Considerations of the Impedance Method, Wave Propagation, and Wireless Systems for Structural Health Monitoring

By

Benjamin Luke Grisso

Thesis submitted to the Faculty of the Virginia Polytechnic Institute and State University
in partial fulfillment of the requirements for the degree of

Master of Science

In

Mechanical Engineering

Dr. Daniel J. Inman, Chair
Dr. Donald J. Leo
Dr. Harry H. Robertshaw

August 31, 2004
Blacksburg, Virginia

Keywords: Structural Health Monitoring, Impedance Method, Wave Propagation, Transverse Matrix Cracking, Edge Delamination, Wireless SHM

Considerations of the Impedance Method, Wave Propagation, and Wireless Systems for Structural Health Monitoring

Benjamin L. Grisso

Abstract

The research presented in this thesis is all based on the impedance method for structural health monitoring. The impedance method is an electro-mechanical technique which utilizes a single piezoelectric transducer as both a sensor and actuator. Due to the high frequencies of excitation used for the method, the sensing area for damage detection can be very localized. Previous work has shown that wave propagation can be added to systems already equipped with hardware for impedance-based structural health monitoring. The work in this thesis shows what happens under varying temperature conditions for a structure being monitored with wave propagation. A technique to compensate for temperature fluctuations is also presented.

The work presented here is an initial study to directly correlate the actual amount of damage in a composite specimen with a damage metric indicated by impedance-based structural health monitoring. Two different damage mechanisms are examined: transverse matrix cracking and edge delamination. With both composite defects, a sample is interrogated with the impedance method before and after damage is introduced. The exact amount of damage in each specimen is found using radiography and compared with the health monitoring results.

Traditional impedance techniques require the use of a bulky and expensive impedance analyzer. With the trend of structural health monitoring moving towards unobtrusive sensors which can be permanently placed on a structure, an impedance analyzer does not lend itself to these small, low power consuming requirements. In this thesis, an initial attempt to miniaturize the hardware is described. A prototype impedance-based structural health monitoring system, incorporating wireless based communications, is fabricated and validated with experimental testing on a number of different structures. The first steps towards a complete self-contained, robust structural health monitoring sensor are presented.

Acknowledgements

I would first like to thank my advisor Dr. Daniel J. Inman for his guidance and advice throughout the duration of my research. I am very glad for the opportunity to work in CIMSS under Dr. Inman. Every time we have a meeting, I always leave with a smile from his wonderful sense of humor. I also want to thank my other committee members Dr. Donald J. Leo and Dr. Harry H. Robertshaw. Dr. Leo is a great teacher, and I enjoyed his classes immensely. Working with Dr. Robertshaw made my teaching assistant days much easier.

I am very blessed to have a wonderful family. My parents have fully supported me throughout my academic career, and graduate school has been no exception. They always share some insightful wisdom and advice at the times I need it most. My sister is always willing to listen and can continually make me laugh. I would also like to thank Erin Elder for her constant encouragement and understanding. All of my great friends at Virginia Tech have made grad school a lot of fun.

Additionally, I would like to thank all of my fellow colleagues at CIMSS. Specifically, I am grateful to Dan Peairs and CIMSS alumnus Dr. Gyuhae Park for all their help with these projects and their insight into the impedance method. Much thanks is extended to following people from the Virginia Tech Engineering Science and Mechanics Department for their help with the composites part of this research: Dr. Jack Lesko, Daniel Reed, Robert Simonds, and Marshall McCord. Finally, I want to thank Los Alamos National Laboratory (grant 44238-001-0245), Extreme Diagnostics, Inc., and the Air Force Office of Scientific Research (contract F49620-03-C-0078) for their financial support of this research.

Table of Contents

List of Figures

List of Tables

Nomenclature

α_v = volume coefficient of thermal expansion

c = longitudinal wave speed

d = damage location on wave propagation beam from PZTs 1 and 2

d' = damage location on wave propagation beam from PZTs 5 and 6

E = Young's Modulus

i = frequency interval for impedance signatures

l = distance to the center of the wave propagation beam

L = length of the wave propagation beam

m = mass

M = RMSD damage metric

n = natural frequency number

N = total number of frequency intervals

ρ = mass density (Chapter 2)

ρ = cross correlation (Chapter 4)

RD = Relative Deviation

s = electric signal measured by the acoustic emission sensors

s_{Z_1} = standard deviation of baseline impedance signature

s_{Z_2} = standard deviation of damaged impedance signature

S = High-Frequency Root Mean Square

t_A = time when the damage reflection arrives at PZTs 3 and 4 on wave propagation beam

t_A' = time when the damage reflection arrives actuated from PZTs 5 and 6

t_1 = time when the first echo arrives at PZTs 3 and 4 on wave propagation beam

t_1' = time when the first echo arrives actuated from PZTs 5 and 6

T = time duration of the acoustic emission signal (Chapter 1)

T = temperature in degrees Celsius (Chapter 2)

$u(x,t)$ = displacement at position x and time t for wave propagation beam

V = volume

V_0 = original volume of wave propagation beam

ω_n = longitudinal natural frequency

Y^{I}_{ij} = admittance after the i th connector at any node is loosened at frequency interval j

Y^{0}_{ij} = admittance before the i th connector at any node is loosened at frequency interval j

Y^{I}_{1j} = admittance after connector 1 at node A is loosened

Y^{0}_{1j} = admittance before connector 1 at node A is loosened

$Z_{i,1}$ = baseline impedance signature

$Z_{i,2}$ = damaged impedance signature

$\overline{Z}_1$ = mean of baseline impedance signature

$\overline{Z}_2$ = mean of damaged impedance signature

Chapter 1

Introduction

1.1 Structural Health Monitoring Challenges

The introduction of smart structures into real world applications is one of the more challenging engineering problems today. Many different aspects of a complete structural health monitoring (SHM) system must be investigated before such a project can be confidently employed. Once a SHM system is in place, continuous or routine interrogation of the desired structure should yield valuable information into the current state of operation for the configuration.

One of the common challenges facing SHM researches in coming up with a robust damage detection scheme for comprehensive structural evaluation. Many detection methods and algorithms are specifically configured to detect damage in an area very local to the sensor. Conversely, some methods are very good at providing indications of damage in a very broad, or global, area. A combination of these confined and expansive sensing techniques may be necessary for deployment of SHM on a large bridge, aircraft, or edifice.

Certain types of defects may cause a SHM system to respond in a different manner. For this reason, the sensitivity of the sensor and detections algorithms to various kinds of damage should be known. The operator must know what type of signal to expect for a specific kind, or

amount, of damage. Without some sort of system calibration, the SHM output signal may indicate little or no damage for a very significant change in the structural condition.

Each individual component of a SHM system, hardware, sensors, and even software, will have to undergo extensive laboratory testing before in can be used in a critical application. After the fabrication of the complete system, experimentation must be performed to ensure the hardware and damage indication results are not adversely affected by any harsh environmental conditions. A mature SHM system has the potential to be fully integrated into the operational hardware of a host structure. If a defect is sensed, the system should have the intelligence to determine what the best course of actions should be, whether it is to shut the entire assembly down, or proceed with caution until the area can be inspected.

1.2 Motivation

On May 23, 2004, after only a year of operation, the vaulted roof on the newest terminal of Paris' Charles de Gaulle airport collapsed (www.cnn.com). The cause of the collapse was attributed to weak concrete being perforated by the struts used to support it. Apparently, the concrete slowly deteriorated over time.

In a 2001 report, the Federal Highway Administration stated that 5 percent of the United States' Interstate bridges are structurally deficient, while 16 percent are functionally obsolete. Structurally deficient bridges are defined as bridges which may have vehicle weight restrictions or may need to be completely closed for repairs before being reopened. Functionally obsolete bridges may be structurally sound, but do not match the conditions of the surrounding interstate. As the class of road decreases from Interstate, the percentages of deficient or obsolete bridges increase.

Pyles (2003) reports that, unlike in previous generations, the US Air Force can no longer rely on the retirement of aircraft to decrease maintenance costs. Many of the aircraft in operation have been extended well beyond their designed service life. In addition, the capital required to train maintenance technicians and acquire the proper materials is ever increasing. Finally, it may take 20 to 35 years to fully replace a fleet of aging aircraft including the lead times for productions.

These are only three of the many examples where an effective structural health monitoring system can decrease maintenance costs and downtime. With a SHM system installed on aging aircraft, scheduled maintenance could be reduced to a minimum, or only be performed when the monitoring system indicates cause for inspection. Bridges can be continuously monitored for defects, and damage can be repaired in insipient stages before the bridges are deemed structurally deficient. Monitoring the integrity of buildings can prevent unnecessary catastrophes leading to loss of human life, or simply hasten post-earthquake inspections. Most importantly, the safety of the people operating or occupying structures with SHM systems will be significantly improved.

1.3 Literature Review

The purpose of this literature review is to discuss research which has been previously carried out in the fields of composites damage detection and wireless structural health monitoring. Damage detection in composites is a very active field of research, and much literature has been published for various detections schemes. Wireless SHM is a relatively new topic, and only a small amount of papers describe systems with local processing capabilities.

1.3.1 Damage Detection in Composites

Composites have become exceedingly popular as a material for use in the construction of many structures. In comparison to many materials, composites have a high strength and modulus to weight ratio. Due to their layered, heterogeneous, and anisotropic nature, however, flaws are inherent in the manufacturing and service life of composites (Bar-Cohen, 1986). These flaws lead to failure mechanisms more complex than those in metals and are therefore more difficult to detect. To provide assurance for the use of composites in critical structures, many methods have been employed to observe the presence of damage in composites.

Bar-Cohen (1986) presents a good review of many of the early nondestructive evaluation (NDE) techniques for monitoring the integrity of fiber-reinforced plastic composites. The damage detection process starts in the production stage of the composites. While the laminate is still being cured, the dielectric method can be used to help ensure proper heating by monitoring the capacitance and dissipation factor across two electrodes on the composite. The capacitance

and dissipation factor are proportional to changes in the molecular structure and resin viscosity respectively. Similarly, the ion-graphing method can be used to determine the amount of resin that is cured in a composite by measuring the DC potential across two metal electrodes in the resin. Monitoring acoustic emissions can also be helpful in composite fabrication as different emissions are produced during different stages of the resin-cure process.

Ultrasonics are presented as the main method of damage detection once the composite is completely cured. Delamination depths can be measured using pulse-echo techniques and by using a piezoelectric transducer to measure change in resonant frequency and impedance. Ultrasonic wave attenuation is used to monitor inconsistencies in material composition, density, and porosity. Composite fiber orientation can be determined with ultrasonic backscattering. Utilizing ultrasonic visualization techniques, delaminations can be seen by the operator. Combining ultrasonics with computer software, flaws in composites can be characterized using feature-mapping.

Other techniques discussed for detection in cured composites are X- and neutron-radiography, including computerized X-ray tomographic systems and real-time radiography display systems. Eddy currents are used when electrically conductive fibers are present. Acoustic emission methods are not as useful when the composite is out of a structure and in a stationary state.

After composites have been placed in a structure or are in service, acoustic emission monitoring is useful in continuously determining the fatigue state of composite. Ultrasonics are again useful, but cannot be used around adhesive edges. Low-frequency ultrasonic testing via dry coupling can be used for inspecting adhesion at laminate edges. Matrix cracking is detected with ultrasonic backscattering. Radiography can be used to detect matrix cracking, delamination, and fiber-bundle fracture, but a penetrant must used to obtain a visual of the damage. In thin composite structures, thermal imaging, thermography with liquid crystals, vibrothermograpy, holography, and electric charge decay can all be used to observe fatigue.

Unlike most NDE techniques, Structural Health Monitoring (SHM) systems are being developed for permanent deployment on a composite structure. NDE techniques require the structure to be taken out of service or a technician to carefully inspect the area in question. SHM systems for damage detection in composites are a very active topic of research. A good review of

many of the current areas of interest is presented by Soon et al. (2003). Papers which discuss damage detection methods such as Lamb wave testing, modal parameter changes, natural frequency and mode shape changes, optical fiber systems, and acoustic emission detection are included. Sensors and actuators used for analysis include piezoceramics, fiber-optics and Fiber Bragg Gratings, and ferromagnetic particles subjected to an alternating magnetic field. Some of the techniques utilize neural networks or an array of sensors in an attempt to locate both the location and extent of damage, as well as monitor impacts to the composite structure. This literature review is by no means meant to be an exhaustive study, but rather, its intent is to give a general overview of the current and past composite damage detection technology.

Using a network of four piezoelectric sensors in a composite plate, Osmont et al. (2000) describe a method of detecting damage using high frequency acoustic emissions. The piezoelectric discs are embedded in carbon-epoxy plates of 16 and 32 plies. Acoustic emission techniques are passive, so the piezoelectric disks are only used as sensors. To analyze the signal observed by the sensors, a parameter called the High-Frequency Root Mean Square (HF-RMS) value, S, is defined as

$$S = \left(\int_0^T \frac{s^2 dt}{T} \right)^{1/2}, \tag{1.1}$$

where s is the electric signal measured by the sensors, and T is the time duration of the signal. Using the HF-RMS parameter, a full diagnosis of occurrence and location of impacts, as well as the severity of damage caused by these impacts can be determined. A near linear relation between the HF-RMS and the delaminated area was shown. To identify the location of the damage, two unknown parameters must be optimized based on the S value at each sensor (the higher S is, the closer the sensor is to damage). For implementation of this technique to find damage areas and locations, a plate similar to these reference plates must be used.

Prosser et al. (1995) also used acoustic emissions to detect damage in composites. In this case, the damage is matrix cracking in cross-ply graphite/epoxy composite test specimens. Four broad band, high fidelity acoustic emission sensors are used for each sample to monitor the cracking and determine the location and initiation site of the cracks. To verify the presence of the cracks, backscatter ultrasonics, X-rays using dye penetrants, and destructive sectioning with

microscopy are used. Six different specimen thicknesses for a stacking sequence of $[0_n, 90_n, 0_n]$ are used, where n = 1 to 6. When n is greater than two, an exact correlation between matrix cracking and acoustic emission signals is found. Using plate wave analysis, the location of the cracks is determined. In thinner specimens (n less than two), a good correlation between acoustic emission waves and the actual cracks is not established.

Kander (1991) uses acoustic emissions to monitor fatigue in glass fiber reinforced composites. Damage accumulation was monitored using two wide band differential piezoelectric transducers at each end of the specimen under three-point quasi-static bend loading. Using two sensors allows for the determination of crack locations to within 0.3 mm by means of measuring the time-of-flight difference for the acoustic waves seen at each sensor. Three distinct acoustic emission signals, correlating directly to three different damage mechanisms, are observed. The lowest acoustic emission signal correlates to matrix cracking and voiding. Intermediate signals occur with fiber-matrix debonding. The highest amplitude acoustic emission signals are found with glass fiber breakage, ultimately leading to the failure of the composite. In addition to the quasi-static testing, the three-point cyclic fatigue testing was also performed. The same three amplitudes (correlating to the same three damage mechanisms) were shown for cyclic fatigue as seen with the quasi-static testing. Acoustic emission events occurred at the same stains for fatigue as they did for quasi-static break tests.

Lamb waves are the primary technique used by Kessler and Spearing (2002a, b) to detect damage in graphite/epoxy test specimens. Two piezoceramic (PZT) patches act as an actuator inducing lamb waves and a sensor to record the strain-induced voltage outputs. Using a beam with a known delamination, the difference between undamaged and damage specimens can be determined in three other beams. Lamb wave methods are effective for in-situ determination of the presence and severity of delaminations, matrix cracks, and through-holes. Kessler and Spearing also experimented with composite damage detection using frequency response methods. Monitoring the frequency shifts of frequency response plots can indicate the presence of damage, but differentiating between damage types, magnitudes, locations, and orientations is extremely difficult. The authors recommend frequency response methods only for detecting global changes in stiffness for larger structures.

Using an experimental setup made to perform Lamb wave and frequency response analyses, Kessler and Spearing also test the feasibility of incorporating strain monitoring methods

and acoustic emissions to detect composite damage. Their results were inconclusive, but, based on previous results for both methods, strain monitoring can be used to predict failure knowing composite material strain limitations, and acoustic emissions have been shown as a useful tool for monitoring damage events. The authors propose a SHM system consisting of autonomous sensor patches containing piezoelectric sensors with local wiring, a data acquisition and processing device, a rechargeable battery with an inductive coil for power reception, and a wireless transmitter. These sensors would operate passively, collecting acoustic emission and strain data, until a sizable event is registered. With a large impact, the system would become active, and Lamb wave and frequency response techniques would search for the presence of damage. After centrally processing the data, the damage information would be sent to the operator of the system. A good comparison of the strengths, limitations, sensitivity to damage, and power consumption for a number of damage sensing techniques, including X-rays, optical fibers, eddy currents, ultrasonics, etc., is also presented.

To analyze the Lamb wave signals altered by defects in composites, wavelet analysis is often used, such as in systems by Kessler and Spearing. Improving the signal processing techniques of wavelet analysis can yield systems more sensitive to the presence of damage. Sohn et al. (2003b) describe the development of a damage index to locate an area of delamination in a composite plate. The damage index is based on exciting the structure with a specific waveform input. With a known input, the damage index is derived by comparing a baseline signal to a signal with some energy dissipation due to damage. Performing the damage index analysis between all the sensor and actuator paths in the plate gives the location of the delamination. Yuan et al. (2004) also introduce a new wavelet based damage signature for determining the presence and extent of damage in a structure. To eliminate the propagation distance effect between sensors of different distances, the damage signature is defined as the initial peak amplitude of the monitored signal. The greater the extent of damage, the lower the signature will be, regardless of the distance of the defect to the sensor.

By observing modal characteristics, Diaz Valdez and Soutis (1999) study the initiation of delamination in a composite laminate. Specifically, a technique known as resonant ultrasound spectroscopy (RUS) is used to observe the modal frequency shifting as a delamination grows in the laminate. RUS uses two transducers, an actuator to excite the structure with a swept sine signal, and a sensor to detect the amplitude of vibration in the structure. A thin scalpel blade is used to introduce, and then grow, a delamination in the composite. The laminate is tested using

RUS in the range of 8-13 kHz, and the exact delamination area is measured using ultrasonic c-scans. As the delamination grew, the modal frequencies decreased indicating a reduction of stiffness in the structure. Small edge delaminations noticeably reduce the frequencies, and plots of the resonant frequencies versus the damage size show the frequency reduction trends for increasing amounts of delamination.

Xu et al. (2003) use fiber optics to detect delaminaitons. In a usual optical fiber damage detection scheme, fibers are embedded into glass fiber reinforced composites. Damage to the composite results in fiber fracturing, significantly reducing the transmitted light power. To effectively monitor a structure, a large number of embedded fibers need to be used, increasing system costs and potentially decreasing laminate strength. An example of such a system to monitor micrometeoroids and orbital debris is described by Tennyson (2004). Using a fiber optic grid to detect impacts, a correlation between the debris pattern and size of hole in the structure is shown. In Xu's method, an optical fiber is embedded inside the length of the beam which acts as one side of a fiber interferometer. As the beam is loaded, the interferometer output is the optical phase shift, which is proportional to the integral strain along the beam. If a delamination is present in the beam, the integral strain will change from that of an undamaged beam. When a load is moved along the length of the beam, the integral strain can be found as a function of the load position. The first derivative of the integral strain will give peaks at delamination points. Experimental results show that the delamination locations are consistently revealed with the first derivative of the integral strain. Numerical results with two and three dimensional finite element models created to compare with the experiment results were less sensitive to the delaminations and often the gaps were indiscernible. This method, which requires a load to be moved over the surface of the beam, seems more suited as an NDE technique rather than something which can be developed into an on-line SHM system.

As described by Xu et al., many attempts have been made to model damage, particularly delaminations, in composite structures. With a model of a structure, including damage, incorporated into a health monitoring system, the accuracy of the system in detecting damage location and magnitude should greatly increase. A representative model of the system may also allow for and upgrade from simply learning about the damage of the structure in a SHM system to determining how the damage will affect the structure in a damage prognosis setup. Nag et al. (2002) attempt to simplify these models using a damaged spectral element. A single damaged spectral element can be used to represent a delamination in a beam model, irrespective of the

beam length. Spectral element methods are computationally more efficient than finite element models, and only two measurement nodes are needed to find the presence of a delamination using a damage force indicator vector. In building a database of damage scenarios for a structure, spectral element methods, with a single damaged spectral element for each damage location, would significantly reduce data storage sizes.

Using an array of PZTs in a composite plate or structure, multiple detection and analysis techniques can be combined. Dugnani and Malkin (2003) used two data analysis methods to analyze data in a composite airplane structure. The objective of the damage detection was to characterize the location and extent of damage in the structure. To generate an image of the damage, time-of-flight and direct path approaches are described, with the latter being chosen for implementation. Producing graphical image of the damage location is found by analyzing the data with two methods: Signal Time-Windowing and Intensity Weight Factoring. The Signal Time-Windowing technique looks at the amount of scatter in a signal to determine the damage. In Intensity Weight Factoring, the scatter signal is compared to the baseline signal of the healthy structure. Sohn et al. (2004) use different methods to detect damage in a composite structure with an embedded PZT array. Lamb waves are used to locate areas of delamination and estimate its area. To further enhance the capabilities of Lamb wave methods, time reversal acoustics (TRA) are used. The TRA gives a means of reproducing the original actuation signal with wavelet analysis. If a defect is encountered in the wave propagation path, the ability of TRA to reconstruct the original signal breaks down, and the defective reproduced signal can be compared to the original input to identify damage. The impedance method is also used to identify the severity of impact damage to the composite plate. Three different techniques were used to extract features from the impedance signatures: correlation coefficients, frequency domain auto-regressive with exogenous inputs (ARX) time-series modeling, and spectral moments. Each method correctly identified the severity of impact to the structure.

The impedance method is also used by Bois and Hochard (2003, 2004) in an attempt to quantify the level of diffuse damage in composite structures. Bois and Hochard claim that, by observing the level of damping of the modes in an impedance curve, the amount of damage can be deduced. As more damage is incurred, the laminate stiffness decreases lowering the frequency and amplitude of the peaks. Measurements are taken with PZT transducers on two different specimens, one damaged and one undamaged. By looking at the curves, they claim to be able to differentiate between the laminate with delamination and the intact laminate. Bois and Hochard

explain that the transducer dominates the signal from the damaged structure, and the other peaks are damped out. However, especially with composite materials, the number of peaks in a given frequency range can vary greatly. While one sample might have a large number of resonant frequencies in a given range, a second sample which appears identical on the macro scale, might only have one large mode, or even none. Composite materials can be very inconsistent in fabrication with many minor defects that will be seen with high frequency impedance measurements. In using the impedance method, a baseline must be taken for each structure to compare with damage signals. Bois and Hochard also model a composite laminate with a piezoelectric element to model the impedance method. The experiments and simulations are conducted at a frequency range from 500 to 10,000 Hz. However, for samples only 180 mm long, the frequency range would seem to overlap with the global resonant modes of the structure, making it very difficult to detect a small amount of damage. Experimental and analytical results are not directly compared in on the same figure, but error between the simulation and experiments is said to be about 15 percent, even though the frequency locations and amplitudes seem to differ greatly.

In the impedance methods presented by Sohn et al., the level of damage detected with the monitoring system is not directly compared to the actual amount of damage in the structure. Each new damage state is just compared with the previous state. Bois and Hochard do not describe a method to quantify the level of damage in the composite from the acquired signals. The length of delamination is known, but no direct statistical connection is made to the changes seen in the impedance signature. The work presented in this thesis is a first attempt to directly quantify the amount of damage in composite specimens using the impedance method. Each damage metric calculated is directly compared to the actual amount of damage in the composite specimen through the use of radiography.

1.3.2 Wireless SHM Systems

In a laboratory setting, most researchers are simply concerned with proving the validity of a structural health monitoring system. For implementation of SHM in a field setting however, some large challenges need to be overcome. Processing and transmitting data may require expensive hardware. Also, connecting sensors, processors, and other hardware can include complex wiring configurations (Sohn et al., 2003a). For these reasons, the use of stand alone or

networked wireless SHM systems have been proposed as a method to introduce permanent monitoring into real world structures.

Sohn et al. (2003a) review some of the early propositions for including wireless transmissions into SHM systems. Many attempts at designing a wireless based system components are discussed. A cluster of wirelessly connected prototypes was constructed to introduce the architecture needed for communication between individual sensors and a central processing unit. At each cluster node, a microprocessor can analyze the sensor signal or simply pass it on to the host PC. However, this is the only research reviewed that has the capability for local data processing. The rest of the projects simply describe a means to acquire data on a structure and wirelessly transmit the data somewhere else for processing. Different transmission methods and their advantages are discussed, but computing still must be done at a host computer. Wirelessly transmitting all of the data is much more inefficient than local computing which simply transmitting the results and may be as simple as revealing that the structure is or is not damaged. The focus of this literature review will be to present wireless SHM systems with local processing ability.

A network of sensors is used by Basheer et al. (2003) to detect strain in the structure it is applied to. Each sensor has the ability to process the raw strain data using neighboring sensors and transmit the resulting information to an end user. The smart sensor note prototype, called ISC-iBlue, consists of an ARM7TDMI microprocessor, a Phillips Blueberry Bluetooth communications module, a multi-channel analog-to-digital converter (ADC), and a rechargeable battery. The focus of this work was to determine the communications necessary for a self organizing wireless sensor network with master and slave nodes. No experimentation is shown which measures strain and processes data; rather, an algorithm is introduced to achieve a tree network of sensors with self routing capability. The node and communications development here should lead to a SHM system which performs complex feature extraction, with wavelet analysis or other methods, in conjunction with its neighboring sensors to accurately detect faults in structures.

Tanner et al. (2003) demonstrate local processing capabilities with off the shelf components in a wireless SHM system. A Mote, developed at the University of California, Berkeley, from Crossbow Inc. is used as the wireless sensing system. The Mote consists of two circuit boards. One board holds a microprocessor, ADC, and wireless transmitter, and the other is

a sensor board containing two microelectromechanical system (MEMS) accelerometers. The bandwidth of the accelerometers was increased to 1 kHz from its original board settings of 50 Hz, and the microprocessor can sample eight channels at 4 kHz, but only by sequential multiplexing (the sampling rate is divided by the number of channels being used). A Mote can be powered by two standard AA batteries. To detect damage on the structure using the Mote platform, a simple statistical process control, based on the cross-correlation coefficient of the two accelerometers, is programmed in C and downloaded to the board. The structure being tested consisted of two aluminum plates, on top and bottom, connected with aluminum columns, steel angles, and steel bolts. One of the bolts incorporates a PZT ring actuator to modify the bolt preload.

After control limits have been determined for the structure, the Mote platform, with its embedded detection algorithm, can detect the loosening of the bolt preload. As the bolt is loosened, a yellow LED will flash indicating an outlier to the limits. The data is then processed, and if failure of the joint is determined, a red LED will come on. A green LED flashes if the system is healthy or the preload is restored. Major limitations are pointed out by Tanner et al. in using the Mote platform. Sensing resolution and range are limited by the 10 bit ADC and low frequency bandwidth respectively. Making simultaneous measurements on different channels for feature extraction is difficult due to the low sampling rate. The flash memory of the system is small and does not allow for complex programming with floating-point calculations, and data cannot be stored with the small amount of RAM. Overall, the system is not able to resolve high frequencies, where much of the damage would be detected. It should also be noted that the SHM system does not produce its own actuation signal and relies on input from a shaker.

A wireless active sensing unit to monitor civil structures has been designed by Lynch et al. (2004a). The sensing unit is constructed of off-the-shelf components and has the ability to command active sensors and actuators. A computational core is combined with wireless transmission and sensing circuits to allow for control of actuation and sensing, implementation of algorithms to process the acquired data, and broadcasting of the structural status. To control the overall operation of the entire unit, a Motorola PowerPC MPC555 microcontroller is used as the core. The MPC555 has 32-bit architecture and allows for embedded algorithms with floating point calculations. 512 Kbytes of external random access memory is used to store sensor data. When in service, the MPC555 can sample 32 channels at sampling rates up to 40 kHz. To provide an actuation signal of -5 Volts to +5 Volts at up to 40 kHz, a Texas Instruments DAC7624 digital-to-analog converter (DAC) is combined with an Analog Devices AD620

amplifier. Wireless radio communications are integrated into the system with a MaxStream XCite radio. All of the components and software are designed with power efficiency in mind and can be powered with a lithium battery pack.

To demonstrate the capabilities of the wireless active sensing unit, two piezoelectric patches are mounted onto an aluminum plate. One patch is actuated with the system to excite the aluminum bar with acoustic surface waves. The second pad acts as the sensor to measure the received waves. An ARX time-series model of the input-output data is generated with the embedded algorithms in the core. Eventually, this ARX model will be used to detect damage in a structure by observing the shifting of transfer function poles. Lynch et al. (2004b) provide a step-by-step energy analysis for calculating the ARX time-series modeling of a 4000 point time-history record in a previous system, which required communicating with a centralized server, with less efficient wireless transmitters.

Sazonov et al. (2004) also design a system to monitor civil infrastructure. Their Wireless Intelligent Sensor and Actuator Network (WISAN) detects bridge defects based on the method of modal strain energy. The WIMSS claims to consume less power, 67 mJ, for the same amount of data as the 3 J of Lynch's (2004) system. However, this does not include the power required for computation as the WISAN doses not perform any local (at the sensor) data processing, but simply transmits the data to a node with a permanent power supply for computations. Sazonov et al.'s system also does not utilize active sensing, so no power is consumed providing an actuation signal, but rather, it relies on ambient energy provided by the bridge structure. In contrast, the prototype presented in this thesis relies on harvesting ambient vibrations to provide power the system rather than provide excitation. A signal with a predetermined amplitude and frequency range is used to excite the structure at high frequencies known to be sensitive to the presence of damage, breaking the reliance on the structure to provide the necessary frequency content. By providing an actuation signal, the prototype in this thesis is also insensitive to global characteristics which may change the ambient vibrations, but may not be able to characterize small, but crucial, defects.

A review of current smart sensor technologies for monitoring civil infrastructure is presented by Spencer et al. (2004). Smart sensors, as opposed to a standard integrated sensor, are defined as sensors having intelligence capabilities, or an on-board microprocessor. The microprocessor can perform functions including, but not limited to, data processing, ADC,

controlling data flow and its own operation, and interfacing with other systems. Four features must be present in a smart sensor, an on-board central processing unit, small size, wireless communications, and the promise of being low cost. With this somewhat broad definition, much of the work reviewed is smart sensors used to simply acquire and transmit unprocessed data. The original prototype by Lynch et al., as well as the evolution of the Mote system used by Tanner et al., are the only two systems described which allow for localized processing. The original Mote distributed by Crossbow Inc. has been upgraded to the Mica, Mica2, and Mica2dot. A lack of programming memory and processing power noted by Tanner et al. are still problems with the Mica series. To address these issues, Intel has started development of their own Mote platform. The ultimate goal of the Intel-Mote is to include sensors, MEMS wireless, memory, DAC, and a battery into a single microchip. The programming memory will be upgraded to 64 Kbytes and include a 32 bit processor operating at 12 MHz.

As briefly mentioned before, the work in the thesis will include a prototype for a wireless SHM system based on the impedance method. A known input will be measured with the system and used to actuate a piezoelectric patch mounted to the structure. At the same time, the response of the system will be recorded using the low cost impedance method. The response is compared to a previously stored baseline, and a statistical damage metric is calculated. If a set threshold is exceeded, the operator will be notified with a wireless warning signal.

1.4 Thesis Overview

1.4.1 Research Objectives

The objectives of this research are to investigate three areas for the improvement of impedance-based SHM. Specifically, the robustness of the impedance method is increased by providing a means of utilized wave propagations to detect global damage in structures under varying thermal conditions. The sensitivity of the impedance method is defined by quantifying the amount of damage present in composite materials. The ultimate goal of this research is to provide a stepping stone for a smart wireless sensor system which can be adapted to monitor the structural integrity of any structure. This low cost and robust sensor should increase the accessibility of the impedance method and allow for permanent health monitoring applications on

real world structures. Much of the research described in this thesis, especially Chapters 2, 3, and 4, is contained in published conference proceedings (Grisso et al., 2004a, b, c).

1.4.2 Chapter Summaries

Impedance-based structural health monitoring techniques have been shown as a promising method to detect damage in a wide variety of structures. Due to the high frequency excitations used in the impedance method, the ability to specify the location of small structural changes in far-field locations may be a limitation. As a result, a technique was developed to combine the impedance-based method with wave propagation. Wave propagation allows for the exact location of damage to be determined in structures.

In Chapter 2, the effect of temperature variations on the use of wave propagation for damage detection is investigated. Equations used to determine the damage location in simulation are derived. Temperature variations are induced, and the resulting errors are displayed. Using a realistic temperature differential, the affect of temperature changes on a possible application is shown. A curve-fit of the modulus of elasticity is then implemented to correct damage location error.

An impedance-based structural health monitoring system is used to detect the onset of transverse matrix cracking in cross-ply graphite/epoxy composites in Chapter 3. Piezoceramic (PZT) patches are attached to the composite samples to simultaneously excite the structure with high-frequency excitations and monitor any changes in structural mechanical impedance. A symmetric $[0/90]_s$ arrangement is tested during quasi-static tensile loading. Impedance measurements are correlated with the stress-strain relationship of the composite, as well as visual inspection. Matrix cracking is verified with radiography. Results are presented and compared with previously published literature. Experimentation with a similar, but thicker, cross-ply also yields similar results.

Chapter 4 extends the research described in Chapter 3 to detecting a different damage mechanism in the form of edge delamination. Again, impedance method results are directly correlated with actual composite faults via radiography. A brief comparison of different damage metrics is also provided.

The fabrication of a stand alone prototype for SHM is outlined in Chapter 5. A new prototype is designed to provide a starting point for a self-contained impedance-based sensor. The new sensor will incorporate data interrogation of a structure, localized computation of algorithms to analyze the data, wireless communication of the results to the end user, and a renewable power supply via piezoelectric-based power harvesting. Validation of the resulting prototype is carried out with experimentation on a number of different structures.

The final chapter provides a brief overview of all the results found from the research of this thesis. An outline of the specific contributions this thesis makes to the field of structural health monitoring is provided. Recommendations for future work to extend the contributions this thesis provides are detailed at the end of the chapter.

Chapter 2

Temperature Influences on Wave Propagation

2.1 Introduction to SHM and the Impedance Method

In many engineering applications, there is a desire to be able to monitor the current status of a structure. When damage occurs, the system operator would like to be able to know what happened to the structure, how severe the damage is, and where the damage is located. To achieve these goals, the field of damage identification methods is currently a large area of research. Many different methods have been studied as viable means for damage detection implementation.

Many techniques for the evaluation of a structure have been used in various fields for many years. Typical non-destructive monitoring techniques are ultrasonic technology, acoustic emission, magnetic field analysis, penetrant testing, eddy current techniques, X-ray analysis, impact-echo testing, global structural response analysis, and visual inspections (Park et al., 2003). There are, however, some distinct disadvantages to some of these techniques. Some methods, such as using ultrasonics, may yield good results, but can only be employed by highly trained technicians when a system is out of service. Eddy current sensors are localized only over a certain area. In general, the distinction between NDE techniques and SHM is that NDE must be

performed while the structure is non operational. Due to these disadvantages, various other methods have been developed (Park et al., 2003).

Vibration-based methods for detecting damage tend to revolve around changes in the basic modal properties of the system: frequencies, damping, and mode shapes (Doebling et al., 1998). Frequencies have been shown to have much lower statistical variation from random errors than the other two modal properties. However, it is hard to detect which resonant peaks are due to mass loading and other factors, or actual damage. Forms of health monitoring using mode shapes include utilizing the modal assurance criteria to detect localized damage, or using the derivatives of mode shapes to detect damage in finite element structures. Other methods utilize all the modal properties to adapt a system model with any changes, some of which could be caused by damage (Doebling et al., 1998).

Impedance-based health monitoring techniques utilize small piezoceramic (PZT) patches attached to a structure to both excite the structure with high-frequency excitations and monitor any changes in structural mechanical impedance (Park et al., 2003). Mechanical impedance is the ratio of an applied force and the resulting velocity. In comparison, electrical impedance is the ratio of an applied voltage and the resulting current. For a single degree-of-freedom example, an equation can be derived which gives the electrical admittance (inverse of impedance) of a PZT when attached to its host structure (Liang et al., 1994). The equation is a combination of both the mechanical and electrical impedances, thus any change in the mechanical impedance (damage) will show up in the electrical impedance. In other words, when the structure is changed, the PZT will draw more or less current with the same applied voltage. When the impedance is varied over a range of frequencies (30 – 400 kHz), plots similar to frequency response functions can be obtained with useful information relating to the health of a structure (Park et al., 2003).

However, some limitations have been shown in the ability of impedance techniques to detect damage in far-field locations. For this reason, impedance-based structural health monitoring has been combined with other non-destructive sensing techniques in an attempt to further quantify the location of damage. Wave propagation (pulse-echo) was introduced as a supplement to the impedance approach for detecting damage (Kabeya et al., 1998). In this method, a longitudinal wave is generated by a PZT patch and a reflective wave is recorded by a different patch. By monitoring the pulses observed by the second patch, the time of travel, and thus the damage location, can be calculated (Park et al., 2003). Applied to a large structure, such

as aging aircraft, one single PZT patch can be used as an actuator, with multiple other PZTs in a sensing mode able to cover a large area (Giurgiutiu et al., 2002). The results indicate that the impedance-based approach is more suitable for near field damage detection, while wave propagation is more useful for far-field damage detection (Park et al., 2003 and Giurgiutiu et al., 2002).

In this chapter, the effect of temperature variations on wave propagation supplementing impedance health monitoring will be discussed. As a structure undergoes temperature changes, its material properties will change. Many of these changes could be large enough to influence the results of the wave propagation technique used to detect damage. The next section will attempt to quantify the possible changes in the wave propagation techniques, as well as present a solution to any arising problems. A discussion applying the analysis will follow, ending with the main conclusions of the chapter.

2.2 Analysis for One Dimensional Structures

As previously mentioned, a time-domain approach using wave propagation was developed by Kabeya, et al. to detect damage in systems already set up with impedance-based structural health monitoring equipment. The basic premise of the pulse-echo technique is as follows; when a pulse is generated and travels through a test piece, the pulse will be reflected when it strikes a crack or some other form of damage. If the time history of when the pulses reach a certain point is recorded, then, knowing the material properties of the structure, the location of the damage can be determined using the wave speed and the time between pulses (Kabeya et al., 1998).

In this case, PZT patches will act both as actuators and sensors. When a PZT is placed on a free-free beam and actuated, the normal result would be a dominant transverse, or bending, wave. The wave propagation technique uses longitudinal waves, so Kabeya, et al. developed a method, through experimentation, in which a longitudinal wave could be generated. A longitudinal wave is formed by in phase actuation of two PZTs on either side of the same end of a beam. The longitudinal wave equation can be described as

$$\frac{\partial^2 u(x,t)}{\partial t^2} = c^2 \frac{\partial^2 u(x,t)}{\partial x^2}, \tag{2.1}$$

where $u(x,t)$ is the displacement at position x and time t, and the longitudinal wave speed, c, is described as

$$c = \sqrt{\frac{E}{\rho}}, \tag{2.2}$$

where E is Young's Modulus, and ρ is the mass density.

Now that a longitudinal wave could be realized, Kabeya, et al. set up a proof of concept experiment in order to determine if wave propagation was a legitimate damage detection compliment to impedance. A free-free aluminum beam was set-up with 6 PZT patches adhered to it. PZT 1 was bonded on one edge of the beam with PZT 2 on the same end, but opposite side. PZTs 5 and 6 were in the same relation, but on the other end of the beam, while PZTs 3 and 4 were in the middle of the beam. The beam was 1.83 m long. Damage was induced onto the beam by means of a small aluminum clamp. The setup of the beam, with appropriate dimensions, can be seen in Figure 2.1.

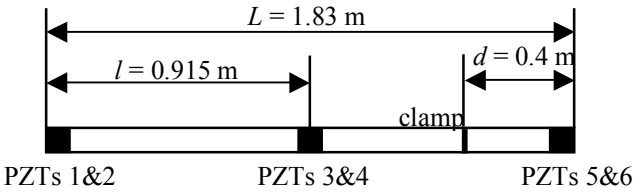

Figure 2.1: Setup for proof of concept experiment with dimensions labeled. Note that PZT patches at each location are on opposite sides of the beam.

To locate damage in the beam, the wave speed of the material was first identified. To calculate the wave speed from a healthy beam the equation

$$c = \frac{l}{t_1} \tag{2.3}$$

can be used, where l is the distance to the center of the beam, and t_1 is the time when the first echo arrives at PZTs 3 and 4 as seen in Figure 2.2.

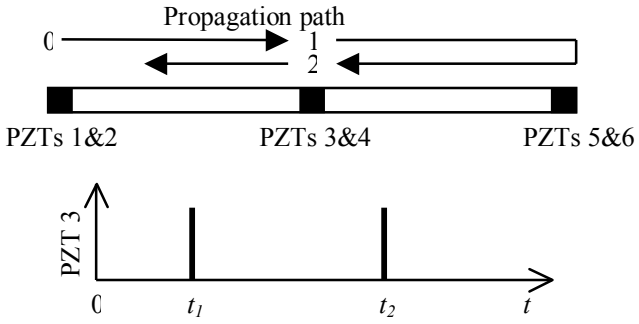

Figure 2.2: The wave propagation path and pulse time history as seen from PZTs 3 and 4.

Next, a longitudinal wave is generated by actuating PZTs 1 and 2 in phase. The damage location from the end with PZTs 5 and 6, *d*, can be determined by using the equation

$$d = L - l - \frac{c(t_A - t_1)}{2}, \tag{2.4}$$

where L is the length of the beam, and t_A is the time when the damage reflection arrives at PZTs 3 and 4 as seen in Figure 2.3.

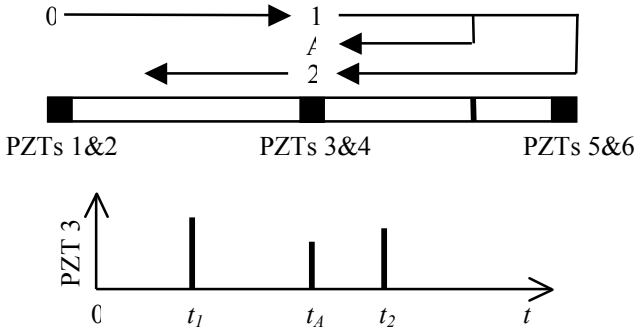

Figure 2.3: The wave propagation and pulse time history as seen from PZTs 3 and 4 when PZTs 1 and 2 are actuated. Time pulse A is the echo from the damage caused by the clamp.

Finally, the damage location is determined again, but this time by actuating PZTs 5 and 6. The damage location from this test, *d'*, can be found with the equation

$$d' = \frac{c(t_A' - t_1')}{2}, \tag{2.5}$$

where t_A' and t_1' are found from Figure 2.4.

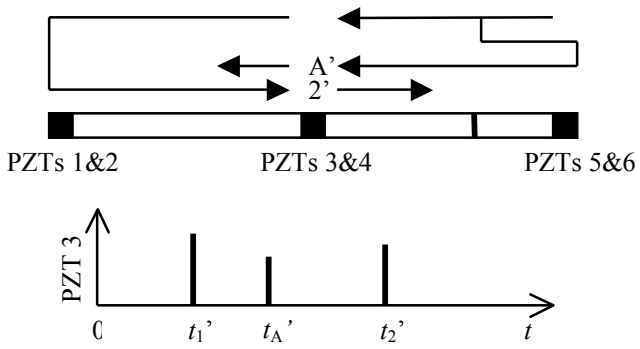

Figure 2.4: The wave propagation and pulse time history as seen from PZTs 3 and 4 when PZTs 5 and 6 are actuated.

If d and d' are the same, then the damage location should be d. If d and d' are not the same, then the damage should be located $L - l - d$ away.

2.2.1 Simulation Setup and Verification

To duplicate the results obtained by Kabeya, et al., a simulation is setup. Pulses are not actually sensed by PZT patches, so a few more equations need to be defined. Looking at Equations 2.4 and 2.5, t_A and t_1, the times seen by PZTs 3 and 4 when PZTs 1 and 2 are actuated, as well as t_A' and t_1', the times seen by PZTs 3 and 4 when PZTs 5 and 6 are actuated, need to be known. From Equation 2.3, both t_1 and t_1' can be determined. Figure 2.3 shows the path the damage pulse takes when PZTs 1 and 2 are creating the longitudinal wave. Knowing the distances from the propagation path, t_A can then be found from the equation

$$t_A = \frac{l + (l-d) + (l-d)}{c} = \frac{3l - 2d}{c}. \tag{2.6}$$

Similarly, Figure 2.4 shows the propagation path when PZTs 5 and 6 are actuated. t_A' can be found from the distances in the equation

$$t_A' = \frac{2d + l}{c}. \tag{2.7}$$

To implement these equations, Matlab is chosen as the simulation tool. The modulus of elasticity and density at room temperature, which are 70 GPa and 2700 kg/m3 respectively, are programmed into the code. Equation 2.2 is used to find the wave speed for aluminum at room temperature, 5092 m/s. Equations 2.3, 2.6, and 2.7 find the pulse times as seen by PZTs 3 and 4, while Equations 2.4 and 2.5 find the damage locations.

The damage location outputs determined by simulation from Equations 2.4 and 2.5 are used to duplicate the results obtained from Kabeya, et al. The initial damage location of d = 0.4 m (from the end with PZTs 5 and 6), is found by exciting the beam from both PZTs 1 and 2 and PZTs 5 and 6. Tracking the damage over a range of values is the next priority. Moving the damage location all over the beam, the equations output the correct location at each value. Table 2.1 shows a few of the iterations for the damage location.

Table 2.1: The damage locations determined from both ends of the beam compared with the actual damage location.

	Kabeya, et al location			
Actual d (m)	0.4	0.8	1.2	1.6
***d* from PZTs 1 and 2 (m)**	0.4	0.8	1.2	1.6
***d'* from PZTs 5 and 6 (m)**	0.4	0.8	1.2	1.6

The damage locations shown in Table 2.1 are all exactly what the actual damage location is. For a simulation, exact locations should be obtained. In Kabeya, et al.'s experimental setup, resolution is a large factor. With the analyzer used to monitor the obtained pulse times, a resolution of 48 mm could be achieved with the analyzer's sampling rate. Resolution is not an issue in simulation because the pulse times are calculated, not measured. In a real system, resolution and external noise will always be an issue.

2.2.2 Damage Detection with Temperature Variations

Equation 2.2 reveals that the wave speed is a function of the modulus of elasticity and density. The wave speed is then used in all of the resulting equations used to find the damage location. The focus of this chapter is now based upon what will happen to the damage location calculated by the pulses, with respect to the actual damage location, when the beam is subjected to a temperature differential.

With increasing temperature, the modulus of elasticity diminishes for most materials (Callister, 1997). The diminishing modulus is especially true for metals. A plot of modulus of elasticity versus temperature can be found for common metals. Using one of these plots for aluminum, the modulus of elasticity is recorded over a large temperature range. Reproducing the modulus versus temperature curve, a curve-fit to the data is generated. Both the curve recreation and curve fit can be seen in Figure 2.5.

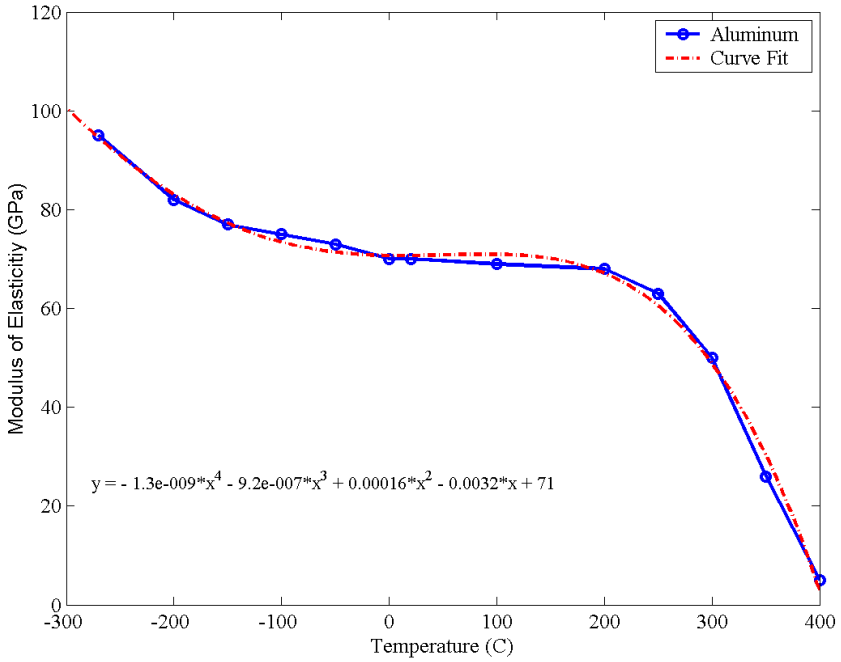

Figure 2.5: The modulus of elasticity versus temperature curve is shown, along with a fourth-order polynomial curve-fit to the data.

The results of the curve-fit yield an equation that can allow the modulus of elasticity for aluminum to be found over a range of temperatures from -270 to 400 degrees Celsius. The equation relating Young's Modulus to temperature can be described as

$$E = -1.3x10^{-9}T^4 - 9.2x10^{-7}T^3 + 0.00016T^2 - 0.0032T + 71, \tag{2.8}$$

where the temperature, T, is in degrees Celsius, and E is in GPa. Now the question is asked, what if the wave speed, as determined from Equation 2.3, is determined at room temperature, but the beam is employed in an atmosphere with a different temperature? The calculations to determine the damage location will be determined with the room temperature wave speed, but the actual

time for the propagation path to reach PZTs 3 and 4 will be a function of the actual wave speed. The actual wave speed is determined by the modulus of elasticity, which is temperature dependent. If measurements are taken in an environment with a temperature different than where the wave speed was calculated, the determined location of damage could be altered.

To determine if the location of damage is indeed influenced by temperature, Equation 2.8 is incorporated into the simulation. As the temperature is varied, the modulus changes, and the actual wave speed is recalculated. The actual wave speed is used to calculate the time required for PZTs 3 and 4 to see the appropriate pulses (Equations 2.3, 2.6, and 2.7). However, when the damage location is found (Equations 2.4 and 2.5), the original room temperature wave speed is used. The results of this simulation shown that as the temperature is varied, the determined damage location does indeed differ from the actual damage location. To show this, the actual damage location, as well as the location found from the room temperature wave speed, are plotted together and can be seen in Figures 2.6 and 2.7.

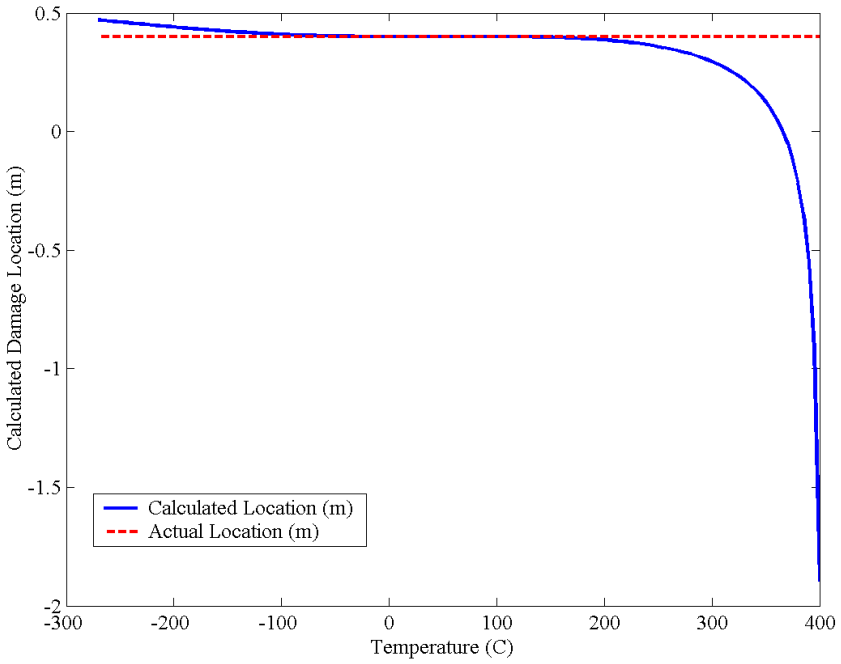

Figure 2.6: The actual damage location, constant at 0.4 meters, is shown with the calculated damage location from PZTs 1 and 2 versus temperature. The wave speed was calculated at room temperature.

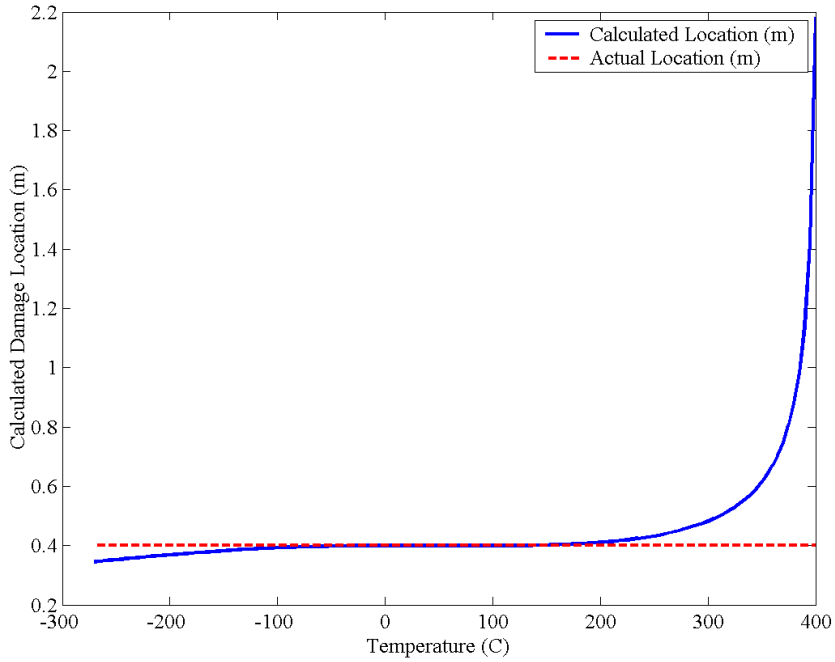

Figure 2.7: The actual damage location, constant at 0.4 meters, is shown with the calculated damage location from PZTs 5 and 6 versus temperature. The wave speed was calculated at room temperature.

Figures 2.6 and 2.7 are shown over a range of temperatures from -270 to 400 degrees Celsius, the range of temperatures for which modulus of elasticity data was available. To place some perspective on these temperatures, -270 degrees (close to 2.7 Kelvin) is the coldest temperature of space, away from all the stars and galaxies. Aluminum has a melting temperature of 600 degrees Celsius, giving a 200 degree cushion between the melting temperature and the highest temperature shown.

At the lowest temperature (-270 degrees Celsius), the damage as determined from PZTs 1 and 2 would be off by 70 mm. PZTs 5 and 6 would show a difference of 55 mm from the actual damage location. However, at the other end of the temperature spectrum, PZTs 1 and 2 would reveal a difference of 2.3 meters, with PZTs 5 and 6 off by 1.8 meters. With higher temperatures, the error is so far off that the damage location determined with the incorrect wave speed would show damage off the beam.

2.2.3 Density Considerations

The wave speed is also a function of density. As the temperature changes, the volume of the beam will change based upon the volume coefficient of thermal expansion (Callister, 1997). The mass of the beam cannot change, so the as the volume changes, the density will change. Volume changes, ΔV, with temperature may be computed from

$$\frac{\Delta V}{V_0} = \alpha_v \Delta T, \tag{2.9}$$

where α_v is the volume coefficient of thermal expansion. The volume coefficient of thermal expansion for an isotropic material is approximately three times the linear coefficient of thermal expansion, which is $23.6x10^{-6}\,(°C)^{-1}$ for aluminum (Callister, 1997). To see if the density will play a significant role the apparent location of damage, the volume of the beam is first found.

$$V = Lwh = 1.83x.0127x.00318 = 7.39x10^{-5}\ m^3$$

Next, the change in volume over a 400 degree Celsius temperature change is found from Equation 2.9.

$$\Delta V = V_0 \alpha_v \Delta T = \left(7.39x10^{-5}\ m^3\right)\left(3x23.6x10^{-6}\,(°C)^{-1}\right)\left(400°C\right) = 2.09x10^{-6}\ m^3$$

The mass of the beam is 0.12 kg, so the apparent change in density can be found with the following procedure.

$$\rho = \frac{m}{V} \quad \Delta\rho = \frac{0.12kg}{7.39x10^{-5}\ m^3} - \frac{0.12kg}{7.60x10^{-5}\ m^3} = 2700kg/m^3 - 2626kg/m^3 = 74kg/m^3$$

The change in wave speed due to the decrease in density can be found using the following procedure.

$$c = \sqrt{\frac{E}{\rho}} \qquad \Delta c = \sqrt{\frac{70GPa}{2700}} - \sqrt{\frac{70GPa}{2626}} = -71m/s$$

Propagating the change in wave speed through the calculations to find damage, the slower speed leads to a difference in the calculated damage location of 2.3 cm from PZTs 1 and 2. Compared to an actual damage location of 40 cm, 2.3 cm is not very far off for such a large temperature change.

Due to this small change in damage location with changes in density, only the modulus of elasticity was considered in the calculations. It should be noted that ignoring the expansion of the beam is only done for a free-free boundary condition. Adding in the affects of the beam's density changing, the apparent damage locations would be a little closer to the actual damage location as seen in Figures 2.6 and 2.7, but not very much. Also, as the object of study gets larger, the change in density plays even less of a role. Only structures with small volumes should be significantly affected by the change in density.

2.2.4 Frequency Considerations

Knowing the modulus changes with temperature, and that the longitudinal natural frequencies are dependent on the modulus, the relationship between temperature changes and frequencies can be determined. The longitudinal natural frequencies, ω_n can be described as

$$\omega_n = \frac{n\pi c}{l}, \tag{2.10}$$

where n is the number of the natural frequency, and c is again the wave speed (Inman, 2001). Using the curve fit of the modulus of elasticity and the density changes considered in the previous section, a plot of the frequencies versus the temperature can be generated. Figure 2.8 shows the first four longitudinal natural frequencies versus temperature with both the modulus of elasticity and density changing.

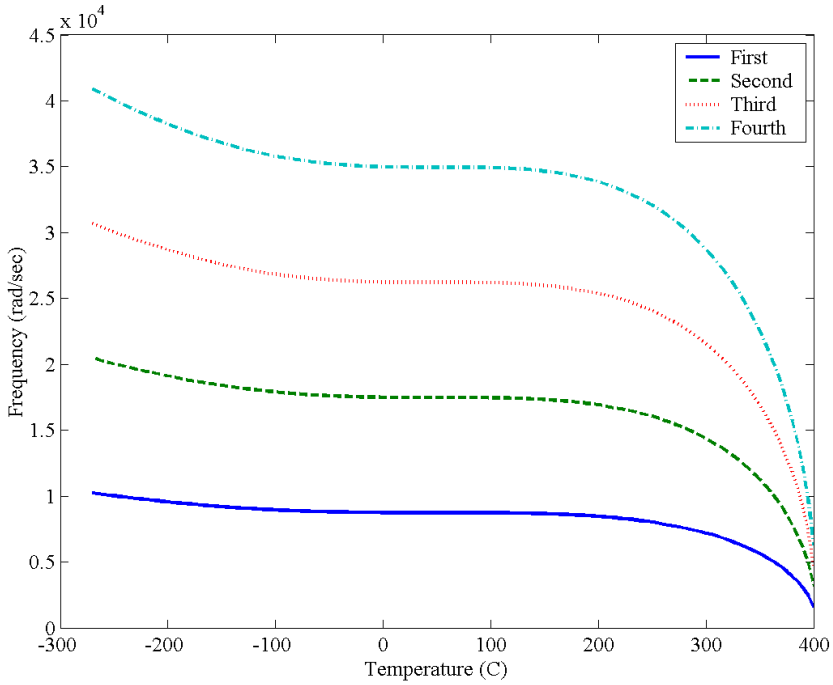

Figure 2.8: The first four longitudinal natural frequencies versus temperature are shown with both the modulus of elasticity and density changing.

As expected, the frequency curves follow the same trend of the modulus versus temperature curve of Figure 2.5. A similar plot to Figure 2.8 can be generated without the density changing, but differences between the two are negligible. This comparison again reaffirms that for large enough structures, the change in density can be ignored.

2.3 Discussion and Applications

In the previous section, plots are generated (Figures 2.6 and 2.7) which show how the calculated damage location changes as a function of temperature. Again, these plots assume that the wave speed was calculated only once at room temperature. Since Figures 2.6 and 2.7 show such a large temperature range, a possible application was looked at to see what would happen to the apparent damage location for a given environment.

2.3.1 Application to Lunar Surface Monitoring

Recently, interest has been shown in developing a base on the moon as a lunching point for manned missions. Critical structures on the moon would serve as ideal candidates for implementing a structural health monitoring system. Initial testing has shown promise in the impedance method being able to detect damage in existing space shuttle ground structures (Peairs et al., 2004a). However, any structural health monitoring system would have to be able to adjust to the temperature differentials incurred as a result of being in a non-atmospheric environment.

The surface temperatures on the moon vary greatly from day to night. The mean surface temperatures are 107 degrees Celsius during the day and -153 degrees Celsius at night (Heiken et al., 1991). The maximum and minimum temperatures at an equatorial location are 123 and -181 degrees Celsius (Heiken et al., 1991). Assuming that the wave speed was measured in a controlled environment on Earth and never recalculated, Figure 2.9 shows what would happen to the calculated location of damage with damage introduced at 0.4 m.

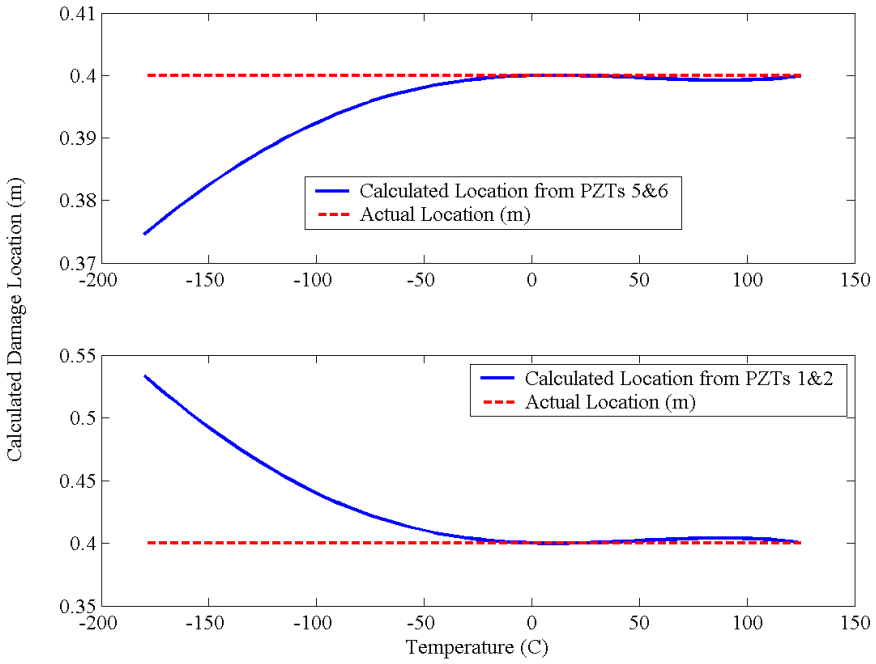

Figure 2.9: The actual damage location, constant at 0.4 meters, is shown with the calculated damage location versus temperature.

From Figure 2.9, the night temperatures on the moon have a much larger influence on the damage location error than the day temperatures. For this system, the largest error occurred at the minimum temperature with a difference of just over 3 cm. For a beam of 1.83 m long, 3 cm is probably an acceptable distance. Depending on the sampling rate of the analyzer monitoring the pulses, the resolution error could be just as large.

However, larger objects with the PZT patches spaced further apart can potentially yield different results. Over the same temperature range, a 5 m long beam will have a damage location error of around 14 cm at the lowest temperature. 14 cm is fairly significant, but could be reduced by using more sensors.

2.3.2 Applying the Modulus Curve-fit

Obviously, the simple solution to possible damage location error is to just recalculate the wave speed of the system before each measurement. However, in situations where measurements are constantly being made, recalculating the wave speed might not be practical. Recalculating the wave speed might not also be realistic if the temperature is changing rapidly. In these cases, the use of a temperature probe might be a solution. If the temperature is known, Equation 2.8 can be implemented in the damage detection algorithm. With the correct modulus of elasticity, the correct wave speed will be used, and the calculations will locate the damage correctly.

2.4 Conclusions

Variations in temperature have theoretically been shown to potentially influence the damage location calculated from the wave propagation approach used to supplement the impedance method. The wave speed is a function of Young's Modulus, which deteriorates with increasing temperature. If the wave speed is not recalculated after a change in structural temperature, the determined damage location may not be an accurate indication of the true damage location.

Of greatest concern would be not recalculating the wave speed after introducing a system into high temperatures. The modulus of elasticity varies most at high temperatures, above 200 degrees Celsius, and simulation has shown that the error in the calculated damage location is also

most influenced at these temperatures. However, if the wave speed is not recalculated, the temperature corrected modulus of elasticity can be found with the determined equation as long as the temperature is known. With the modulus of elasticity correct, the wave speed will also be right.

Another concern would be larger structures with sensors placed too far apart. Larger structures will be more susceptible to temperature variations than smaller structures. However, if a damage location of within a few centimeters is acceptable, then no correction may need to be made for temperatures less than 200 degrees Celsius.

Future work will consist of placing a real structure in a temperature controlled environment to verify the results of this simulation. Due to the difficulty of producing a longitudinal wave with the PZT patches, Lamb waves might be used to generate pulses. Further testing may introduce other factors such as different boundary conditions and more complex structures.

Chapter 3

Detecting Matrix Cracking in Composites

3.1 Introduction

In the previous chapter, wave propagation is utilized to add robustness to the impedance method for structural health monitoring. The concept of the impedance method is introduced, but Chapter 2 only deals with how temperature influences wave propagation and methods to correct these temperature variations. In this chapter and the following chapter, the impedance method is used by itself to detect damage. Specifically, the amount of damage in composite test samples is quantified using impedance-based structural health monitoring.

The ability to detect transverse matrix cracking in composites can be very helpful in many applications where composites are used. In a $[0_m/90_n]_s$ setup, there are m layers of laminate with fibers aligned in a uniform direction of the outside, and n layers of laminate perpendicular on the inside. The total lay-up is symmetric (denoted by s), so there are n more layers of $90°$ in the middle, and m more layers of $0°$ on the other side. If a tensional load is applied along the fiber direction of the $0°$ layers, the first sign of the composite failing will be cracks in the $90°$ layers (Hyer, 1998). These cracks will appear parallel to the fibers in the $90°$ direction. The presence of these cracks causes larger stresses in the $0°$ due to stress concentrations. The stress concentrations and larger stresses lead the laminate failing in the $0°$ direction at a lower load than

would occur if the 90° layers were not present (Hyer, 1998). The same type of cracking has also been shown to occur with fatigue as well (Kander, 1991). Thus, detecting matrix cracking can be essential to verifying the condition of a structure.

Many methods have been implemented in an attempt to detect transverse matrix cracking. Some of these methods include microscopy, edge replication, X-ray techniques using a dye penetrant, backscatter ultrasonics, and acoustic emissions (Kander, 1991, Prosser et al., 1995, and Subramanian et al., 1994). However, these techniques, with the exception of acoustic emissions, are not useful for in situ monitoring of a structure (Prosser et al., 1995). Even during testing, specimens must be taken out of loading conditions to detect cracking. Using penetrant to perform an X-ray will cause permanent damage to the composite, making further testing impossible. Therefore, a reliable method of detecting matrix cracking, whether a sample is being tested in the laboratory, or a real world structure is being used, needs to be able to detect cracking without disrupting the test or normal use.

The impedance method for structural health monitoring utilizes PZT patches as self-sensing actuators, as described in the introduction to Chapter 2 (Park et al., 2003). When the PZT is mounted on a structure, it can be used to actuate a structure at high frequencies. Since the PZT is bonded to the structure, it can be shown that the mechanical impedance of the structure is correlated with the electrical impedance of the PZT (Liang, et. al., 1994). Thus, any change in the mechanical impedance, which could be caused by damage to the structure, will show up in the electrical impedance. Using impedance as a method of detecting damage has been shown effective for many types of structures (Park et al., 2003). Early testing has shown the impedance method to already be useful in structures where composites are commonly used, such as aerospace applications (Chaudhry et al., 1995).

As previously mentioned, acoustic emissions have been used to detect matrix cracking. Specifically, Prosser et al. performed acoustic emissions tests of graphite/epoxy composites with a $[0_m/90_m]_s$ stacking sequence where *m* ranged from 1 to 6 (Prosser et al., 1995). The results of the experiment showed an exact correlation between signals observed with acoustic emissions and actual matrix cracking for samples were *m* is greater that 2 (Prosser et al., 1995). However, for samples where *m* was less than 2, cracking was not always successfully detected (Prosser et al., 1995).

In this chapter, an initial experiment to determine whether or not the impedance-based structural health monitoring method could be used to detect transverse matrix cracking in thin, or cross-ply specimens with only four layers, is described. Composites are fabricated and prepared for testing. Test coupons are loaded in tension to specific values, and impedance testing, utilizing PZT bonded to the coupons, is performed before and after loading. The impedance signatures are then analyzed to show that matrix cracking can be detected using the impedance-based structural health monitoring method. The same method is then used to perform damage detection on a thicker cross-ply composite.

3.2 Test Setup and Experimentation

The material used in this study is Narmco/BASF 5245C/G40/600, which is a prepreg with unidirectional graphite fiber in a bismaleimide resin. Prepreg sheets of 30.48 cm square are arranged to form a stacking sequence of $[0/90]_s$. With only two $90°$ layers, the laminate is considered thin using the definition set by Prosser, et al. After curing the laminates, the panels are cut into fourths in order to allow tabbing material to be applied. The tabs protect the composite from the tensile testing jaws and provide a good surface for the jaws to grip. With tabbed panels test coupons with a length of 147.9 mm along the $0°$ fiber direction and 25.45 mm wide are cut. The samples are 1.29 mm thick. PZT patches are mounted to the composite coupons allowing impedance measurements to be taken. A sample coupon can be seen in Figure 3.1.

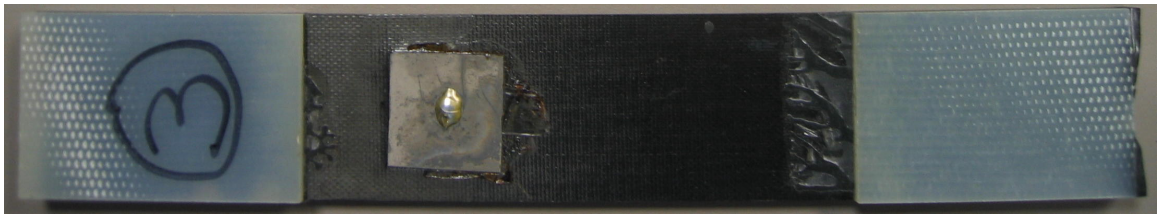

Figure 3.1: Sample 3 is shown after the tensile testing is completed. The leads to the PZT have been removed.

To induce transverse matrix cracking in the specimens, a quasi-static tensile test is performed. Different samples are subjected to different loads using an Instron machine with a 50 kN load cell. The different loading conditions allow a different number of cracks to form in each coupon. The loading is stroke controlled at a rate of 1 mm per minute.

Before each sample is loaded, and out of the Instron machine jaws, two baseline impedance measurements are taken with an HP 4192A impedance analyzer. Two more impedance measurements are acquired after the samples are loaded, again out of the grips. Impedance frequency ranges of 10-20 kHz and 40-60 kHz are chosen to take measurements over. Generally, there are a large number of peaks in these frequency ranges to compare the before and after loading condition impedance curves. A sample impedance measurement can be seen in Figure 3.2.

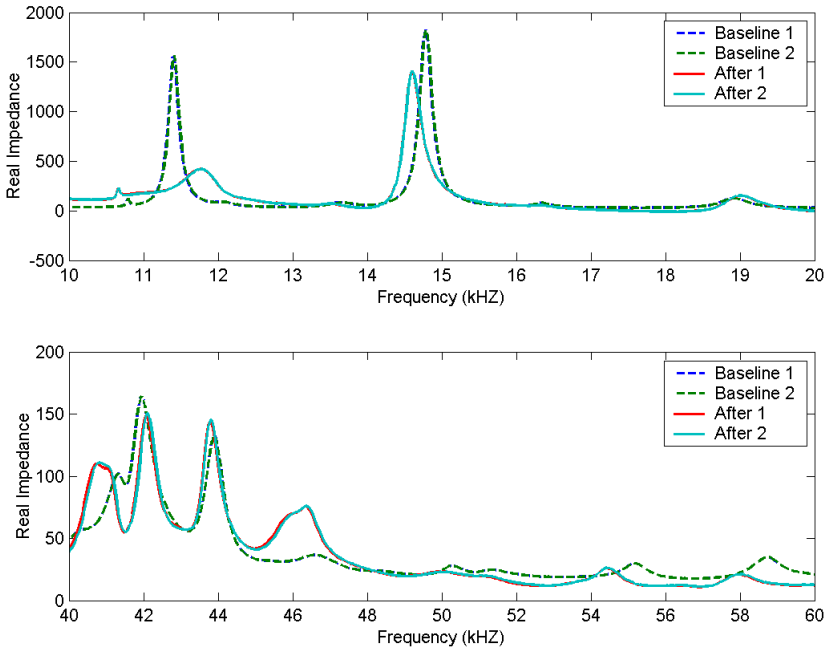

Figure 3.2: The real impedance measurements versus frequency are shown for Sample 6. The top plot shows the 10-20 kHz frequency range, and the bottom plot shows 40-60 kHz.

As seen in Figure 3.2, the impedance signature after the sample has been loaded is significantly different from the baseline. These changes are what will be used to determine how much damage, seen in cracking, is present in the sample. It should be noted that these curves have been normalized in the vertical direction to reduce the effect of drift or other variations. Also, the lengths of specimens were measured before and after loading, and no residual strain was noticeable. The stress-strain curve for a sample composite specimen is shown in Figure 3.3.

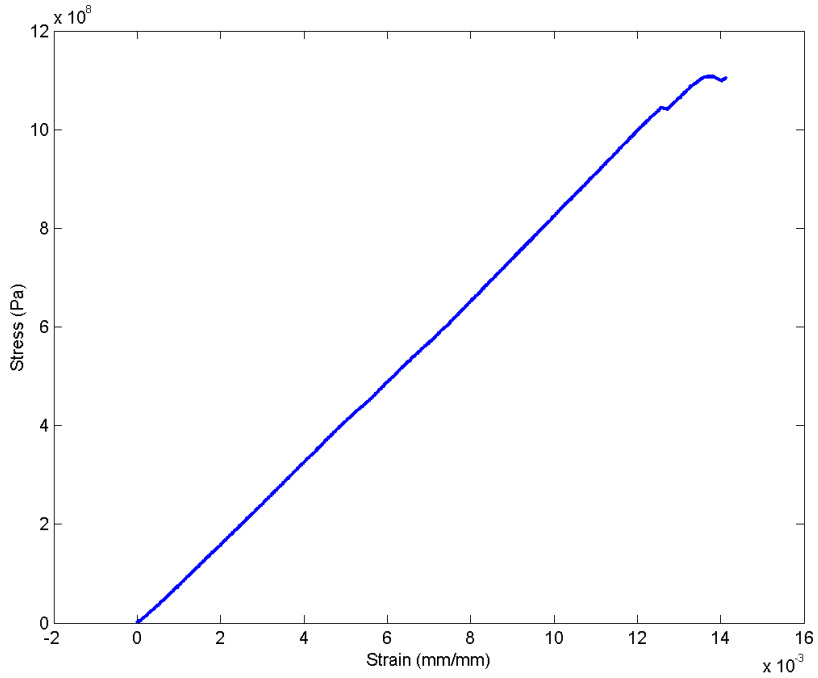

Figure 3.3: The stress-strain curve for a $[0/90]_s$ sample. The curve is typical for a symmetric cross-ply composite.

The strain before failure looks fairly elastic, as Figure 3.3 reveals. Elastic deformations would account for the lack of any residual strain in specimens. The shifting of the curve near 0.012 mm/mm strain is due to large accumulations of fiber fracture.

3.3 Analysis

After each sample is tested, they are soaked in a dye penetrant and X-rayed. The penetrant soaks into the cracks, allowing the cracks to appear in the X-rays. The X-ray is used as verification for the number of cracks present. The length of the sample in between the tabs is 7.54 cm. To get a standard for the damage in a sample, the total number of cracks in between tabs are counted, and divided by the length to get cracks per centimeter. An enlarged view of an X-ray showing cracking can be seen in Figure 3.4.

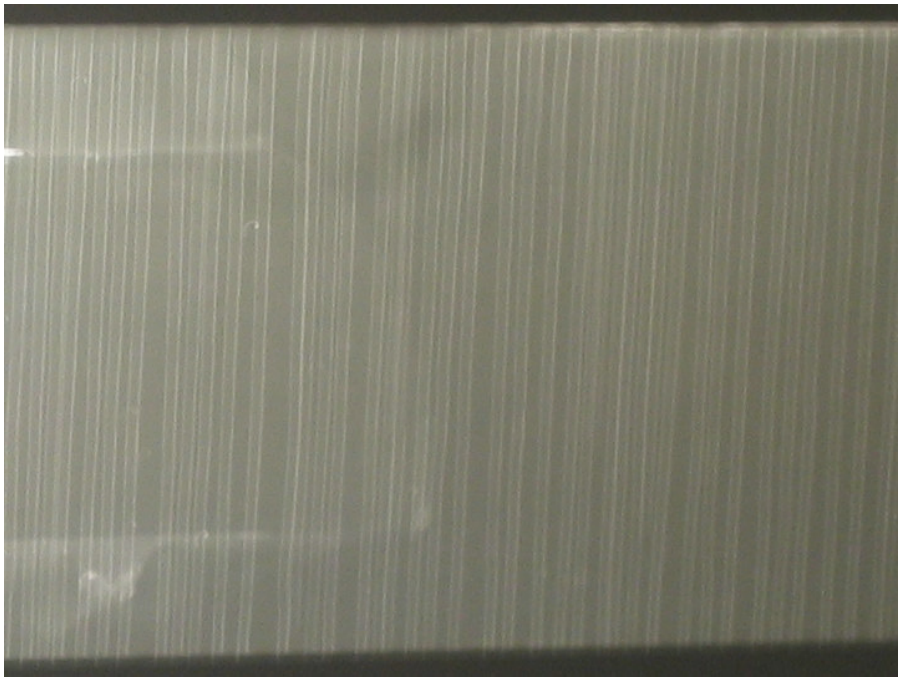

Figure 3.4. An enlarged X-ray shows the cracks for a portion of one of the samples. The total number of cracks are counted to get a value of cracks per centimeter.

Now that the actual damage for each sample is known, the impedance curves can be analyzed to determine how much damage was observed using structural health monitoring. In order to determine the amount of damage, some sort of damage metric must be implemented. A damage metric gives a standard interpretation of the difference between two impedance curves. For these test, a simple variation Root Mean Square Deviation (RMSD) is applied. The RMSD compares individual peaks to see how much they changed. The RMSD method for finding the damage metric, M, can be described as

$$M = \sqrt{\sum_{i=1}^{n} \frac{[\mathrm{Re}(Z_{i,1}) - \mathrm{Re}(Z_{i,2})]^2}{[\mathrm{Re}(Z_{i,1})]^2}}, \tag{3.1}$$

where $Z_{i,1}$ is the baseline, or healthy, impedance of the PZT, and $Z_{i,2}$ is the impedance used for comparison with the baseline measurement at frequency interval i. For the RMSD, the higher the damage metric value, the more difference there is between the baseline impedance signature and the impedance signature indicating damage. More complicated damage metric algorithms are available which take into account temperature and other variables, but for this initial experiment, temperature is assumed to remain constant during testing in a laboratory environment (Park et al., 2003). A brief discussion of different statistical damage algorithms can be found in Section 4.4.

Appling the RMSD to the impedance curves for each sample, damage metrics for each specimen are calculated. The damage metrics are normalized with the damage metric for the sample that is loaded to 20 kN. A bar chart that compares the baselines to the damaged signatures can be used to show the damage metrics graphically. The resulting plot can be seen in Figure 3.5.

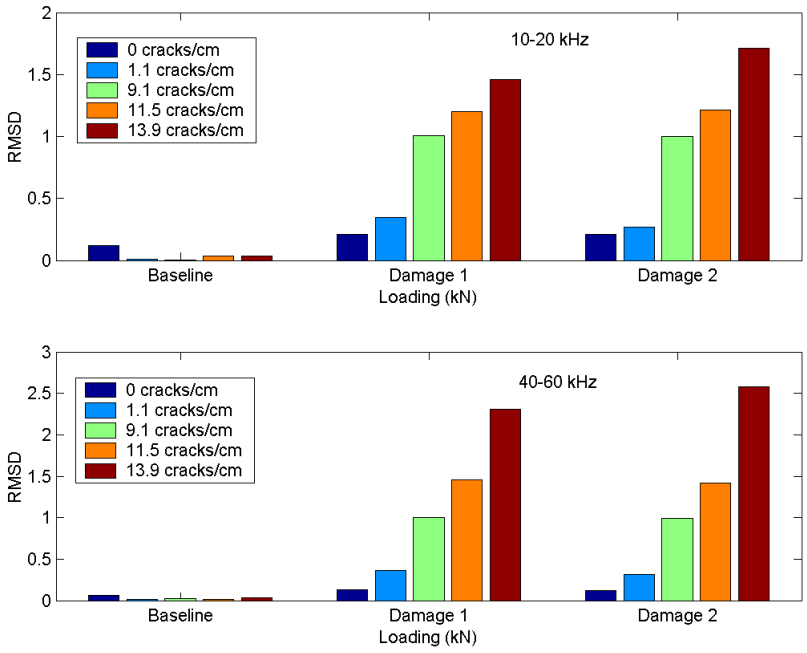

Figure 3.5: The Root Mean Square Deviation, normalized to the sample with a 20 kN load, is shown and compared to the cracks per centimeter. The top plot shows the 10-20 kHz frequency range, while the bottom plot shows the 40-60 kHz frequency range.

The first group of bars compares the baselines with each other. The next two groups compare both damage readings with the baseline. As Figure 3.5 shows, the damage metric increases as the cracks per centimeter increase. Knowing both the damage metric and the crack per centimeter values, a plot of RMSD damage metrics versus cracks per centimeter can be created, and is shown in Figure 3.6.

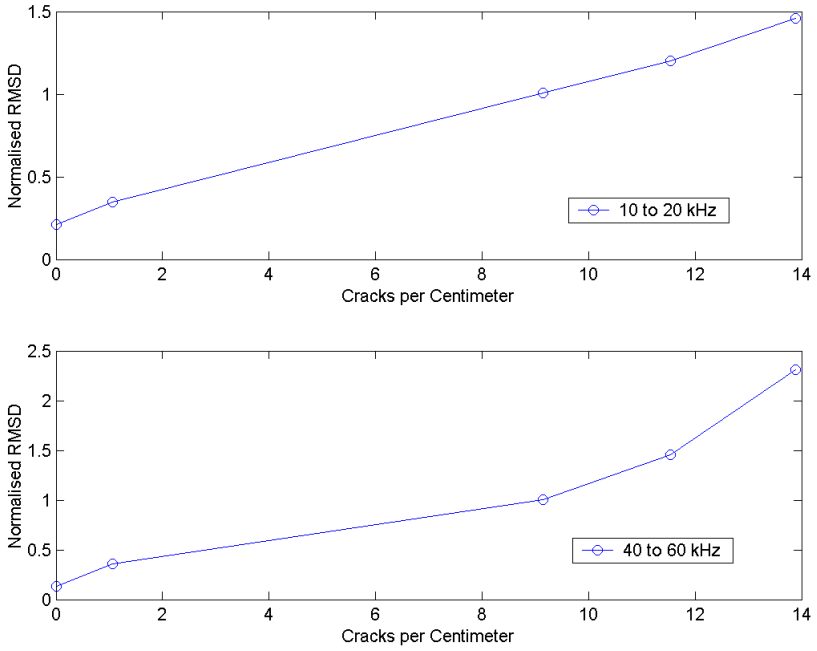

Figure 3.6: Root Mean Square Deviation, normalized to the sample with a 20 kN load, is shown versus the cracks per centimeter. The top plot shows the 10-20 kHz frequency range, while the bottom plot shows the 40-60 kHz frequency range.

Figure 3.6 shows an almost linear correlation between the damage detected using impedance-based structural health monitoring and the actual number of cracks per centimeter. This linear correlation is especially true in the 10-20 kHz frequency range. A linear correlation between the actual damage and the damage metric can be very useful. With a linear correlation, a threshold of what amount of damage is acceptable can be set fairly easily. In normal use of many structures, the user should not have to worry about the damage metric suddenly jumping up to unacceptable levels.

Table 3.1 summarizes the load applied and damage incurred for each sample, along with the damage metric for each frequency range. The number of cracks correlates well with the applied load. The same correlation can be found between the damage metric and the number of cracks, which is ultimately the relationship of interest.

Table 3.1: A summary of the damage for each sample is summarized and displayed in increasing order of load.

Sample	Load (kN)	Cracks/cm	Damage Metric 10-20 kHz	Damage Metric 40-60 kHz
7	5	0	4.2	0.7
3	10	1.1	6.9	2.0
4	20	9.1	20.2	5.5
6	25	11.5	24.0	7.9
8	30	13.9	29.1	12.6

Similar testing with glass-reinforced composites has shown that the same matrix cracking is formed with cyclic fatigue as with quasi-static testing (Kander, 1991). Assuming the same relationship between quasi-static and fatigue testing is true for graphite-reinforced composites, the results shown here should be the same for cracks formed during cyclic testing. Many structures undergo cyclic loading, so being able to detect matrix cracking could prove to be very helpful.

3.4 Detecting Matrix Cracking in Thicker Specimens

Now that the impedance method has been shown to detect matrix cracking in thinner cross-ply specimens, the same technique is applied to a composite with more layers. For the thicker specimen, a stacking sequence of $[0/90_2]_s$ is used. Acoustic emissions were able to detect cracking in a laminate with the same lay-up and a similar material (Prosser et al., 1995). The impedance method should detect matrix cracking with this stacking sequence as was shown with a thinner stacking sequence. Impedance measurements are taken with a HP 4192A impedance analyzer in the ranges of 40-60 kHz and 90-110 kHz. The bar chart for the stacking sequence of $[0/90_2]_s$ used to generate matrix cracks can be seen in Figure 3.7.

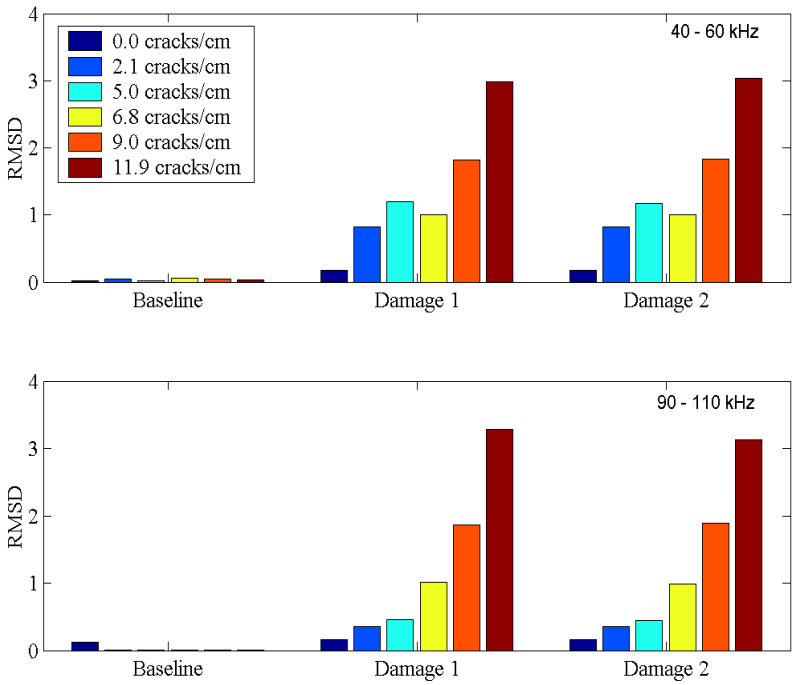

Figure 3.7. The RMSD, normalized to the 20 kN load sample, is plotted for the $[0/90_2]_s$ stacking sequence and compared to the cracks per centimeter. The top plot shows the 40-60 kHz frequency range and the bottom shows 90-110 kHz.

As with Figure 3.5, the first group of bars in Figure 3.7 shows the two baseline measurements compared with each other. Comparing the baselines gives an estimate of the variability in the measurements. The other two groups of bars compare the impedance measurements taken after loading to the baseline. With an increase of the number of cracks per centimeter, the RMSD increases accordingly.

As Figure 3.7 shows, the impedance method successfully detects damage in specimens with various amounts of transverse matrix cracking. In a real world structure, a threshold level can be set based on the acceptable amount of damage that can be accumulated before the integrity of the structure is compromised. Table 3.2 summarizes the applied load and induced damage for each sample.

Table 3.2: The loading, cracks per centimeter and damage metrics (normalized to sample 7) are shown for the $[0/90_2]_s$ samples.

Sample	Load (kN)	Cracks/cm	Damage Metric 40-60 kHz	Damage Metric 90-110 kHz
3	5	0	0.17	0.16
8	10	2.1	0.82	0.36
1	15	5.0	1.17	0.45
7	20	6.8	1.00	1.00
6	25	9.0	1.82	1.89
4	35	11.9	3.04	3.13

The number of cracks shown in Table 3.2 is proportional to the applied load. There is also a strong relationship between the damage metric and the number of cracks per centimeter, which is ultimately the relationship of interest. One bad correlation is seen in the 40-60 kHz range of sample 7, which has 6.8 cracks per centimeter. The damage metric for sample seven is lower than the damage metric for sample 1, which has 5.0 cracks per centimeter. This disparity can be explained by not having an optimized frequency range for each sample. If a large peak shifts out the chosen range after loading, the damage metric may be significantly lowered. Discrepancies such as this are one reason for testing multiple frequency ranges. With multiple frequency ranges, or a frequency range chosen specifically for a certain structure, the ability to accurately detect damage increases.

3.5 Conclusions

In this chapter, an initial attempt at quantifying the amount of damage in graphite/epoxy composites is described. Using the impedance method, an almost linear correlation between the damage metric and actual amount of damage, matrix cracking in this case, is shown. The impedance method is shown to be more sensitive to damage in thin composite lay ups than previous studies utilizing acoustic emissions.

Thicker specimens, where acoustic emissions were able to sense matrix cracking, are also tested. Again, the results are very promising. As the amount of cracks in a specimen increases, the damage metric also increases. Utilizing the relationship between the amount of damage in the sample and the determined damage metric, an acceptable threshold level can be set. A damage threshold level can give an early warning alert to the operator of a structure and possibly avert a failure or operational costs.

Each specimen has a different impedance signature. As some of the results presented here revealed, the same frequency range does not always work for each sample. For experimental setup in a laboratory, it is not practical to determine a specific frequency range with centered peaks for each sample. However, in a real world composite structure, the user, or a pre-programmed algorithm, should find an optimal frequency range containing a lot of structural content to perform health monitoring. An optimal impedance signature will allow for less variability in the detection of damage to the structure.

Damage detection with impedance-based SHM continues in the next chapter. The same methods of testing and analysis are utilized, but the damage mechanism of interest is different. Composites are fabricated with stacking sequences know to delaminate under a tensile load. The correlation between the RMSD and percent area of delamination will then be examined.

Chapter 4

Detecting Delaminations in Composites

4.1 Introduction

The inclusion of composites in many of today's products is becoming increasingly common. However, many industries have concerns over the fatigue reliability of composite materials. For this reason, the ability to detect various kinds of damage in composites should be useful in convincing companies to incorporate the benefits of using composites in appropriate applications. Designers should then be less concerned with the uncertainty of composite material failure. A structural health monitoring system would allow for real-time testing of composite structures.

Graphite-fiber reinforced materials are often used by stacking multiple layers on top of each other at different orientation angles to form a laminate (Hyer, 1998). With certain stacking sequences, the laminates will tend to come apart in the thickness direction with applied loads (Hyer, 1998). This phenomenon is referred to as delamination. Obviously, the presence of delaminations may adversely affect the performance of the composite. Delaminations may lower the stiffness and strength of the composite (Diaz Valdes et al., 1999). As with matrix cracking, many different methods, including the addition of modal characteristics and fiber optics, have been utilized to detect composite delaminations (Diaz Valdes et al., 1999 and Xu et al., 2003).

In the previous chapter, the ability of the impedance method to detect transverse matrix cracking in thinner cross-ply laminates is experimentally verified. These initial results are promising with regard to the difficulties of acoustic emissions in detecting cracking of similar thin specimens (Prosser et al., 1995). The experimentation with thin cross-ply composites was then successfully extended to thicker specimens. In this chapter, an initial study to detect the onset of edge delamination is described. Composite test coupons are manufactured and prepared for quasi-static tensile loading. Impedance signatures are collected before and after loading, and the resulting data is analyzed to determine whether impedance techniques are suitable to composite damage detection. Radiography is again used to verify the results obtained from impedance-based damage detection. A comparison of different damage metric algorithms is also presented.

4.2 Test Setup and Experimentation

Square composite panels (30.48 cm) are made up of Narmco/BASF 5245C/G40/600, the same prepreg used for matrix cracking detection in Chapter 3. The same methods of curing, cutting, and tabbing the laminates are applied as described in Section 3.2. Testing coupons of length 14.79 cm and width 2.54 cm are the result of this process. In order to facilitate impedance testing, PZT patches are bonded to the samples. Figure 3.1 shows what a sample test coupon looks like.

Stacking sequences for delamination testing are chosen based upon similar lay-ups that are known to delaminate at low tensile strains (O'Brien et al., 1987). Two different stacking sequences of $[+30/-30/0/90]_s$ and $[+30/0/-30/90]_s$ are fabricated. Impedance signatures are acquired with a HP 4194A impedance analyzer. Frequency ranges of 40-60 kHz, 90-110 kHz and 190-230 kHz are chosen to perform structural health monitoring.

Damage is again induced in each specimen using an Instron machine with a 50 kN load cell by means of tension testing stroke controlled at a rate of 1 mm per minute. Loading each specimen to a different level allows for a different amount of edge delamination to form. The amount of change determined by the impedance method should correlate to the loading of the sample, and therefore the amount of damage actually present. As in Chapter 3, two baseline

impedance measurements and two post loading impedance measurements are taken. Figure 4.1 shows the impedance signatures for all three frequency ranges for sample four.

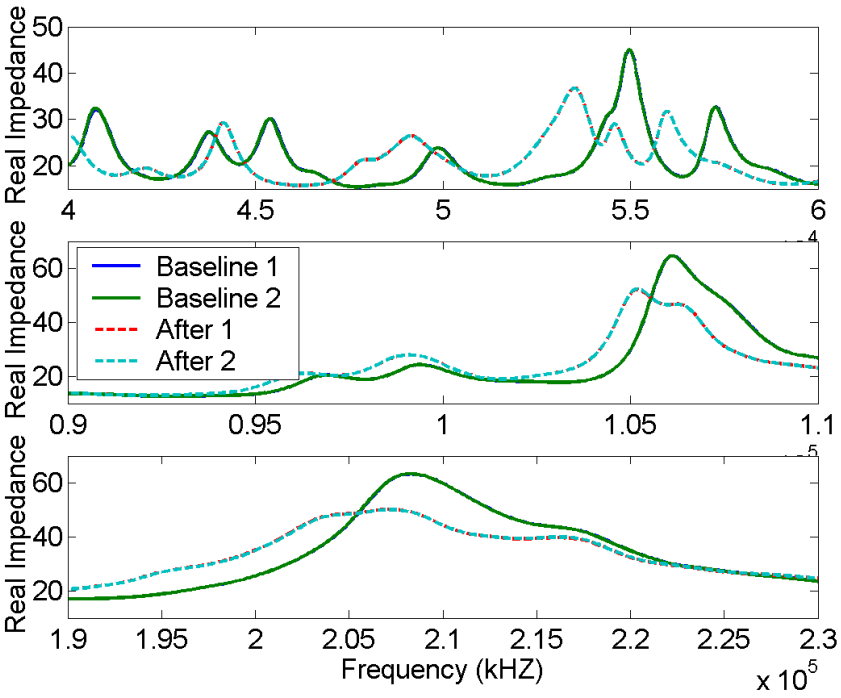

Figure 4.1: Impedance signatures are shown for sample four of the $[+30/0/-30/90]_s$ composite samples, which was loaded to 20 kN.

All three frequency ranges in Figure 4.1 show significant changes between the undamaged and damaged states of the sample. Using a simple statistical algorithm, the changes in these curves will ultimately be used to determine the amount of delamination in the composites. The next section describes the process of extracting features from these curves to obtain damage information.

4.3 Analysis

Just as dye penetrant was used to soak into the matrix cracking in Chapter 3, the penetrant is also used to soak into the delaminated areas of each specimen. With the dye penetrant fully saturated into the delaminated areas, the edge delaminations will show up in an X-ray. Figure 4.2 shows a sample radiograph revealing the delaminated area of a specimen.

Figure 4.2: A sample radiography shows both transverse matrix cracking and areas of edge delamination.

In the case of these specimens, the damage mechanism is edge delamination. The delamination will start at the top and bottom of the specimen shown in Figure 4.2 and spread towards the center of the specimen with further loading. The area of delamination is determined by thresholding the X-ray using image processing software. The delaminations are quantified by determining the total area out of the exposed area that is delaminated.

With the exact amount of damage known for each specimen, the impedance signatures are analyzed to find how much change is noticed using structural health monitoring. The RMSD compares the individual peaks of each curve and quantifies how much subsequent readings differ from the baseline reading (Park et al., 2003). The RMSD damage metric, M, used for quantifying delaminations can be described as

$$M = \sum_{i=1}^{n} \sqrt{\frac{[\mathrm{Re}(Z_{i,1}) - \mathrm{Re}(Z_{i,2})]^2}{[\mathrm{Re}(Z_{i,1})]^2}}, \tag{4.1}$$

where $Z_{i,1}$ is the baseline, or healthy, impedance of the PZT and $Z_{i,2}$ is the impedance used for comparison with the baseline measurement at frequency interval i (Park et al., 2003). Larger values of the damage metric indicate larger amounts of damage.

Using the RMSD on each set of curves, the damage metric is generated for each sample. Each damage metric is normalized to the damage metric of the sample loaded to 20 kN. The bar charts displaying the RMSD results are seen in Figures 4.3 and 4.4.

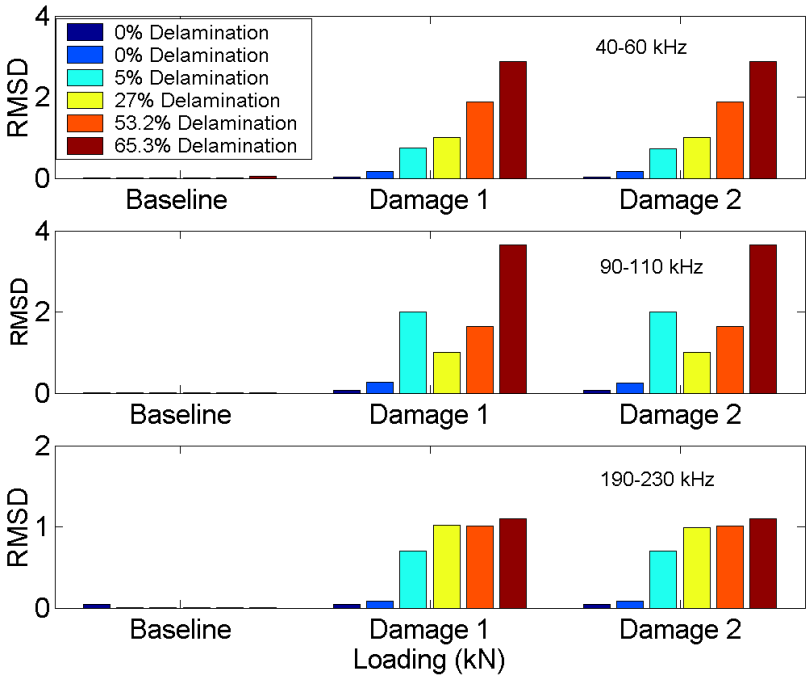

Figure 4.3: The RMSD is shown for each sample and correlated with the delaminated area for the $[+30/-30/0/90]_s$ samples. RMSD values are normalized to the sample with 27% delamination.

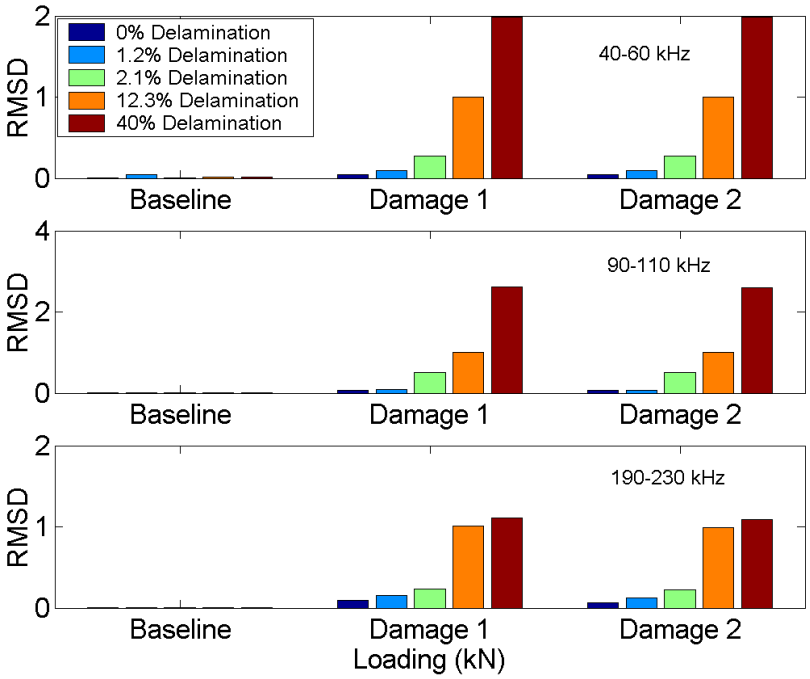

Figure 4.4: The RMSD is shown for each sample and correlated with the delaminated area for the $[+30/0/-30/90]_s$ samples. RMSD values are normalized to the sample with 12.3% delamination.

In both Figure 4.3 and 4.4, the damage metric consistently increases as the area of delamination expands. Results are very similar to those seen in Chapter 3 when the RMSD increased as the amount of matrix cracking increased. Similar to Figures 3.5 and 3.7, the first group of bars compares the two baseline impedance curves. The next two groups of bars compare the curves acquired after loading to the first baseline. Ideally, the damage metric should increase linearly as the delaminated area increases. To determine whether this is true, plots of the damage metric versus the actual damage are generated and shown in Figures 4.5 and 4.6.

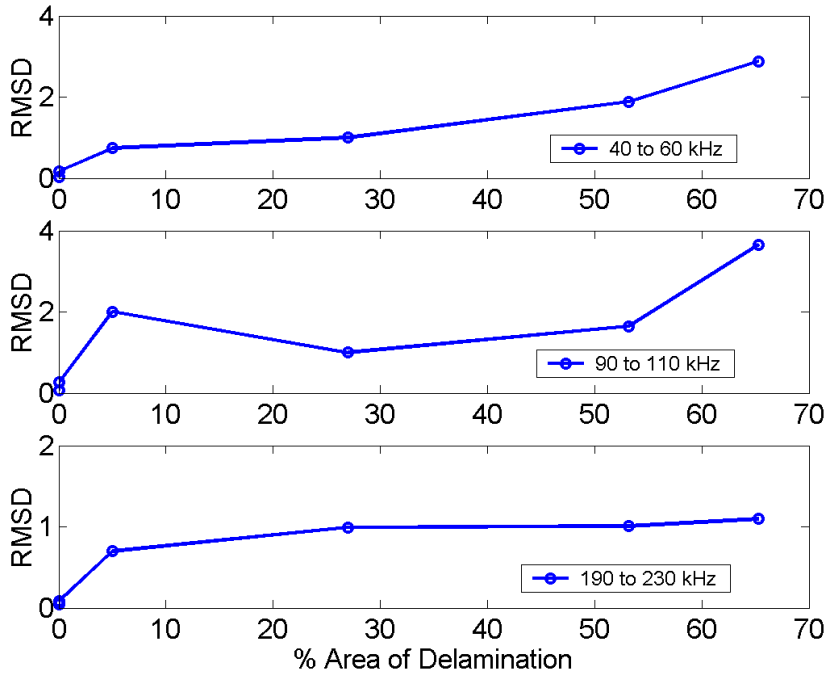

Figure 4.5: The RMSD versus the percent area of delamination curve is shown for each frequency range in the $[+30/-30/0/90]_s$ samples. RMSD values are normalized to the sample with 27% delamination.

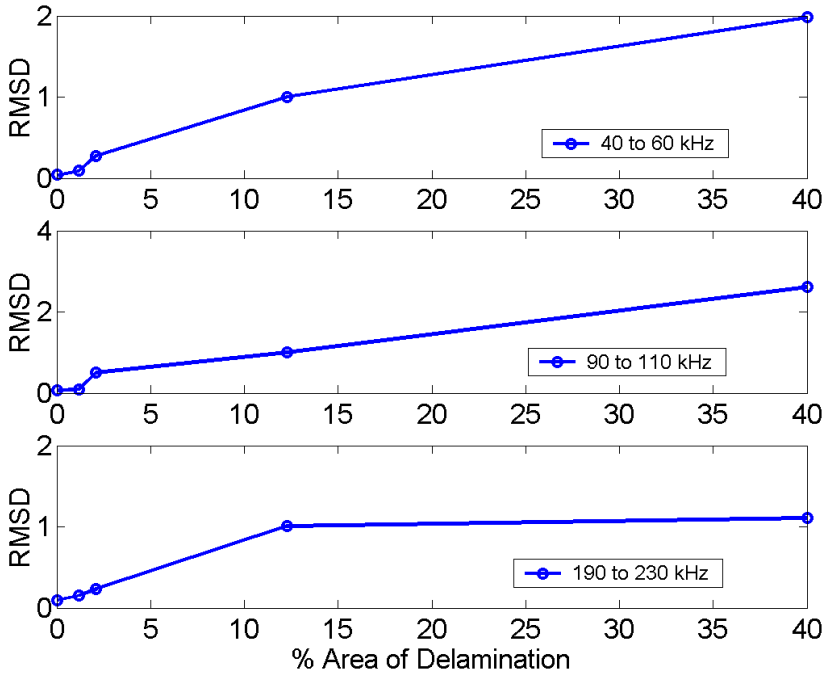

Figure 4.6: The RMSD versus the percent area of delamination curve is shown for each frequency range in the $[+30/0/-30/90]_s$ samples. RMSD values are normalized to the sample with 12.3% delamination.

The 40-60 and 90-110 kHz ranges show more of a linear agreement between the damage metric and the percent of area delaminated. In the 190-230 kHz range, the change indicated by the damage detection algorithm between not having damage and having damage is more abrupt. The higher frequency range reveals damage in a fashion more like a switch, either on (damage) or off (no damage), and the RMSD versus percent delamination plots in Figures 4.5 and 4.6, show more of a constant value when a certain amount of damage is accumulated. In the impedance signatures for these curves, a much larger amount of damping is shown in the peaks (Figure 4.1). The peaks have lower amplitudes, and the resonances are spread out over a larger range of frequencies. As a result, the changes to these curves with damage are much more subtle than in the lower frequency ranges. The RMSD still indicates damage, but not nearly as much in the linear fashion as seen in the lower frequency ranges.

The presence of edge delaminations are detected quite well with the impedance method. Results similar to those seen for detecting matrix cracking are seen with the damage metric increasing as the delaminated area increases. Table 4.1 shows a summary of the results for the $[+30/-30/0/90]_s$ laminate samples.

Table 4.1: The loading, delamination area, and damage metrics (normalized to sample 4) are shown for the $[+30/-30/0/90]_s$ samples.

Sample	Load [kN]	Percent Delaminated [%]	Damage Metric 40-60 kHz	Damage Metric 90-110 kHz	Damage Metric 190-230 kHz
8	5	0	0.04	0.06	0.05
6	10	0	0.17	0.26	0.09
5	15	5.0	0.74	2.00	0.70
4	20	27.0	1.00	1.00	1.00
3	25	53.2	1.89	1.65	1.01
2	30	65.3	2.87	3.66	1.10

A deviation from the expected results can be seen in the 90-110 kHz range of sample 5. In this case, the damage metric is larger than what would normally be expected. The rest of the values correlate very well to the amount of delamination present in the samples. Results for the $[+30/0/-30/90]_s$ laminate are displayed in Table 4.2.

Table 4.2: The loading, delamination area and damage metrics (normalized to sample 4) are shown for the $[+30/0/-30/90]_s$ samples.

Sample	Load [kN]	Percent Delaminated [%]	Damage Metric 40-60 kHz	Damage Metric 90-110 kHz	Damage Metric 190-230 kHz
7	5	0	0.04	0.06	0.10
6	10	1.2	0.09	0.09	0.15
5	15	2.1	0.28	0.51	0.23
4	20	12.3	1.00	1.00	1.00
3	25	40.0	1.98	2.61	1.11

Damage metrics correspond very well to the delaminations for the $[+30/0/-30/90]_s$ test coupons. With good damage detection sensitivity, structures can be closely monitored for any changes which may occur as a result of use. The next section describes some of the difference between various damage metrics.

4.4 A Comparison of Damage Metrics

In Chapter 3, a modified version of the RMSD is used for feature extraction to quantify the extent of matrix cracking. Equation 3.1 is based on the standard definition of the root mean square deviation described as

$$M = \sqrt{\sum_{i=1}^{N} \frac{(Z_{i,1} - Z_{i,2})^2}{N}}, \tag{4.2}$$

where $Z_{i,1}$ is again the baseline impedance of the PZT, and $Z_{i,2}$ is the impedance used for comparison with the baseline measurement at frequency interval i for N amount of frequency intervals. In the standard RMSD definition, the results are scaled by the number of points, whereas Equation 3.1 is scaled by the baseline.

Delaminations are measured in this chapter using the RMSD damage metric of Equation 4.1 defined by Park et al. (2003). This statistical algorithm is based on the Relative Deviation (RD) statistical algorithm first introduced by Sun et al. (1995). The RD comparison is defined as

$$RD_i = \frac{\sum_{j=1}^{N} (\mathrm{Re}(Y^1{}_{ij}) - \mathrm{Re}(Y^0{}_{ij}))^2}{\sum_{j=1}^{N} (\mathrm{Re}(Y^1{}_{1j}) - \mathrm{Re}(Y^0{}_{1j}))^2}, \tag{4.3}$$

where $Y^1{}_{ij}$ and $Y^0{}_{ij}$ are the admittance (inverse of impedance) of the PZT at frequency interval j after and before the i th connector at any node in a truss structure is loosened. $Y^1{}_{1j}$ and $Y^0{}_{1j}$ are described as the admittance after and before connector 1 at node A in the structure is loosened. At connector 1 of node A, the RD will always be one. As connectors at different nodes are loosened, the RD is expected to be less than one due to the increase of distance, yielding a damage metric scaled between zero and one (Sun et al., 1995).

Another scalar damage metric commonly used is simply the sum of the squared differences between the real impedance signatures (Peairs et al., 2004). This damage metric does not utilize any scaling and is implemented with the equation

$$M = [\mathrm{Re}(Z_{i,1}) - \mathrm{Re}(Z_{i,2})]^2. \tag{4.4}$$

The variables are the same as in Equations 4.1 and 4.2.

A damage metric based upon the cross correlation was first implemented by Raju et al. (1998). The expression for the correlation coefficient, ρ, between two impedance signatures can be described as

$$\rho = \frac{1}{n-1} \frac{\sum_{i=1}^{n} \left(\mathrm{Re}(Z_{i,1}) - \mathrm{Re}(\bar{Z}_1)\right)\left(\mathrm{Re}(Z_{i,2}) - \mathrm{Re}(\bar{Z}_2)\right)}{s_{Z_1} s_{Z_2}} , \tag{4.5}$$

where $Z_{i,1}$ and $Z_{i,2}$ are again baseline and damaged impedance curves, $\bar{Z}_1$ and $\bar{Z}_2$ are the means of the two signals, and s_{Z_1} and s_{Z_2} are the standard deviations of each signal (Rutherford, et al., 2004). To yield damage metrics with higher values indicating higher amounts of damage, the quantitly (1 – abs(ρ)) is used for the correlation coefficient algorithm. With impedance curves which look very similar, a higher correlation coefficient should be obtained, indicating (with one minus the correlation coefficient) a low amount of damage.

Zagrai and Giurgiutiu (2001) compared several damage metric algorithms including RMSD, mean absolute percentage deviation, covariance change, and correlation coefficient deviation. For thin plate structures, the third power of the correlation coefficient deviation $(1 - R^2)^3$, was found to be the most consistent metric in detecting cracking.

In any of the described algorithms, the results of the equations yield similar results. The trend for each damage metric equation is the same; the resulting values increase for an accumulating amount of damage to the structure. The following figure shows the results of using four of the above described damage metrics on the same group of data.

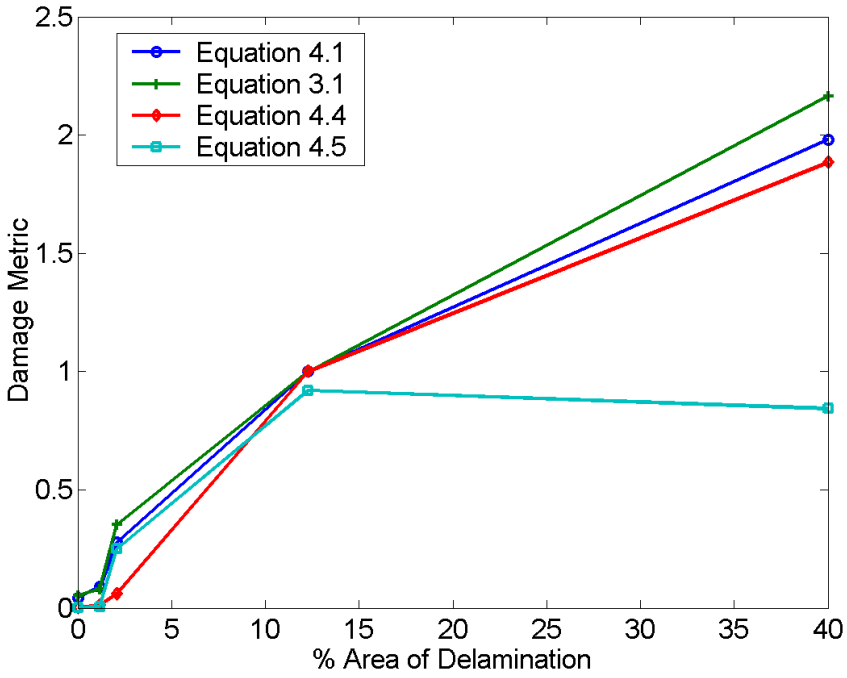

Figure 4.7: The results using four different damage metric algorithms are shown for the 40-60 kHz range of the $[+30/0/-30/90]_s$ composite samples. Note that the damage metric values of Equations 4.1, 3.1, and 4.4 are normalized to the value from the sample loaded to 20 kN.

As Figure 4.7 shows, each of the damage metrics follows the same general trend. The correlation coefficient damage metric described in Equation 4.5 shows a slight variation when the value decreases for an increasing amount of damage from 12.3 percent to 40 percent area of delamination. The rest of the correlation coefficient curve follows both of the RMSD variation algorithms (Equations 3.1 and 4.1) very well. In each of the metrics, minus the last value of the correlation coefficient curve, the damage metric versus delamination curve is fairly linear. Using any of the algorithms, the operator of a SHM system on a structure will be able so set a threshold damage limit. In order to see each of the correlation coefficient values with the rest of the curves, the other damage metric values are normalized to the value obtained at 12.3 percent delamination. The actual non-normalized numbers for each of the algorithms can be seen in Table 4.3.

Table 4.3: The results using four different damage metric algorithms are shown for the 40-60 kHz range of the $[+30/0/-30/90]_s$ composite samples.

Sample	Percent Delaminated [%]	Equation 4.1	Equation 3.1	Equation 4.4	Equation 4.5
7	0	4.28	0.38	55.71	0.00
6	1.2	9.08	0.52	256.22	0.01
5	2.1	27.47	2.26	1255.80	0.25
4	12.3	99.18	6.40	20,596.00	0.92
3	40.0	196.49	13.84	38,801.00	0.84

As Table 4.3 shows, the numbers generated for each of the damage metrics compared can vary quite a bit from one to another. However, the general trend stays the same; when the amount of damage is increased in the sample, the damage metric will increase to indicate this damage. In many cases, there is an almost linear correlation between the damage metric value and the actual amount of damage seen in the specimen.

4.5 Conclusions

This testing has successfully monitored damage in graphite/epoxy composites with stacking sequences arranged to delaminate under tensile loading. Composite specimens with two different lay-ups are fabricated, and in both cases, the presence and quantity of damage are readily identified. Comparing the damage metric to the actual amount of damage, lower frequency ranges of 40-60 kHz and 90-110 kHz the metric increases in an almost linear fashion with respect to the area of the composite that is delaminated. The higher 190-230 kHz range is also effective in detecting damage, but damage metric tends to increase and then stay at a relatively constant value (increasing only slightly with more delamination) in the presence of damage.

In the implementation of impedance-based SHM, many different statistical based damage detection algorithms have been used. Several of these damage metrics are defined in this chapter and the previous chapter. Each algorithm will generate a different value for the same amount of damage on a structure. However, the general trends for each of these metrics remain the same; as the accumulated amount of damage increases, the damage metric value will increase. An acceptable damage level can be used as a threshold warning level when using any of the described damage metrics.

Future work will continue to expand testing of various composite lay-ups that will produce different damage mechanisms under tensile loading. Efforts will also be made to expand the number of samples used for each test. With increased amounts of data, confidence intervals can begin to be defined. A reliability analysis can also be performed in the presence of different types of uncertainty.

Chapter 5

Developing a Wireless System for Impedance-based SHM

5.1 Introduction to MASSpatch Project

Many investigations have been performed into the use of remotely operated wireless-based systems to perform structural health monitoring (Spencer Jr. et al., 2004). However, a large number of these projects are focused on civil structural applications. Certainly, no system has been developed which uses the impedance method as a means of detecting damage.

The Center for Intelligent Material Systems and Structurs (CIMSS) at Virginia Polytechnic Institute and State University saw an opportunity to develop such a wireless system for use on existing aerospace structures. The MEMS-Augmented Structural Sensor (MASSpatch) for is a joint effort between Virginia Tech, Extreme Diagnostics, and The Air Force Office of Scientific Research. A complete MASSpatch system should incorporate the use of piezoelectric based Macro-Fiber Composite (MFC) sensors and actuators, compute all impedance-based SHM on an inexpensive chip-sized computer, be self powered with the utilization of piezoelectric-based power harvesting, and communicate by means of wireless telemetry.

5.2 MASSpatch Hardware Development

MASSpatch is an attempt to miniaturize the equipment needed to perform impedance based SHM. The final goal is to develop a sensor which can be permanently attached to a structure and provide meaningful information regarding the structure's integrity. The sensor will utilize energy from the ambient environment, excite its host structure with a high-frequency excitation, analyze the results, and wirelessly provide the status of the structure to an end user. The following sections will describe the development of a MASSpatch prototype to perform impedance-based SHM.

5.2.1 Low Cost Impedance Method

A major goal of the MASSpatch project is to develop a small, inexpensive impedance analyzer that can be deployed in the field. With these restrictions, normal methods of measuring impedance cannot be used. Peairs et al. (2004b) developed a low-cost impedance method to get around the requirements of using traditional impedance measuring techniques (Peairs et al., 2004b). Using the low cost method requires only a sensing circuit, shown in Figure 8, and an FFT analyzer.

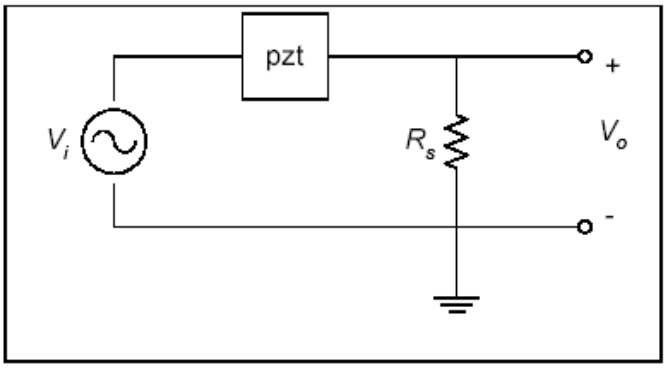

Figure 5.1: The low cost circuit for approximating impedance (Peairs et al., 2004b).

As seen in Figure 8, the circuit is simply a voltage divider. The output voltage across the sensing resistor is proportional to the current through the resistor. With small resistance, this current is close to the current through the piezoelectric device, as though the circuit were not there. With the current known, the impedance can be determined.

The MASSpatch project takes this concept one step further. FFT analyzers can still be expensive, bulky, and require a lot of power. Instead of using a FFT analyzer, a single chip could carry out the data acquisition, process the data with an FFT algorithm, perform a damage metric, and wirelessly alert the user if damage as occurred. A chip-sized processor could be small enough to permanently leave on a structure and be inexpensive compared to traditional impedance measurements.

5.2.2 MASSpatch Components

To implement the impedance-based SHM method, the hardware shown in Figure 5.2, and described in the following sections, is assembled and programmed. The low cost impedance method is used to monitor the structure of interest, as previously described. This method provides accurate approximations of the structural impedance without using massive and complex external electronics. Figure 5.2 shows the general components of the initial design used to construct the MASSpatch prototype. Most of the basic impedance method hardware is condensed into a single electronic board.

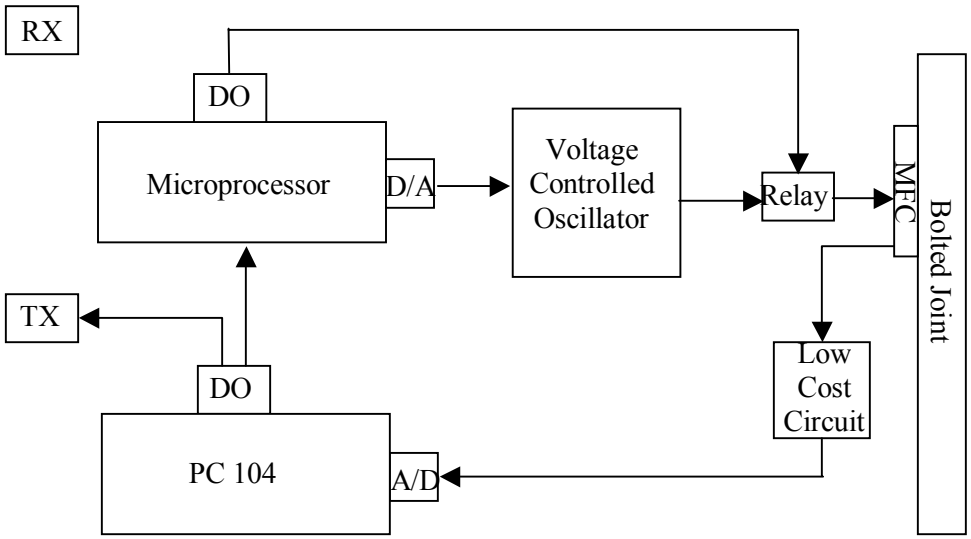

Figure 5.2: The MASSpatch prototype couples PC 104-based computing with the low cost impedance circuitry.

The Figure 5.2 components are all that are needed to use a piezoelectric device bonded to a structure as SHM self-sensing actuators. Descriptions of major components follow. Appendix C presents photographs of each component.

Microprocessor

A PIC16F877 from Microchip (www.microchip.com) is used as the microprocessor. The microprocessor controls the actuator input. Activating the PIC generates and outputs a varying voltage. The microprocessor then shuts down until it is needed again.

Voltage Controlled Oscillator

A voltage controlled oscillator (VCO) acts like a function generator. The VCO generates a frequency when it receives an input voltage. This output frequency changes linearly as the voltage changes. Eventually, an ICL8038 waveform generator from Intersil (www.intersil.com) or some similar component will be used; this device has an output frequency range of 0.001 Hz to 300 kHz. Typically, impedance curves are acquired at frequency intervals from 30 – 400 kHz, so the waveform generator has an output to encompass most of this range.

PC 104 Board

The PC 104 board is the heart of the system and controls all other MASSpatch components. The prototype uses Prometheus, a PC 104 board from Diamond Systems (www.diamondsystems.com). Prometheus comes as an all-inclusive system ready to perform data acquisition. The analog to digital converter operates at a sampling frequency of 100 kHz, which permits impedance measurements on the low range of the impedance frequency range. The A/D converter sampling-rate is split between eight differential analog inputs, so a 50 kHz maximum sampling frequency can be achieved with two channels. All data analysis is done locally on the PC 104 board. A 32 megabyte flash disk is included to load the DOS operating system and save executable and storage files. Attached to the PC 104 board is a 3.5-inch floppy drive used to load executables and download data files.

Wireless Transmitter and Receiver

The wireless transmitter and receiver are the TX and RX shown in Figure C.3 (Appendix C). The transmitter is attached to a digital output of the PC 104 board. The receiver is located across the room and alerts the operator to damage by means of a blinking LED. The current

prototype uses Radiometrix RX2M-458-5 and TX2M-458-5 wireless sensors (www.radiometrix.com).

Several things were discovered while incorporating the microprocessor and voltage controlled oscillator board. The frequency range produced with the existing circuitry is much too low for impedance measurements. Additionally, more voltage (fifteen Volts) was required to achieve the desired amplitude of excitation than the five Volts the PC 104 board supplied. A voltage booster can be implemented to solve the voltage problem. However, the circuitry would have had to be rebuilt to adjust the frequency range. In the current setup, the microprocessor and voltage controlled oscillator are replaced with a function generator. Current efforts are centered on obtaining higher and more adjustable frequency ranges from the board, as well as simplifying and miniaturizing the board. Figure 5.3 shows the existing setup.

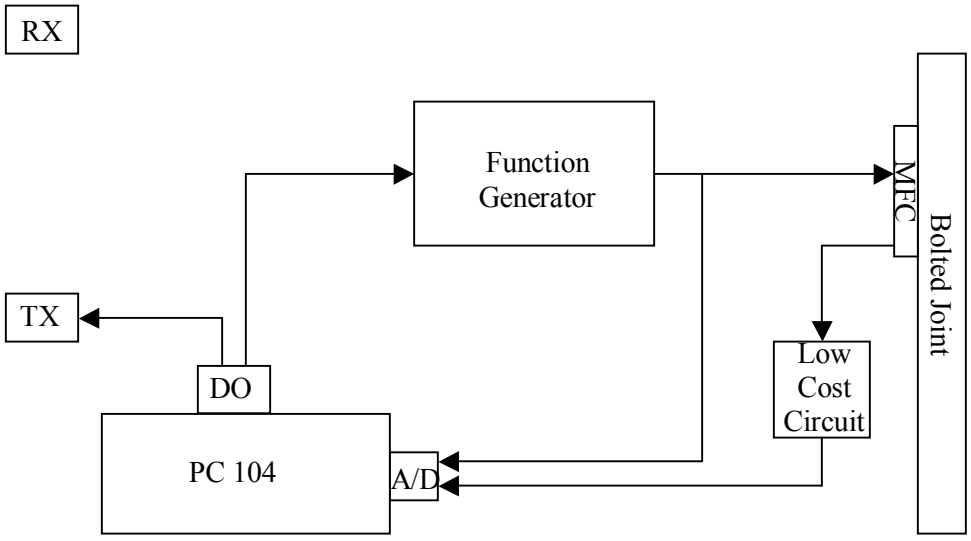

Figure 5.3: The MASSpatch prototype shown with the function generator replacing the voltage-controlled oscillator.

The Figure 5.3 system works in exactly the same manner as the system described in Figure 5.2. The PC 104 board still triggers the function generator, which in this case is a HP 3314A. A signal from the function generator is sent to the MFC and back to the PC 104 board. Table 5.1 summarizes the specifications of the current MASSpatch prototype. Figure 5.4 displays each component in the current configuration.

Table 5.1: Specifications for the current MASSpatch prototype.

Processing/Programming		Sensing/Sampling		Wireless Transmission	
Processor	ZFx86 100 MHz CPU	**ADC**	16 bit	**Usable Range**	over 1 km
Programming Memory	64 Kb (limited by Dos OS)	**Max Sampling Frequency**	100 kHz with interrupts	**Operating Frequencies**	458.5-491.5 MHz 433.05 – 434.79 MHz
Flash Memory	2 MB	**Sensor Types and Ranges**	Analog 8 at up to +10 to -10 V Digital 3.3 or 5 V	**Data Bit Rate**	5 kbps

General	
Power Supply	+5 VDC @ 900 mA
Weight	79 g

Figure 5.4 includes a monitor and keyboard. These are attached to the PC 104 board in order to facilitate easy modification of the executable code. In the next iteration, the PC 104 board will not have extra attachments or the interfaces (top layer of the board) to connect them. Additionally, the bulky function generator will be replaced with improved microcontroller and voltage controlled oscillator electronics. The objective of all of this research is to lay a foundation to produce a single chip which incorporates every component contained in the current prototype. Future work will be discussed further at the end of this chapter.

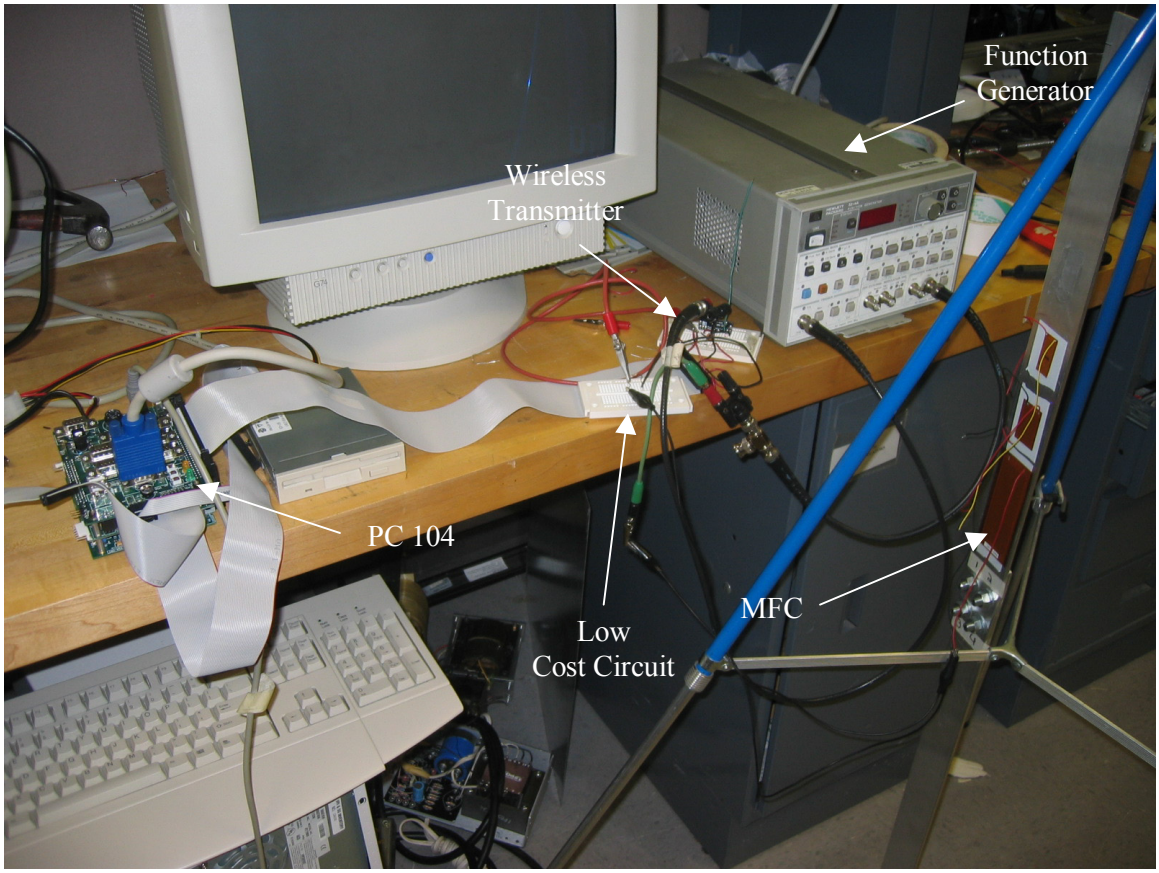

Figure 5.4: The MASSpatch prototype, with individual components labeled.

Power Harvesting

In a permanent setting, MASSpatch will operate off battery power. To minimize battery changes and avoid the demands of a periodic maintenance schedule, MASSpatch uses piezoelectric power harvesting to recharge the system battery. Piezoelectric materials can transform mechanical strain into electrical charge. Therefore, piezoelectrics can harvest energy from an environment's ambient motion and transform mechanical energy into electrical energy. Appropriate power harvesting circuitry can store electrical energy, power other devices, or recharge a battery (Sodano et al., 2003b).

In the MASSpatch prototype, the PC 104 board supplies power to the rest of the components. This excludes the function generator that is temporarily replacing the voltage-controlled oscillator. The PC 104 board operates with a DC power supply of 5 Volts. Circuitry has been developed that will power the MASSpatch prototype with a battery that can be completely recharged from power harvesting alone. However, in the current configuration, the

PC 104 board draws just under one Amp at 5 Volts. The PC 104 board draws a high current because of the extra devices used for prototype programming. The board supplies power to the floppy drive and keyboard and sends a signal to the monitor. Without these accessories, the current draw will be much less, and a mature system will be energy-independent and autonomous.

Furthermore, even the relatively large needs of the current setup can be satisfied with piezoelectric-based power harvesting. For example, the current prototype could be operated for twelve minutes with five 1.2V, 200 mAh capacity batteries. A 1 Ah capacity means a battery will last for 1 hour if it is subjected to a discharge current of 1 A. A 200-mAh battery can be recharged to 90% capacity in 1.2 hours with a random vibration signal at 0-500 Hz if a 2.5 x 2.375 inch PZT is used (Sodano et al., 2003b). This random signal is similar to the motion generated by an automobile compressor. An operational Air Force structure should have ambient vibration of at least this magnitude.

5.2.3 Impedance-based Health Monitoring Algorithm

As previously stated, the PC 104 board uses DOS as an operating system. All of the code used to control the PC 104 board is written in C language. Borland C++ 5.02 is used as the code editor and compiler. A fundamental sample program that read one data point per specified channel was expanded into the eventually complex code to perform impedance-based structural health monitoring data acquisition, analysis, and wireless output.

Appendix D outlines the final impedance measurement program in detail. The following steps describe the basic measurement procedure for each cycle using the current setup.

- A digital output signal from the PC 104 board triggers the function generator.
- The function generator sends a swept sine signal at the desired frequency range, amplitude, and sweep rate.
- The input signal is sent to both the PC 104 board and the MFC.
- The PC 104 samples at the desired rate, and reads the voltage from the sensing resistor of the impedance approximation circuit, as well as the output from the function generator.
- The time history signals are saved into files.
- The time data files are opened, undergo a Fast Fourier Transform over all the data points, and are saved into new files.

- The above procedure is repeated for the desired number of averages, with an equal number of function generator and response FFT files saved.
- The FFT files for each signal are averaged into two files.
- An impedance curve is generated by calculating the frequency response function (FRF) of the sensing resistor voltage with respect to the input voltage.
- The impedance signature is compared to a stored reference baseline using the RMSD.
- The damage metric is computed, and an alert is wirelessly sent out to blink an LED across the room if the damage threshold is exceeded.
- The system then ends until the next measurement is required, when the entire procedure repeats.

5.2.4 MASSpatch Experimental Validation

The final MASSpatch PC 104 program acquires 2048 sample time histories for two channels, the function generator and sensing resistor voltage, at a 50 kHz sampling rate. Twenty averages are taken, so twenty FFTs are performed; this creates forty FFT files (twenty for each channel). The averaged FFT files are then used to calculate the electrical impedance of the MFC sensor/actuator. A MFC has been shown to be an effective self-sensing actuator (Sodano et al., 2003a). Only the real part of electrical impedance is analyzed as it has been shown to be more sensitive to the presence of damage than the imaginary part (Park et al., 2003).

The function generator sweeps from 5 to 8 kHz in 40 ms. The amplitude of the swept sine is 5 Volts. A 1000 Ohm sensing resistor is used for the low cost circuit.

Many data acquisition runs were made in order to determine the program and function generator variables. The 5 to 8 kHz range is chosen by comparing impedance curves generated with the new system to an HP 4192A impedance analyzer. Responses with large, discernable peaks are shown in this range, even though the system would operate at higher frequencies. By adding additional PC 104 boards, a 100 kHz sampling frequency could be readily maintained for each channel. With the program and function generator variables set, some additional experiments were carried out to demonstrate the capability of the MASSpatch prototype. Figure 5.5 shows impedance signatures for one of these tests.

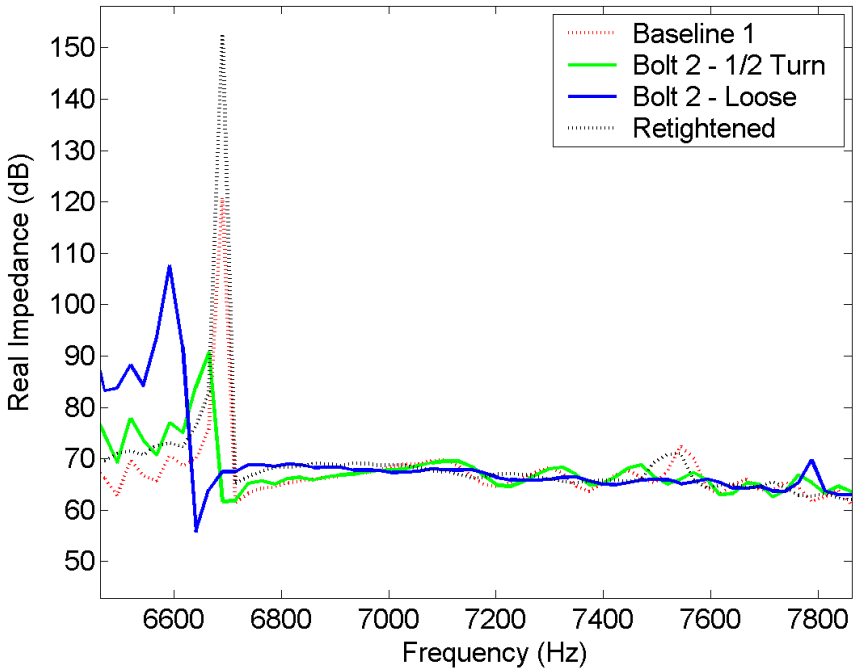

Figure 5.5: The impedance curves are shown for the loosening and retightening of bolt 2.

Figure 5.5 clearly shows peak shifts and other changes in the impedance signature that arise as damage occurs. Impedance curves are only shown for the structural excitation range. The current MASSpatch prototype automatically compares these curves and finds the damage metric. Figure 5.6 shows the resultant RMSD values.

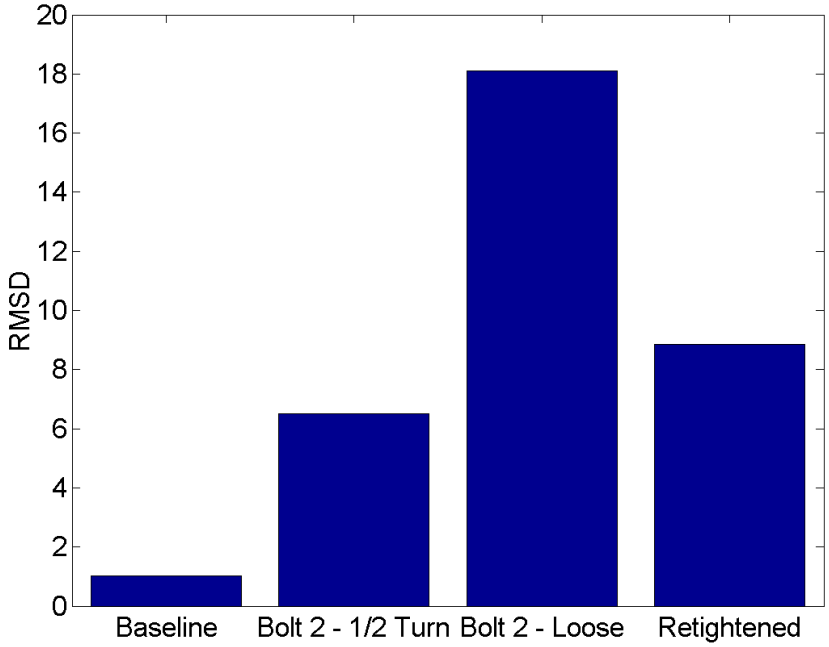

Figure 5.6: The RMSD of the impedance curves of Figure 8. The baseline damage metric is compared to a curve not shown in Figure 8.

Figure 5.6 shows that the damage metric increases if damage is induced into the system. The RMSD damage metric is computed over the range of 6500–7800 Hz. Figure 5.5 reveals that when the bolt is retightened, the curve peaks shift back very close to where the baseline was established. However, the damage metric still shows potential damage. Even though the curves are similar, this is a good example of why baselines need to be reestablished when a structure is repaired. An accurate baseline is crucial if false positives are to be avoided.

In previous experiments, the damage metric threshold is set to twenty based on initial experiments performed to set the prototype variables. In the final setup, if the calculated metric never exceeded twenty; the wireless system would never have indicated damage. The current configuration averages twenty times, and uses an optimum frequency range. With a higher number of averages, system noise had been reduced, and therefore the damage metric threshold was able to be reduced. After some additional experimentation, a new damage metric threshold of ten was chosen. Figure 5.7 shows the impedance curves of the experiment used to determine whether this threshold is reasonable for the bolted joint structure.

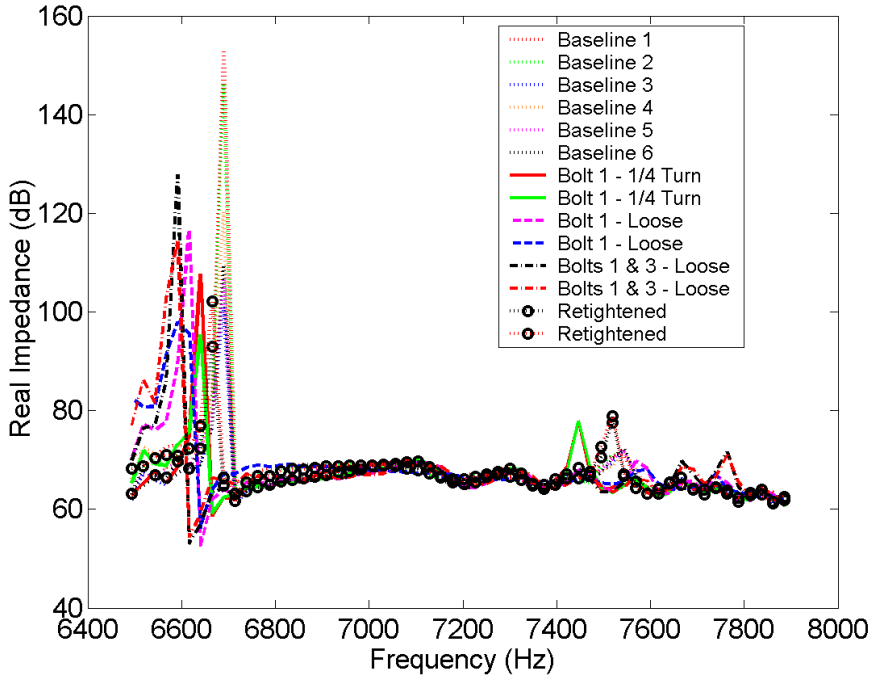

Figure 5.7: Impedance curves for the damage threshold determination.

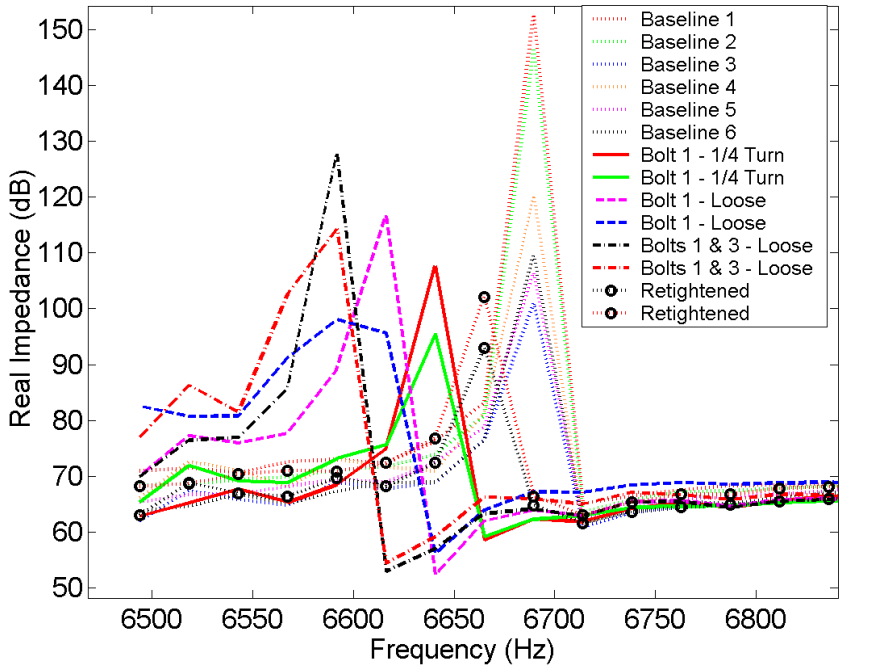

Figure 5.8: An improved view of the first peak of Figure 5.7.

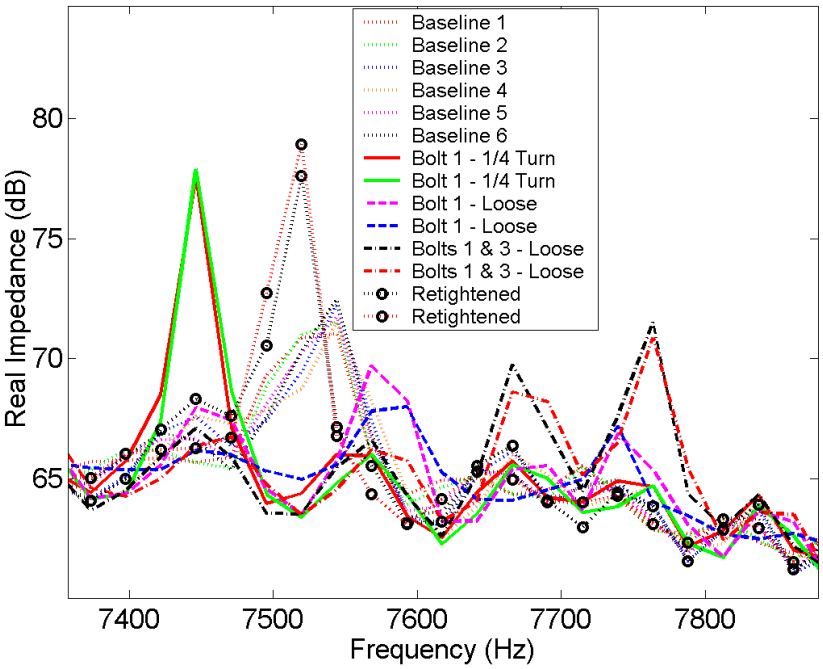

Figure 5.9: An improved view of the second peak of Figure 5.7.

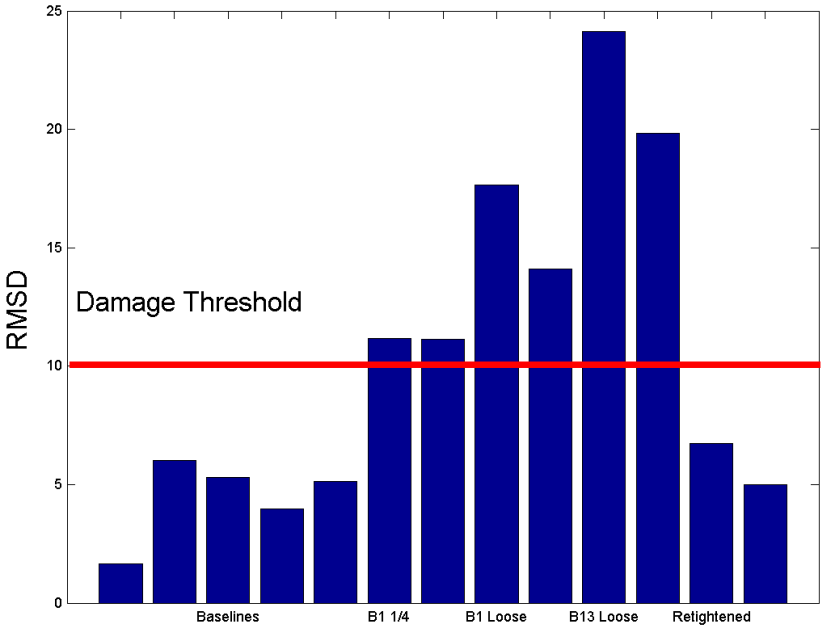

Figure 5.10: The RMSD of the impedance signatures of Figure 5.7 with the damage metric threshold level shown.

The first five bars of Figure 5.10 compare the baseline curves with the first baseline. The next two compare the curves for loosening bolt 1 one-quarter turn with the baseline. Bolt 1 is loose in the next two bars, bolts 1 and 3 are loose in the next two, and both bolts are retightened in the final two bars. This data indicates that the damage threshold appears to be set correctly. With a small amount of damage, the threshold is exceeded. In the code, when the damage metric threshold (ten for this case) is exceeded, a signal is sent to a digital output channel. This output sends a signal of a certain length and interval to the wireless transmitter. When the wireless receiver gets the signal from the transmitter, the LED indicates damage by turning on for the same length at the same interval, essentially blinking. With no damage, and with the bolts retightened, no damage is indicated.

5.2.5 Comparison to Traditional Impedance-based SHM

In comparison to traditional methods based on the HP impedance analyzer shown in Figure 5.11, MASSpatch is compact, lightweight, and can be operated off rechargeable battery power. Data is collected, averaged twenty times, and analyzed with MASSpatch produces results much faster than can be done with an off-the-shelf impedance analyzer. The MASSpatch single board computer prototype is currently set up to acquire 20 averages at any frequency range. 98 seconds are required to acquire the data. To completely acquire and process the data, compare it with a baseline, and notify the operator of damage exceeding the specified threshold, the system takes 150 seconds (only 52 seconds for processing). In comparison, a HP 4194A impedance analyzer is setup to acquire date from 30 - 50 kHz. Normally, only four averages are taken, and 33 seconds are required to interrogate the structure. For a more direct comparison, the impedance analyzer is set to perform 16 averages at the same frequency range. 90 seconds are now required to collect the impedance signatures, which is very comparable to the MASSpatch system. However, data taken with the traditional impedance analyzer is still unprocessed and must be analyzed with Matlab or some other programming technique, which will require more than 52 seconds.

Furthermore, a typical impedance analyzer costs around $40,000. All the components used in the MASSpatch prototype were acquired for around $1,500, and, with the knowledge gained during this experience, a similar system could be built for much less. MASSpatch has many advantages over the traditional method of impedance-based structural health monitoring.

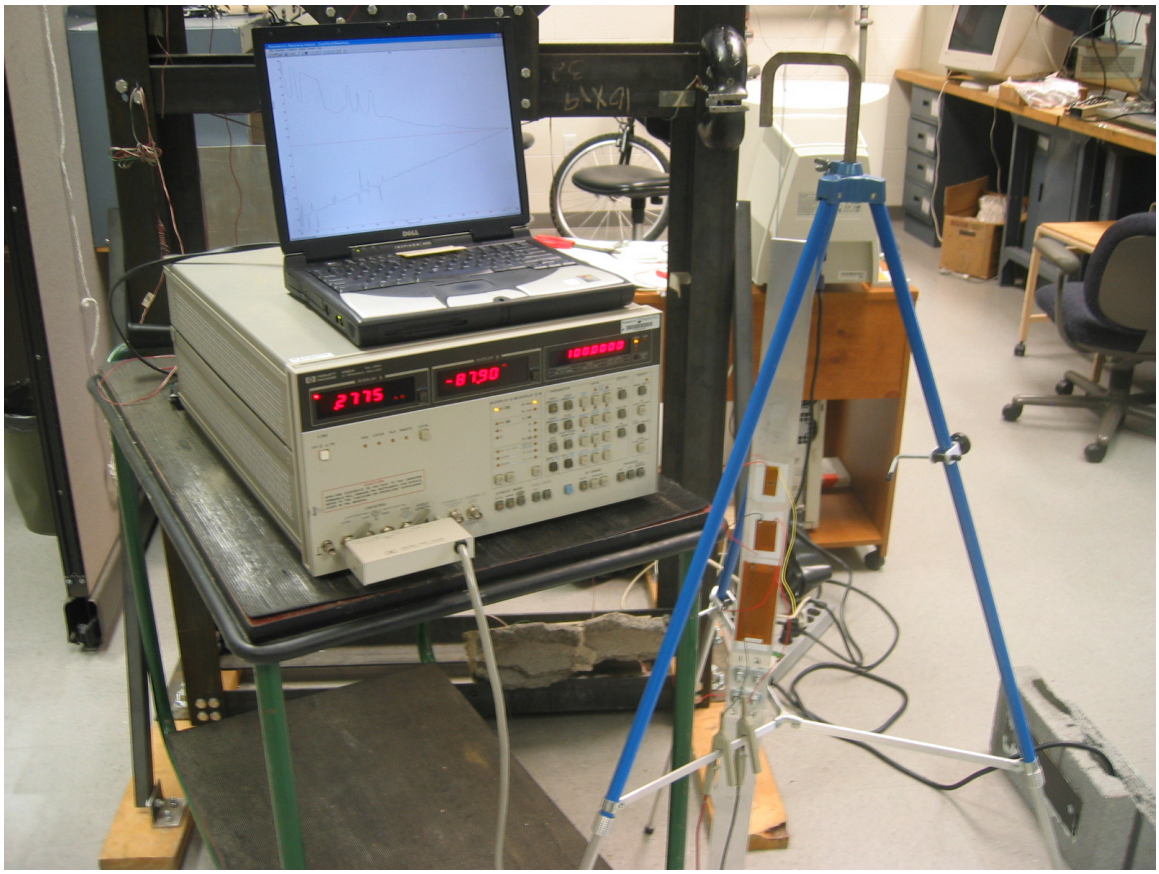

Figure 5.11: Bolted joint impedance measured with a traditional impedance analyzer.

5.3 Extending the MASSpatch Capabilities

In Chapters 3 and 4, damage in graphite/epoxy composite samples is detected using traditional impedance method hardware. Chapter 2 describes a simulation where longitudinal waves are generated by exciting two PZT patches, and the resulting pulses are monitored to detect and locate damage. In the following sections, MASSpatch will be shown as an effective alternative for measuring damage in composites, as well as pulses in a beam.

5.3.1 Composite Delamination Detection

The impedance-based SHM method is shown to be very useful in detecting delaminations in composite samples in Chapter 4. In this section, the MASSpatch prototype is used to monitor the extent of damage in composite specimens rather than using an impedance analyzer. The

results of the MASSpatch composite testing are presented, as well as a comparison to results obtained with a HP 4194A impedance analyzer.

For this experiment, samples with a stacking sequence of $[+30/0/-30/90]_s$ are fabricated, cut, and tabbed, as described in Chapter 4. PZT patches are mounted to each of the five samples. Each sample undergoes the same experimental procedure to test the impedance-based SHM capabilities of MASSpatch.

A baseline measurement is taken with the HP4194A impedance analyzer on each sample for comparison with the curve generated with the prototype. Two baseline curves are taken with MASSpatch. The first baseline curve is saved on to the PC 104 flash disk to allow a damage metric calculation. Each sample is then loaded to a different level using an Instron machine with a 50 kN load cell. Two impedance signatures are again taken with the MASSpatch system and another reference curve is taken with the impedance analyzer.

The HP 3314A function generator is set to sweep from 10-20 kHz in 40ms at an amplitude of 5 Volts. MASSpatch acquires data as described in detail in Section 5.2.3 with the parameters set in Section 5.2.4. The function generator output and voltage across the resistor are sampled at 50 kHz. 20 averages of 2048 samples are taken. The low cost circuit consists of a 1000 Ohm resistor.

Figure 5.12 shows a sample impedance signature of a composite sample taken with MASSpatch. Peaks are readily identifiable, and changes in the signature are easily seen after loading. Figures 5.13 and 5.14 compare the impedance measurements taken with the MASSpatch prototype to those taken with an impedance analyzer. The impedance analyzer curves have been scaled to appear in the same range as the new system's curves. Figure 5.13 shows the baseline curves, while Figure 5.14 compares the curves showing a change in the sample. Major peaks in both signatures occur at the same frequencies. With this comparison, the MASSpatch system, utilizing the low cost method, is shown to be accurately measuring impedance for SHM. All figures are shown in frequency ranges where structure is excited, the same range that the damage metric is calculated over.

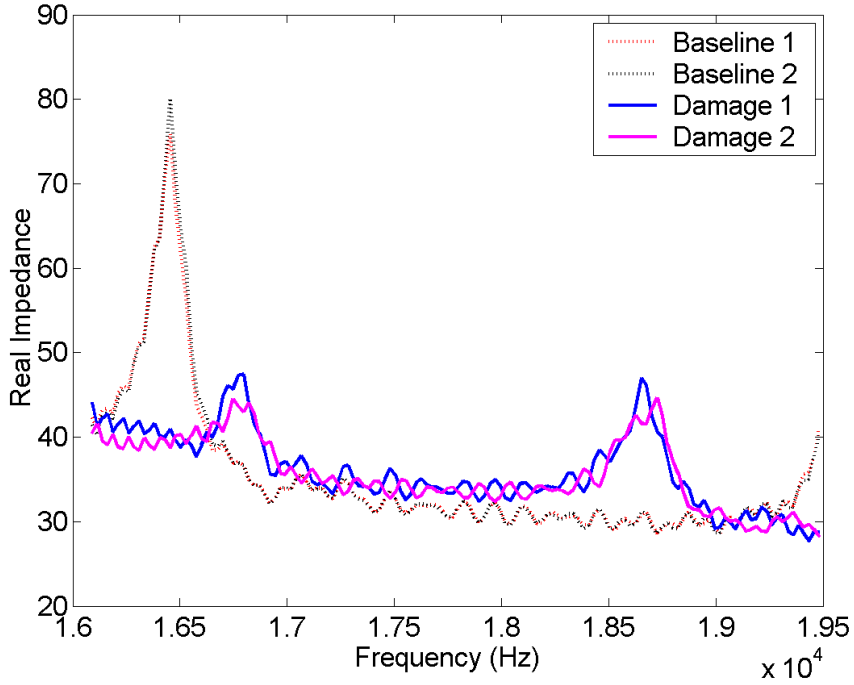

Figure 5.12: The impedance signatures for Sample Three measured with MASSpatch.

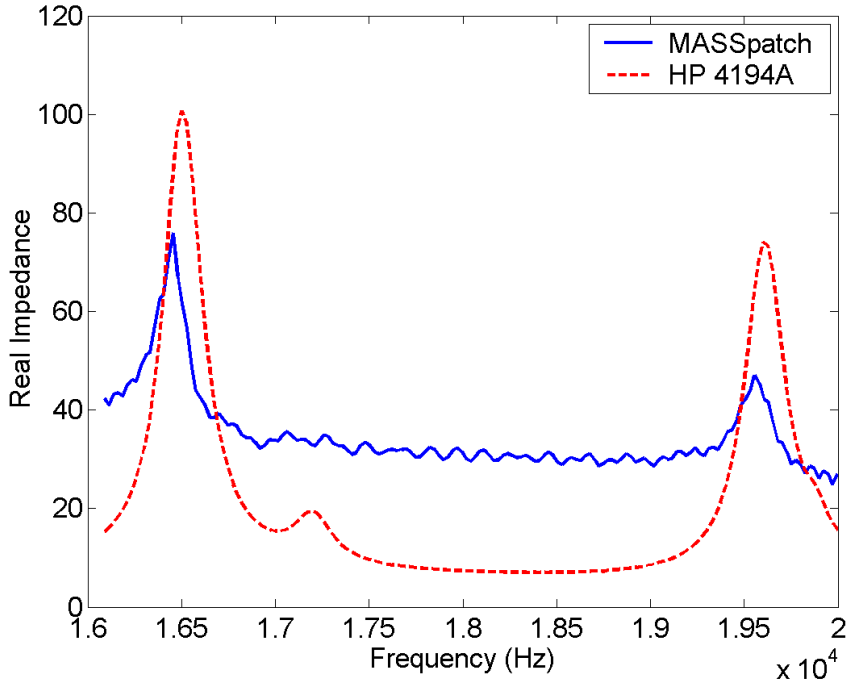

Figure 5.13: A comparison between the baselines of the MASSpatch and HP 4194A impedance analyzer. Note that the impedance analyzer curve is scaled.

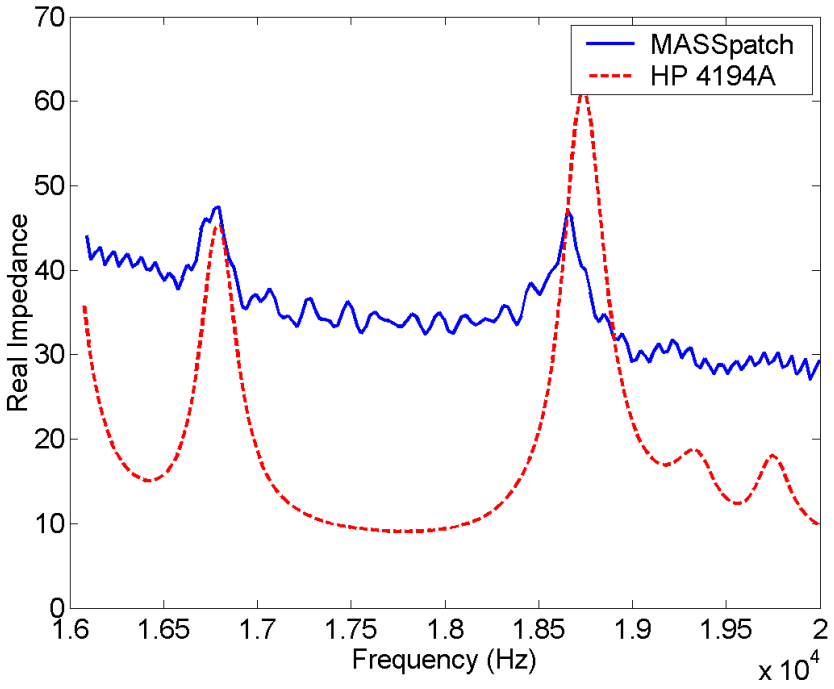

Figure 5.14: A comparison between the damaged curves of the MASSpatch and HP 4194A impedance analyzer. Note that the impedance analyzer curve is scaled.

After the samples are tested, the actual amount of damage to the structure is determined using radiography. The damage metrics are automatically calculated with the MASSpatch prototype. Table 5.2 displays the damage metrics and the actual amount of delamination induced in each specimen. The loading for each sample is also summarized.

Table 5.2: Summary of sample loading, damage metrics, and delaminated area.

Sample	Load (kN)	RMSD 1	RMSD 2	RMSD 3	Delaminated Area (%)
1	10	30.3	80.82	88.86	0.0
2	15	56.56	326.92	330.53	0.0
3	20	2.63	33.8	32.24	6.6
4	25	27.6	108.69	149.0	29.3
5	30	51.4	93.28	95.0	35.6

In Table 5.2, RMSD 1 compares the two baseline measurements. RMSD 2 and 3 compare the impedance curves after loading to the first baseline measurement. In each sample, the calculated damage metrics indicate damage, as is shown by the different curves before and after loading. However, the damage metrics do not correlate with the actual amount of damage in

the specimens determined through radiography. To ensure the bad correlation is not a MASSpatch programming error, the damage metrics are calculated with Matlab using the same impedance signatures. Table 5.3 shows the results of this analysis.

Table 5.3: Summary of the damage metrics calculated with Matlab.

Sample	RMSD 1	RMSD 2	RMSD 3
1	57.0	119.1	169.1
2	59.5	327.3	331.6
3	2.9	35.8	35.1
4	30.3	218.3	204.9
5	52.3	92.9	96.0

The damage metrics calculated with Matlab compare very well with the RMSD values MASSpatch calculated. In Samples Two, Three, and Five, the numbers are very close. The same trend is shown in the other two samples, but the calculated values are not as close. Similar values are generated using two different methods. The algorithm for both the MASSpatch prototype and the Matlab program are very similar, so comparable results are expected.

A possible reason for the bad correlation is the low number of points the damage metric is calculated over. With an impedance analyzer, the RMSD is determined over 401 points. However, these calculations were only calculated over 139 points. Increasing the sampling rate, and therefore generating more samples in the frequency range of interest, should lead to more accuracy in quantifying the amount of damage.

MASSpatch has a couple advantages over taking impedance measurements for SHM in the traditional manner. The MASSpatch system cuts down on the analysis needed to quantify damage. With the traditional method, each impedance curve must be saved and later analyzed to generate a damage metric. In the MASSpatch setup, the damage metric is calculated automatically. Traditional impedance measurements require the operator to choose appropriate frequency ranges and name and save files for each measurement. With the MASSpatch setup, the executable name is entered and everything else is fully automated. Overall, the MASSpatch prototype decreases time spent testing samples and increases the ease of use in performing SHM.

5.3.2 Wave Propagation

Chapter 2 describes a simulation where longitudinal wave pulses are monitored to detect and locate damage in an aluminum beam. The longitudinal wave speed, which is determined by the temperature dependent Young's Modulus, is used to determine the location of damage. By monitoring the temperature, the correct wave speed, and thus the correct damage location, can be determined.

This section describes an experimental setup used to show that MASSpatch can be used to trigger the generation of longitudinal waves and monitor the resulting pulses. In Chapter 2, the beam and results are a result of simulation. Here, MASSpatch will monitor actual waves generated on a physical beam.

A free-free aluminum beam of dimensions 1830 mm long, 12.7 mm wide, and 3.18 mm thick is used for the experiment, just like the simulated beam of Chapter 2. Three PZT patches, 12.7 mm square, are bonded to the beam. PZT's 1 and 2 are on opposite sides of each other on an edge of the beam. PZT 3 is mounted in the center of the beam. The setup of the beam can be seen in Figure 5.15.

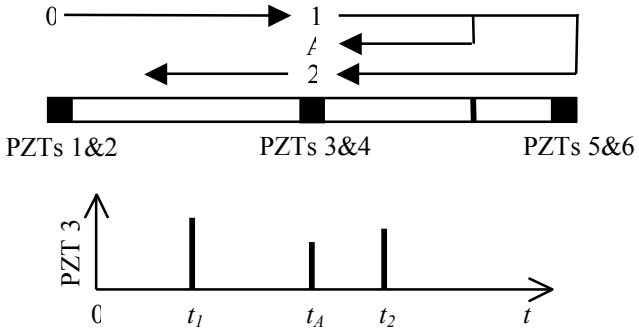

Figure 5.15: The beam setup and wave propagation path for damage located at 0.4 m from the right side of the beam are shown. Note that PZTs 4, 5, and 6 are not mounted for this experiment.

The MASSpatch program is set up to trigger the HP 3314A function generator and then acquire 2048 samples at a sampling rate of 50 kHz. PZT 1 is monitored on the first data acquisition input to observe the longitudinal wave generation. The second channel monitors PZT 3 and is used to record the pulse time history. The HP 3314A function generator is set to half cycle burst mode with a 3 Volt sine wave to generate the pulse. When the function generator is

triggered by the MASSpatch program, PZT's 1 and 2 are actuated with this pulse in phase to generate the longitudinal wave. The input pulse and resulting wave are shown in Figure 5.16.

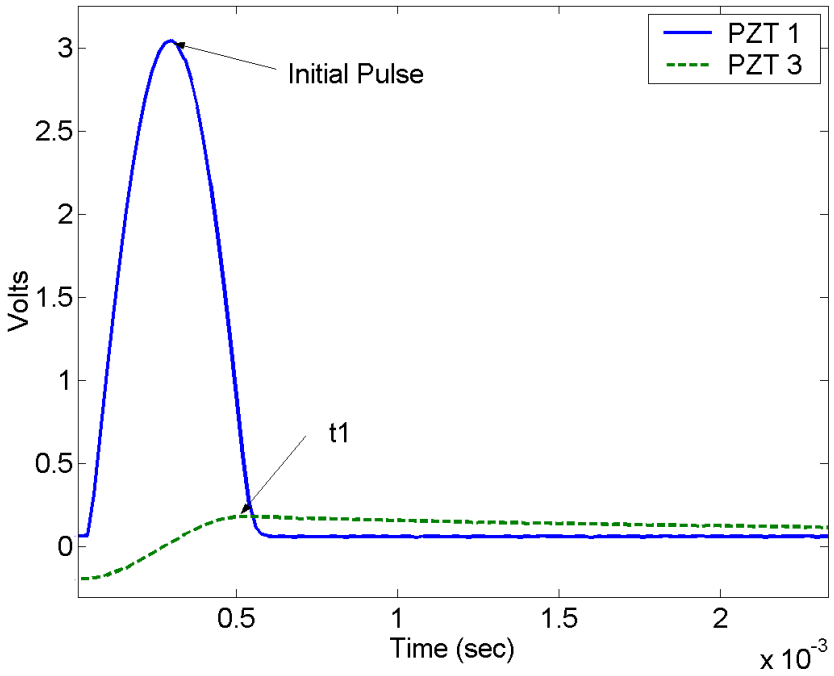

Figure 5.16: The initial pulse generated by triggering the function generator and the response as the wave reaches PZT 3 are shown.

To see if a longitudinal wave was indeed generated, the pulse time histories can be used to determine the wave speed. Taking a closer look at the curves shown in Figure 5.16, individual pulses can be seen, as shown in Figure 5.17. By taking the time difference between when the wave reaches PZT 1 and PZT 3, the wave speed can be determined.

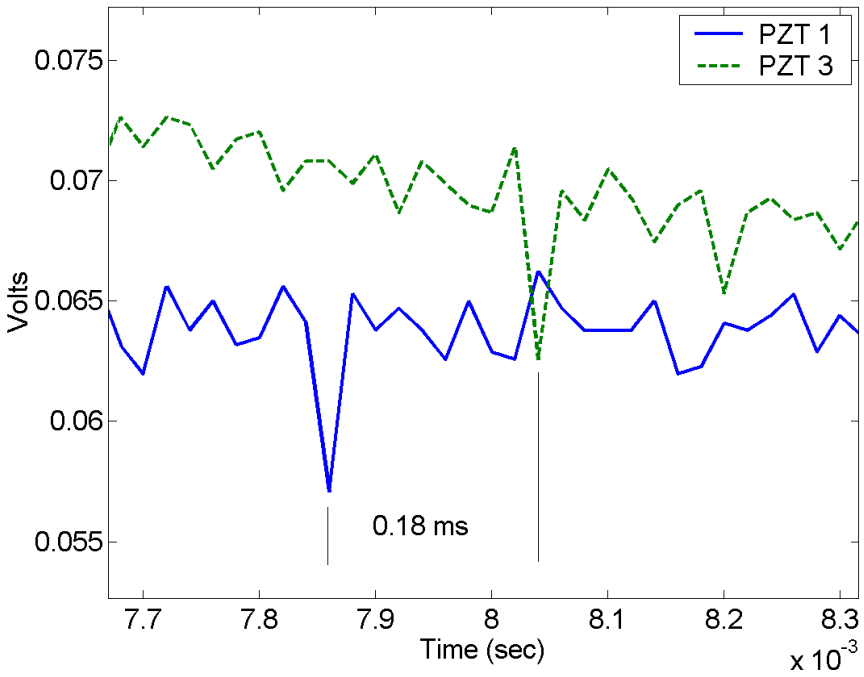

Figure 5.17: An enlarged view of the curves shown in Figure 5.16.

Figure 5.17 shows that the time differential between pulses at PZTs 1 and 3 is 0.18 ms. The distance between these PZTs, *l*, is 0.915 m. Plugging these numbers into Equation 2.3, the wave speed can be determined.

$$c = \frac{l}{t_1} = \frac{0.915\,m}{0.18\,ms} = 5083.3\,\frac{m}{s}$$

The calculated wave speed of 5083 meters per second is very close to the actual wave speed of aluminum at room temperature of 5092 meters per second.

With PZTs 1 and 2 producing a longitudinal wave, damage can be induced on the beam by means of a small hand clamp. The clamp was placed 0.4 meters from the end of the beam opposite PZTs 1 and 2, as seen in Figure 5.15. Damage on the beam causes additional wave reflections, and therefore additional pulses. The time history with beam damage can be seen in Figure 5.18.

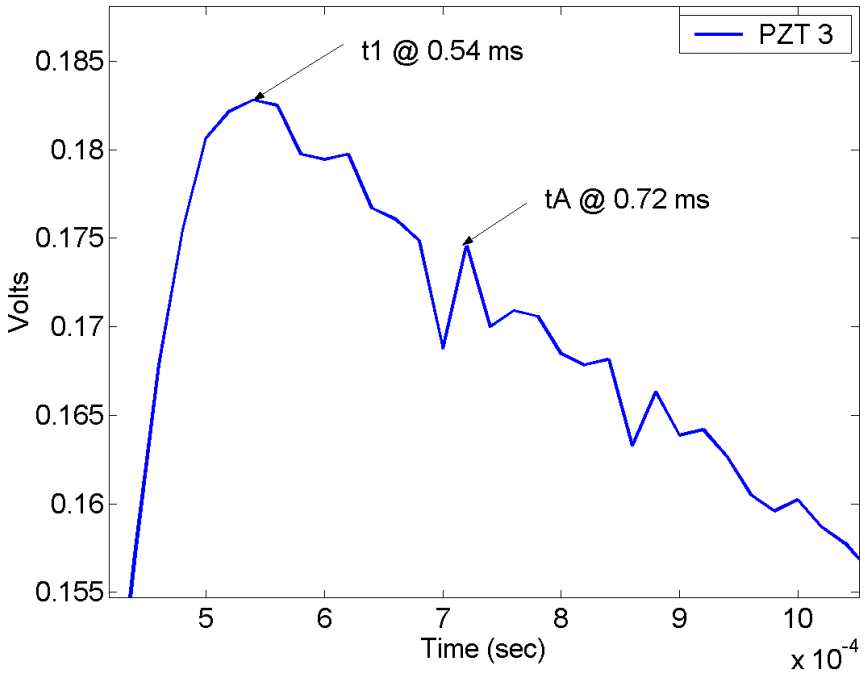

Figure 5.18: t_1 and t_A are labeled on the time history of PZT 3.

Figure 5.18 shows the location of pulse times t_1 and t_A. t_1 is the time for the wave to initially reach the center of the beam, and t_A is when the wave reflected from the damage reaches PZT 3. The wave propagation path showing how t_1 and t_A are related is shown in Figure 5.15. Using Equation 2.4, the damage location, d, can be found by plugging in the values for t_1 and t_A.

$$d = l - \frac{c(t_A - t_1)}{2} = 0.915\,m - \frac{5083\,m/s\left(0.18x10^{-3}\,s\right)}{2} = 0.457\,m$$

To determine whether a calculated damage location of 0.457 meters is accurate, the spatial resolution of the system is considered. The spatial resolution, Δd , is calculated with the equation

$$\Delta d = ct_s\,, \tag{5.1}$$

where c is the speed of the wave generated in the beam, and t_s is the sampling period of MASSpatch (Kabeya et al., 1998). Plugging in the numbers, the spatial resolution is found to be 0.103 meters.

$$\Delta d = (5083 m/s)(2x10^{-5} s) = 0.103 m$$

The calculated damage location of 0.457 meters is well within the resolution range of the prototype, $d \pm \Delta d$ (0.503 to 0.297 meters), so the estimated damage location is accurate.

This experiment verifies the MASSpatch prototype can be used to monitor pulses. Longitudinal waves are generated in a free-free aluminum beam. By monitoring the pulses recorded from a PZT patch in the center of the beam, the correct damage location is identified.

5.4 Chapter Summary

The initial steps in the development of a fully automated, self-contained, wireless system for impedance-based SHM are described in this chapter. A prototype is constructed and the hardware development is described in detail. The programming steps are also described. An experiment was developed to show the functionality of the new system. Damage was readily detected in a bolted joint.

The new prototype is found to be easier to use that traditional method of impedance based SHM. The system is also much cheaper and less bulky. Future work will focus on development of an even more robust system. Eventually, all of the functionality of the current system and more will be included on a single small chip. To incorporate all of these complex components into one functional chip, very-large-scale integration (VLSI) design will be utilized. VLSI allows for analysis and design of very dense and complicated electronic integrated circuits. A higher sampling rate will allow for higher excitation frequencies to be used. The chip will also be equipped with advanced signal processing techniques and allow for temperature compensation. Validation of the completed project will occur on a variety of existing operational systems.

Impedance signatures are acquired on composite specimens that delaminate under tensile loading. The MASSpatch system generated curves very similar to those of an impedance analyzer. A system with a faster sampling rate would allow for more data points in the range of interest. Stronger correlations between the damage metric and actual amount of damage may then be seen; the traditional impedance method has been shown effective in quantifying damage, and similar curves are generated with MASSpatch.

MASSpatch is also used to monitor wave propagation in a free-free aluminum beam. By analyzing pulses generated by these waves at a specific PZT patch bonded to the beam, damage can be correctly located. Additional programming could allow features to be added such as finding the damage automatically and monitoring the temperature to correct the damage location.

Chapter 6

Conclusions

This thesis discusses different components related to structural health monitoring systems. All of the research is centered on the impedance method for SHM. In the impedance method, high frequency excitations are used to excite the structure of interest with a piezoelectric patch bonded to the surface. The piezoelectric acts as a self-sensing actuator, so, at the same time the excitation signal is being applied, the response of the structure is monitored by measuring the current. By comparing response signatures to a baseline of the structure, indications to the health of the structure can be inferred. Work performed in this thesis looks to make the damage detection scheme more robust, directly quantify the amount of damage in specific structures, and increase the accessibility of the method. This chapter will provide a brief summary of the results, indicate research contributions, and provide recommendations for future work.

6.1 Brief Thesis Summary

In Chapter 2, the influences of temperature variations on the use of wave propagation for damage detection are investigated for use with impedance-based structural health monitoring. The equations used to determine the damage based upon a longitudinal wave are presented as derived by Kabeya et al. (1998). Equations are defined in order to determine the damage location in a simulation. Temperature variations are induced, and the resulting errors are presented. A

possible application using a realistic temperature differential is proposed. A curve-fit of the modulus of elasticity is implemented to correct damage location error.

The impedance-based structural health monitoring method is used to successfully detect different composite damage mechanisms and correlate impedance measurement changes with structural changes in Chapters 3 and 4. Specifically, graphite/epoxy composite samples are manufactured and tested. PZT patches are attached to the composite coupons to actuate the structure with high-frequency excitations. Bonding the patches to the sample allows changes in the structural mechanical impedance to be monitored with the electrical impedance of the PZT. Samples are tested using quasi-static tensile loading to introduce damage. To determine the extent of damage incurred, impedance signatures are acquired before and after the tensile load is applied. A change in impedance from the baseline shows the presence of damage. The amount of damage is characterized using a damage metric. Radiography is used to verify the extent of damage.

Finally, the development, fabrication, and validation of a self-contained prototype for wirelessly employing impedance-based SHM are described. Each component of the new sensor is discussed, along with the algorithms needed to control data collection and processing and reveal the status of the structure to the end user. The prototype is successfully compared with traditional impedance measurement techniques on a number of relevant structures. The capabilities of the smart sensor are extended to test the composite specimens used in Chapter 4 and monitor the wave propagation pulses of the beam described in Chapter 2.

6.2 Contributions

Previously, the wave propagation technique was discussed as a procedure for making impedance-based SHM more robust. In structures equipped to perform local impedance method detection at critical points, wave propagation can be used to detect global damage. The work described in this thesis describes what happens to the wave propagation technique under temperature variations. In previous work, the structure was assumed to be in a constant temperature environment, which is not always realistic. A simulation is performed here to determine how the damage location, calculated by monitoring the time history of pulses reflecting off damage, changes with temperature. A curve fit of the modulus of elasticity versus temperature is used as a technique to correct the wave speed, and thus the damage location, for a

given temperature. With the correction algorithm developed in this thesis, the wave speed does not have to be continuously recalculated in environments with shifting temperatures to obtain accurate damage locations.

In Chapters 3 and 4, the first direct comparison of damage metrics calculated with the impedance method and the actual amount of damage present in a composite specimen is shown. The impedance method has been used to detect the presence of damage in composites in earlier work, but the exact amount of damage was never known. Usually, a comparison of the state of damage, as indicated by a metric, is compared with the previous measurement or metric to gain some relative notion of how much more damage is present. Radiography on the composite samples in this thesis is used to gain insight into the exact amount of damage present after loading. The damage metric is then compared to the exact amount of damage. In many cases, an almost linear correlation between the amount of damage indicated with the SHM system and the actual damage is shown. These correlations are made with samples containing two kinds of damage mechanisms: transverse matrix cracking and edge delaminations.

A comparison of various damage metrics is also discussed in Chapter 4. For impedance-based SHM, many different statistical algorithms have been used to extract features from the data. In this thesis, four of these damage metrics are directly compared on one set of data. After scaling the results, it is shown that the compared metrics, for the most part, follow the same trends. The numbers generated by the metrics will vary greatly in magnitude, but each algorithm shows a significant increase for a significant amount of damage. The results show that a limiting threshold value can be set which corresponds to the actual amount damage in a structure, no matter which damage metric is utilized.

Chapter 5 describes the fabrication of the first prototype for wireless SHM specifically using the impedance method. Traditional impedance measurements require the use of a large and expensive impedance analyzer. At best, the low cost impedance method can be used with an FFT analyzer, which may still be rather obtrusive. The new system combines the low cost impedance method with single board computing to increase the accessibility of, and decrease the overhead in, using impedance-based SHM. The prototype successfully detected damage in a number of structures, including the onset of edge delamination in composite specimens. Wave propagation was also performed with the prototype to supplement the impedance method.

Much of the research described in this thesis lends itself to the development of a robust smart sensor for impedance-based SHM. The first steps in including all of the components in Chapter 5 on a single chip are shown. The final sensor should integrate the impedance method and wave propagation for local detection and global monitoring of a wide variety of structures. Wireless communications can alert the end users of any problems with structural integrity.

6.3 Future Work and Recommendations

To extend the scope of this research, recommendations for future work are presented. In Chapter 2, a numerical simulation representative of wave propagation is performed on an aluminum beam. Future work will consist of placing the beam discussed in Chapter 5 in a temperature controlled environment to verify the results of this simulation. The wireless based system of Chapter 5 can be used to automate the pulse generation, and embedded algorithms can detect the presence and location of damage. The impedance method can be combined with this system for a complete damage detection scheme. Further testing may introduce other factors such as different boundary conditions and more complex structures.

In Chapters 3 and 4, large resonant peaks in the impedance signature were noted to shift in or out of the frequency range of interest as a result of flaws in the composite. The incorporation of an algorithm to find an optimal frequency range centered around larger peaks could help in the progression towards a completely autonomous SHM system adaptable to a wide range of structures. An optimal impedance signature will allow for less variability in the detection of damage to the structure. Also, future work will consist of quantifying the amount of damage in more composites with different stacking sequences. Increasing the amount of samples used for each test will generate more confidence in the ability of the impedance method to readily detect imperfections, hopefully in a linear fashion, with respect to the amount of damage.

VLSI design will be used to incorporate everything needed for an impedance-based damage detection scheme onto a single chip. With higher processing power and more computational memory, complex signal processing techniques and advanced feature extraction algorithms can enhance the damage detection capabilities of the smart sensor. The chip design will focus on energy efficiency, while still maintaining a reasonably low cost and maintaining a highly robust structural interrogation scheme. The presence and severity of damage can be detected with the impedance method, while the location of global damage can be found with

wave propagation. By monitoring the temperature, shifts in impedance signatures and wave propagations pulses can be accounted for and corrected. Such a system that adds structural modeling both increases the accuracy of damage detection and can be upgraded to perform damage prognosis.

References

Bar-Cohen, Y., 1986, "NDE of Fiber-Reinforced Composite Materials-A Review," *Materials Evaluation*, Vol. 44, pp. 446-454.

Basheer, M.R., Rao, V., and Derriso, M., 2003, "Self Organizing Wireless Sensor Networks for Structural Health Monitoring," Proceedings of the 4th International Workshop on Structural Health Monitoring, September 15-17, Stanford, CA, pp. 1193-1207.

Bois, C., and Hochard, C., 2003, "Damage Monitoring in CFRP Laminated Composites Using Dynamic Measurements," Proceedings of the 4th International Workshop on Structural Health Monitoring, September 15-17, Stanford, CA, pp. 742-748.

Bois, C., and Hochard, C., 2004, "Monitoring of Laminated Composites Delamination Based on Electro-mechanical Impedance Measurement," *Journal of Intelligent Material Systems and Structures*, Vol. 15, No. 1, pp. 59-67.

Callister, Jr., W.D., 1997, *Materials Science and Engineering: An Introduction*, John Wiley & Sons, Inc., New York, NY.

Chaudhry, Z., Lalande, F., Ganino, A., and Rogers, C.A., 1995, "Monitoring the Integrity of Composite Patch Structural Repair via Piezoelectric Actuators/Sensors," 45th AIAA/ASME//ASC Structures, Structural Dynamics & Materials Conference, New Orleans, LA, pp. 2243-2248.

Diaz Valdes, S.H., and Soutis, C., 1999, "Delamination Detection in Composite Laminates from Variations of their Modal Characteristics," *Journal of Sound and Vibration*, Vol. 228-1, pp. 1-9.

Doebling, S.W., Farrar, C.R., and Prime, M.B., 1998, "A Summary Review of Vibration-Based Damage Identification Methods," *The Shock and Vibration Digest*, Vol. 30**,** No. 2, pp. 91-105.

Dugnani, R., and Malkin, M., 2003, "Damage Detection on a Large Composite Structure," Proceedings of the 4th International Workshop on Structural Health Monitoring, September 15-17, Stanford, CA, pp. 301-309.

Giurgiutiu, V., Zagrai, A., and Bao, J.J., 2002, "Piezoelectric Wafer Embedded Active Sensors for Aging Aircraft Structural Health Monitoring," *International Journal of Structural Health Monitoring*, Vol. 1, pp. 41-61.

Grisso, B.L., Leo, D.J., and Inman, D.J., 2004a, "Temperature Influences on the Wave Propagation Technique for use in Supplementing Impedance-Based Structural Health Monitoring," Proceedings of SPIE's 9th International Symposium on NDE for Health Monitoring and Diagnostics, March 14-18, San Diego, CA, Vol. 5394, pp. 222-232.

Grisso, B.L., Peairs, D.M., and Inman, D.J., 2004b, "Impedance-based Health Monitoring of Composites," Proceedings of IMAC XXII, January 26-29, Dearborn, MI.

Grisso, B.L., Peairs, D.M, and Inman, D.J., 2004c, "Detecting Damage in Graphite/Epoxy Composites using Impedance-based Structural Health Monitoring" Proceedings of the International Conference on Advances in Experimental Mechanics, September 6-8, York, UK, pp. 185-190.

Heiken, G.H., Vaniman, D.T., and French, B.M., 1991, *Lunar Sourcebook: A User's Guide to the Moon*, Cambridge University Press, New York, NY.

Hyer, M.W., 1998, *Stress Analysis of Fiber Reinforced Composite Materials*, The McGraw Hill Companies, Inc., New York, NY.

Inman, D.J., 2001, *Engineering Vibration*, Prentice Hall, Upper Saddle River, NJ.

Kabeya, K., Jiang, Z., and Cudney, H.H., 1998, "Structural Health Monitoring by Impedance and Wave Propagation Measurement," Proceedings of the 4th International Symposium on Motion and Vibration Control, August 25-28, Zuric, Switzerland, pp. 207-212.

Kander, R.G., 1991, "A Study of Damage Accumulation in Unidirectional Glass Reinforced Composites via Acoustic Emission Monitoring," Polymer Composites, Vol. 12, No. 4, pp. 237-245.

Kessler, S.S. and Spearing, S.M., 2002a, "Design of of a piezoelectric-based structural health monitoring system for damage detection in composite materials," Proceedings of SPIE's 9th International Symposium on Smart Structures and Materials, March 17-21, San Diego, CA, Vol. 4701, pp. 86-96.

Kessler, S.S. and Spearing, S.M, 2002b, "In-Situ Sensor-Based Damage Detection of Composite Materials for Structural Health Monitoring," Proceedings of the AIAA/ASME/ASCE/AHS/ASC 43rd Structures, Structural Dynamics, & Materials Conference, April 22-25, Denver, CO.

Liang, C., Sun, F.P., and Rogers, C.A., 1994, "An Impedance Method for Dynamic Analysis of Active Material System," *Journal of Vibration and Acoustics*, Vol. 116, pp. 121–128.

Lynch, J.P., Sundararajan, A., Law, K.H., Sohn, H., and Farrar, C.R., 2004a, "Design of a Wireless Active Sensing Unit for Structural Health Monitoring," Proceedings of SPIE's 11th Annual International Symposium on Smart Structures and Materials, March 14-18, San Diego, CA. Vol. 5394, pp. 157-168.

Lynch, J.P., Sundararajan, A., Law, K.H., Kiremidjian, A.S., and Carryer, E., 2004b, "Embedding Damage Detections Algorithms in a Wireless Sensing Unit for Operational Power Efficiency," *Smart Materials and Structures*, Vol. 13, pp. 800-810.

O'Brien, T.K., Johnston, N.J., Raju, I.S., Morris, D.H., and Simonds, R.A., 1987, "Comparisons of Various Configurations of the Edge Delamination Test for Interlaminar Fracture Toughness," *Toughened Composites ASTM STP 937*, pp. 199-221.

Osmont, D., Dupont, M., Gouyon, R., Lemistre, M, and Balageas, D., 2000, "Damage and Damaging Impact Monitoring by PZT Sensors-Based HUMS," Proceedings of SPIE Smart Structures and Materials 2000: Sensory Phenomena and Measurement Instrumentation, Vol. 3986, pp. 85-92.

Park, G., Sohn, H., Farrar, C.R., and Inman, D.J., 2003, "Overview of Piezoelectric Impedance-Based Health Monitoring and Path Forward," *The Shock and Vibration Digest*, Vol. 35, Issue 6, pp. 451-463.

Peairs, D.M., Grisso, B.L., Margasahayam, R.N., Page, K.R., and Inman, D.J., 2004a, "Impedance-based Health Monitoring of Space Shuttle Ground Structures," Proceedings of SPIE's 9th International Symposium on NDE for Health Monitoring and Diagnostics, March 14-18, San Diego, CA, Vol. 5394, pp. 99-107.

Peairs, D.M., Park, G., and Inman, D.J., 2004b, "Improving Accessibility of the Impedance-based Structural Health Monitoring Method," *Journal of Intelligent Material Systems and Structures*, Vol. 15, No. 2, pp. 129-140.

Prosser, W.H., Jackson, K.E., Kellas, S., Smith, B.T., McKeon, J., and Friedman, A., 1995, "Advanced, Waveform Based Acoustic Emission Detection of Matrix Cracking in Composites," *Materials Evaluation*, Vol. 53, No. 9, pp. 1052-1058.

Pyles, R., 2003, *Aging Aircraft: USAF Workload and Material Consumption Life Cycle Patterns*, RAND, Arlington, VA.

Raju, V., Park, G., and Cudney, H., 1998, "Impedance-based Health Monitoring Technique of Composite Reinforced Structures," Proceedings of 9th International Conference on Adaptive Structures and Technologies, October 14-16, Cambridge, MA, pp. 448-457.

Rutherford, A.C., Park, G. Sohn, H., and Farrar, C.R., 2004, "Structural Health Monitoring Using Macro-Fiber Composites and Impedance Methods," 45th AIAA/ASME/ASCE/AHS/ASC Structures, Structural Dynamics & Materials Conference, April 19-22, Palm Springs, CA.

Sazonov, E., Jonoyan, K., and Jha, R., 2004, "Wireless Intelligent Sensor Network for Autonomous Structural Health Monitoring," Proceedings of SPIE's 11th Annual International Symposium on Smart Structures and Materials, March 14-18, San Diego, CA, pp. 5384-5394.

Siggerud, K., 2002, "Highway Infrastructure: Physical Conditions of the Interstate Highway System Have Improved, but Congestions and Other Pressures Continue," Testimony before the Subcommittee on Highways and Transit, Committee of Transportation and Infrastructure, United States House of Representatives.

Sodano, H.A., Park, G., and Inman, D.J., 2003a, "An Investigation into the Performance of Macro-Fibers Composites for Sensing and Structural Vibration Applications," *Mechanical Systems and Signal Processing*, Vol. 18, pp. 683-697.

Sodano, H.A., Park, G., Leo, D.J., and Inman, D.J., 2003b, "Use of Piezoelectric Energy Harvesting Devices for Charging Batteries," Proceeding of SPIE's 10th Annual International Symposium on Smart Structures and Materials, Vol. 5050.

Sohn, H., Farrar, C.R., Hamez, F.M., Shunk, D.D., Stinemates, D.W., and Nadler B.R., 2003a, "A Review of Structural Health Monitoring Literature: 1996-2001," Los Alamos National Laboratory Report, LA-13976-MS.

Sohn, H., Park, G., Wait, J.R., and Limback, N.P., 2003b, "Wavelet Based Analysis for Detecting Delamination in Composite Plates," Proceedings of the 4th International Workshop on Structural Health Monitoring, September 15-17, Stanford, CA, pp. 567-574.

Sohn, H., Wait, J.R., Park, G., and Farrar, C.R., 2004, "Multi-Scale Structural Health Monitoring for Composite Structures," Proceedings of the Second European Workshop on Structural Health Monitoring, July 7-9, Munich, Germany, pp. 721-729.

Spencer, Jr., B.F., Ruiz-Sandoval, M.E., and Kurata, N., 2004, "Smart Sensing Technology: Opportunities and Challenges," in press *Journal of Structural Control and Health Monitoring*.

Subramanian, S., Lesko, J.J., Reifsnider, K.L., and Stinchcomb, W.W., 1994, "Damage Mechanism and Failure Modes in Cross-Ply Laminates Under Monotonic Tensile Loading: The Influence of Fiber Sizing," Applied Composite Materials, Vol. 1, pp. 283-300.

Sun, F.P., Chaudhry, Z., Liang, C., and Rogers, C.A., 1995, "Truss Structure Integrity Identification Using PZT Sensor-Actuator," *Journal of Intelligent Material Systems and Structures*, Vol. 6, pp. 134-139.

Tanner, N.A., Wait, J.R., Farrar, C.R., and Sohn, H., 2003, "Structural Health Monitoring Using Modular Wireless Sensors," *Journal of Intelligent Material Systems and Structures*, Vol. 14, No. 1, pp. 43-55.

Tennyson, R., 2004, "SHM System for Detecting Foreign Object Impact Damage on Spacecraft," Proceedings of the Second European Workshop on Structural Health Monitoring, July 7-9, Munich, Germany, pp. 399-406.

Xu, Y., Leung, C.K.Y., Yang, Z., Tong, P., and Lee, S.K.L., 2003, "A New Fiber Optic Based Method for Delamination Detection in Composites," *Structural Health Monitoring*, Vol. 2-3, pp. 205-223.

Yuan, S., Wang, L., Wang, X., and Chang, M., 2004, "A New Damage Signature for Composite Structural Health Monitoring," Proceedings of the Second European Workshop on Structural Health Monitoring, July 7-9, Munich, Germany, pp. 1058-1064.

Zagrai, A.N. and Giurgiutiu, V., 2001, "Electro-Mechanical Impedance Method for Crack Detection in Thin Plates," *Journal of Intelligent Material Systems and Structures*, Vol. 12, pp. 709-718.

http://www.cnn.com/2004/WORLD/europe/07/06/airport.collapse/index.html

http://www.diamondsystems.com

http://www.intersil.com

http://www.microchip.com

http://www.radiometrix.com

Appendix A

Matlab Code for Wave Propagation Simulation

```
close all
clear all

rho = 2700; %density kg/m3 for Al
T = 20;     %Temp in Celsius

%Define Modulus of Elasticity Temperature Dependence
temp = [-270 -200 -150 -100 -50 0 20 100 200 250 300 350 400];
modulus = [95 82 77 75 73 70 70 69 68 63 50 26 5];

figure, plot(temp,modulus,'o-'),xlabel('Temperature (C)'), ylabel('Modulus of Elasticitiy (GPa)')
title('Modulus of Elasticitiy versus Temperature for Aluminum')

%Curvefit for Modulus (GPa) based upon temp
E = - 1.3025e-009*T^4 - 9.2053e-007*T^3 + 0.00016173*T^2 - 0.0031899*T + 70.0067;
E = E*1e9;

RoomTemp_E = 70e9;

ca = sqrt(E/rho);
crt = sqrt(RoomTemp_E/rho);

%Define Beam Parameters
L = 5;   %Length of beam
l = 2.5;   %length to center PZT patch
d = .4;     %damage location



%ROOM TEMP DAMAGE LOCATION CALCULATIONS

%Measuring from PZT 5&6
t11 = l/crt;
ta1 = (2*d+l)/crt;
dloc1 = crt*(ta1-t11)/2

%Measuring from PZT 1&2
t12 = l/crt;
ta2 = (3*l -2*d)/crt;
dloc2 = L - l - crt*(ta2-t12)/2


%DAMAGE LOCATION CALCULATIONS FOR ANY OTHER TEMPERATURE

%Measuring from PZT 5&6
t13 = l/ca;
ta3 = (2*d+l)/ca;
dloc3 = crt*(ta3-t13)/2

%Measuring from PZT 1&2
t14 = l/ca;
```

```
ta4 = (3*l -2*d)/ca;
dloc4 = L - l - crt*(ta4-t14)/2



%WHOLE RANGE OF TEMPERATURES
T1 = [-180:5:125];
E1 = - 1.3025e-009*T1.^4 - 9.2053e-007*T1.^3 + 0.00016173*T1.^2 - 0.0031899*T1 + 70.0067;
E1 = E1*1e9;

ca1 = sqrt(E1./rho);

for ii = 1:length(ca1)
   %Measuring from PZT 5&6
   t1_56(ii) = l/ca1(ii);
   ta_56(ii) = (2*d+l)/ca1(ii);
   dloc_56(ii) = crt*(ta_56(ii)-t1_56(ii))/2;

   %Measuring from PZT 1&2
   t1_12(ii) = l/ca1(ii);
   ta_12(ii) = (3*l -2*d)/ca1(ii);
   dloc_12(ii) = L - l - crt*(ta_12(ii)-t1_12(ii))/2;
end

figure, subplot(211), plot(T1,dloc_56), ylabel('Calculated Damage Location (m)')
hold on, plot(T1,d*ones(length(T1)),'--'), hold off, title('Calculated and Actual Damage Locations
versus Temperature')
legend('Calculated Location from PZTs 5&6','Actual Location (m)')

subplot(212), plot(T1,dloc_12), xlabel('Temperature (C)'), ylabel('Calculated Damage Location
(m)')
hold on, plot(T1,d*ones(length(T1)),'--'), hold off
legend('Calculated Location from PZTs 1&2','Actual Location (m)')

figure, plot(T1,t1_56), xlabel('Temperature (C)'), ylabel('t1 (sec)')
title('t1 Time versus Temperature From PZTs 5&6')
```

```
close all
clear all

rho = 2700; %density kg/m3 for Al


%Define Beam Parameters
L = 1.83;   %Length of beam
l = .915;   %length to center PZT patch
d = .4;     %damage location

%Find Longitudinal Natural Frequencies
%Curvefit for Modulus (GPa) based upon temp

T = [-270:5:400];
E = - 1.3025e-009*T.^4 - 9.2053e-007*T.^3 + 0.00016173*T.^2 - 0.0031899*T + 70.0067;
E = E*1e9;

RoomTemp_E = 70e9;

ca = sqrt(E/rho);

n=4;
for ii = 1:n;
   for jj = 1:length(ca);
      wn(ii,jj) = ii*pi*ca(jj)/L;
   end
end

figure, plot(T,wn(1,:),T,wn(2,:),T,wn(3,:),T,wn(4,:))
title('Beam Longitudinal Natural Frequencies vs Temperature (Modulus Change)')
xlabel('Temperature (C)'), ylabel('Frequency (rad/sec)')
legend('First','Second','Third','Fourth')


%Add in Density

av = 3*23.6e-6;  %Coefficient of Volumetric Expansion
Vo = .00183;     %Room Temp Volume
m = 4.941;       %Mass in kg

dV = Vo - Vo*av*(T-20);
drho = m./dV;

dc = sqrt(E./drho);

m=4;
for ii = 1:m;
   for jj = 1:length(dc);
      wn1(ii,jj) = ii*pi*dc(jj)/L;
   end
```

```
end

figure, plot(T,wn1(1,:),T,wn1(2,:),T,wn1(3,:),T,wn1(4,:))
%title('Beam Longitudinal Natural Frequencies vs Temperature (Modulus and Density Change)')
xlabel('Temperature (C)'), ylabel('Frequency (rad/sec)')
legend('First','Second','Third','Fourth')
```

Appendix B

Sample Matlab Code for Composites Damage Detection

```
close all
clear all

%load impedance signatures
load after40to60
load after40to60A
load after90to110
load after90to110A
load after190to230
load after190to230A
load baseline40to60
load baseline40to60A
load baseline90to110
load baseline90to110A
load baseline190to230
load baseline190to230A

%%%%%%%%%%%%%%%%%%%%%%%%%%%%%%%%%%%%
%40 to 60 kHz frequency range
%%%%%%%%%%%%%%%%%%%%%%%%%%%%%%%%%%%%

% normalize impedance signatures
baseline40to60A(:,2) = baseline40to60A(:,2) - (mean(baseline40to60A(:,2))-
        mean(baseline40to60(:,2)));
after40to60(:,2) = after40to60(:,2) - (mean(after40to60(:,2))- mean(baseline40to60(:,2)));
after40to60A(:,2) = after40to60A(:,2) - (mean(after40to60A(:,2))- mean(baseline40to60(:,2)));

figure, plot(baseline40to60(:,1),baseline40to60(:,2),baseline40to60A(:,1),baseline40to60A(:,2),
        after40to60(:,1),after40to60(:,2), after40to60A(:,1),after40to60A(:,2))
legend('Baseline 1','Baseline 2','After 1','After 2')
title('Impedance Measurements of Sample Two (15 kN Loading)'), xlabel('Frequency (kHZ)'),
ylabel('Real Impedance')

%compute damage metrics
M1 = sum(sqrt(((baseline40to60A(:,2) - baseline40to60(:,2)).^2)./(baseline40to60(:,2)).^2));
M2 = sum(sqrt(((after40to60(:,2) - baseline40to60(:,2)).^2)./(baseline40to60(:,2)).^2));
M3 = sum(sqrt(((after40to60A(:,2) - baseline40to60(:,2)).^2)./(baseline40to60(:,2)).^2));

Mtot40 = [M1,M2,M3]
figure, bar(Mtot40)


%%%%%%%%%%%%%%%%%%%%%%%%%%%%%%%%%%%%
%90 to 110 kHz frequency range
%%%%%%%%%%%%%%%%%%%%%%%%%%%%%%%%%%%%

% normalize impedance signatures
baseline90to110A(:,2) = baseline90to110A(:,2) - (mean(baseline90to110A(:,2))-
        mean(baseline90to110(:,2)));
after90to110(:,2) = after90to110(:,2) - (mean(after90to110(:,2))- mean(baseline90to110(:,2)));
```

```
after90to110A(:,2) = after90to110A(:,2) - (mean(after90to110A(:,2))-
mean(baseline90to110(:,2)));

figure,
plot(baseline90to110(:,1),baseline90to110(:,2),baseline90to110A(:,1),baseline90to110A(:,2),
        after90to110(:,1),after90to110(:,2), after90to110A(:,1),after90to110A(:,2))
legend('Baseline 1','Baseline 2','After 1','After 2')
title('Impedance Measurements of Sample Two (15 kN Loading)'), xlabel('Frequency (kHZ)'),
ylabel('Real Impedance')

%compute damage metrics
M4 = sum(sqrt(((baseline90to110A(:,2) - baseline90to110(:,2)).^2)./(baseline90to110(:,2)).^2));
M5 = sum(sqrt(((after90to110(:,2) - baseline90to110(:,2)).^2)./(baseline90to110(:,2)).^2));
M6 = sum(sqrt(((after90to110A(:,2) - baseline90to110(:,2)).^2)./(baseline90to110(:,2)).^2));

Mtot90 = [M4,M5,M6]
figure, bar(Mtot90)

%%%%%%%%%%%%%%%%%%%%%%%%%%%%%%%%%%%%
%190 to 230 kHz frequency range
%%%%%%%%%%%%%%%%%%%%%%%%%%%%%%%%%%%%

% normalize impedance signatures
baseline190to230A(:,2) = baseline190to230A(:,2) - (mean(baseline190to230A(:,2))-
mean(baseline190to230(:,2)));
after190to230(:,2) = after190to230(:,2) - (mean(after190to230(:,2))-
mean(baseline190to230(:,2)));
after190to230A(:,2) = after190to230A(:,2) - (mean(after190to230A(:,2))-
mean(baseline190to230(:,2)));

figure, plot(baseline190to230(:,1),baseline190to230(:,2),baseline190to230A(:,1),
        baseline190to230A(:,2),after190to230(:,1),after190to230(:,2),
        after190to230A(:,1),after190to230A(:,2))
legend('Baseline 1','Baseline 2','After 1','After 2')
title('Impedance Measurements of Sample Two (15 kN Loading)'), xlabel('Frequency (kHZ)'),
ylabel('Real Impedance')

%compute damage metrics
M7 = sum(sqrt(((baseline190to230A(:,2) -
baseline190to230(:,2)).^2)./(baseline190to230(:,2)).^2));
M8 = sum(sqrt(((after190to230(:,2) - baseline190to230(:,2)).^2)./(baseline190to230(:,2)).^2));
M9 = sum(sqrt(((after190to230A(:,2) - baseline190to230(:,2)).^2)./(baseline190to230(:,2)).^2));

Mtot190 = [M7,M8,M9]
figure, bar(Mtot190)
```

Appendix C

MASSpatch Component Photographs

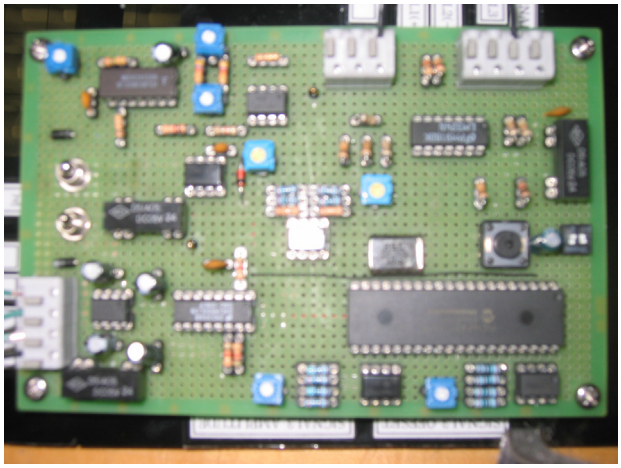

Figure C.1: The microprocessor and voltage oscillator board.

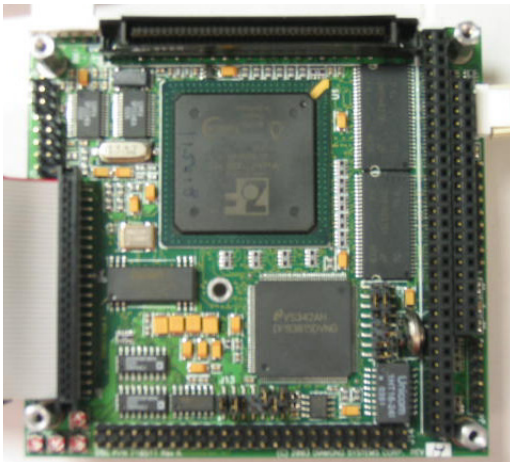

Figure C.2: The Prometheus PC 104 single board computer. The data acquisition board is not attached.

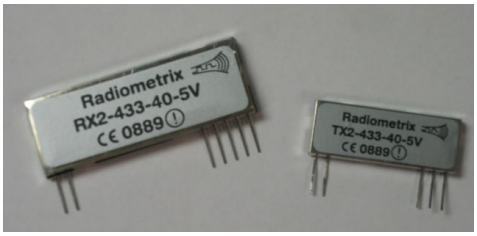

Figure C.3: The wireless transmitter and receiver used to indicate damage.

Appendix D

MASSpatch C Program Flowchart

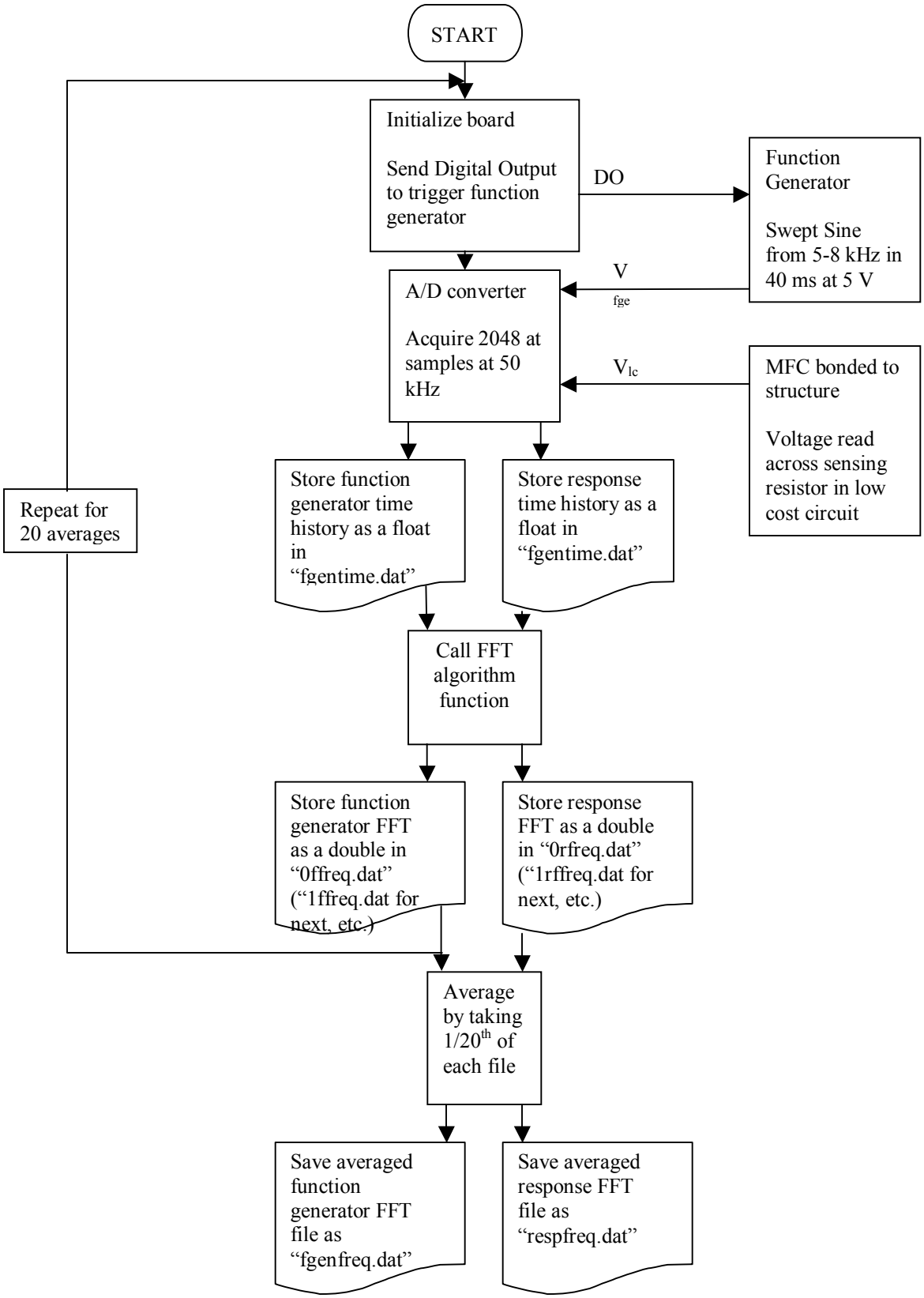
START
Initialize board
Send Digital Output to trigger function generator
DO
Function Generator
Swept Sine from 5-8 kHz in 40 ms at 5 V
V fge
A/D converter
Acquire 2048 at samples at 50 kHz
V lc
MFC bonded to structure
Voltage read across sensing resistor in low cost circuit
Repeat for 20 averages
Store function generator time history as a float in "fgentime.dat"
Store response time history as a float in "fgentime.dat"
Call FFT algorithm function
Store function generator FFT as a double in "0ffreq.dat" ("1ffreq.dat for next, etc.)
Store response FFT as a double in "0rfreq.dat" ("1rffreq.dat for next, etc.)
Average by taking 1/20th of each file
Save averaged function generator FFT file as "fgenfreq.dat"
Save averaged response FFT file as "respfreq.dat"

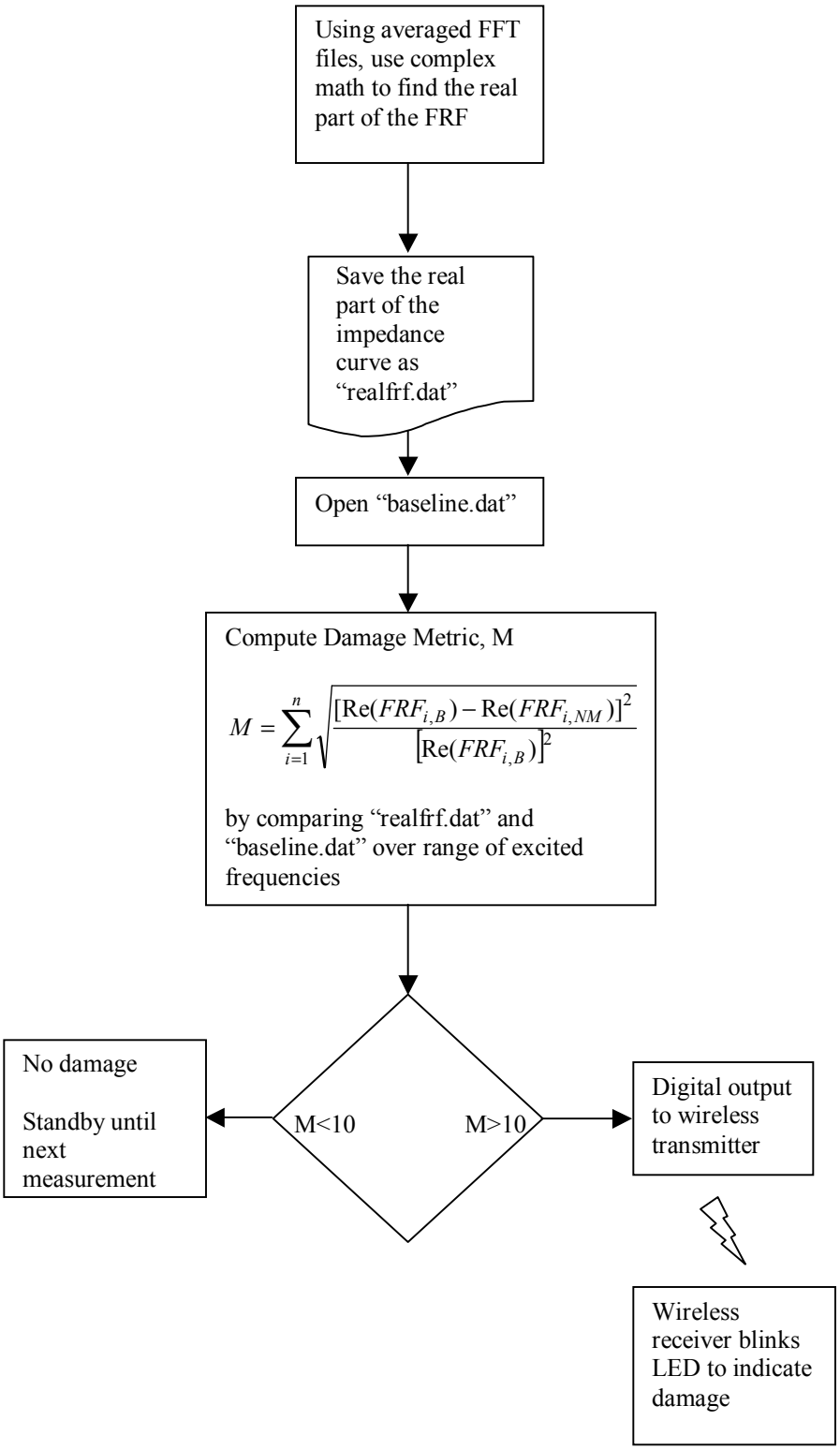
Using averaged FFT files, use complex math to find the real part of the FRF
Save the real part of the impedance curve as "realfrf.dat"
Open "baseline.dat"
Compute Damage Metric, M
$M = \sum_{i=1}^{n} \sqrt{\frac{[\mathrm{Re}(FRF_{i,B}) - \mathrm{Re}(FRF_{i,NM})]^2}{[\mathrm{Re}(FRF_{i,B})]^2}}$
by comparing "realfrf.dat" and "baseline.dat" over range of excited frequencies
M<10
M>10
No damage
Standby until next measurement
Digital output to wireless transmitter
Wireless receiver blinks LED to indicate damage

Vita

Benjamin L. Grisso was born on March 9, 1980 to Kenneth and Suzanne Grisso in Warsaw, Indiana. Ben was raised in Grandville, Michigan and graduated from Grandville High School in June of 1998. In the fall of 1998, he started pursuing his undergraduate degree from Michigan Technological University. Ben graduated Summa Cum Laude from Michigan Tech with a Bachelor of Science degree in Mechanical Engineering in May of 2002. Deciding to continue his mechanical engineering education, he started graduate studies at Virginia Polytechnic Institute and University in August of 2002. In May of 2003, he was offered a Graduate Research Assistant in the Center for Intelligent Material Systems and Structures (CIMSS). His research focused on using the impedance method for structural health monitoring to detect damage in composites and constructing a self-contained wireless system prototype utilizing the impedance method. After completion of his Masters of Science degree at Virginia Tech, Ben will continue working in CIMSS towards his Doctorate of Philosophy in Mechanical Engineering under the support of a National Science Foundation grant.

Address: Virginia Tech/CIMSS
310 Durham Hall MC 0261
Blacksburg VA 24061